at Maden Dere near MJT-1, contained more than 1 % Cu, and 0.01% Mo was detected in 14 samples from Hasan Dere. Good correlation between Cu and Mo values of the chipped samples is not recognizable as is the case of the soil geochemical survey.

1-3-2 Alteration

Samples for X-ray diffraction analysis were collected in the area of the Pgl stock and surrounding andesite at Maden, Mat and Hasan Deres in order to unravel zoning of alteration by mineralization. These 55 samples (44 samples from surface and 16 samples from drilling core) were analysed using the X-ray diffraction meter. The result was compiled in the map of alteration zoning, together with microscopic observations of thin sections. Results of X-ray diffraction analysis are presented in Table 2; the alteration zoning map of ground surface is in Fig.10, and the alteration zoning map of drilling core is in Fig.58.

Altered clay minerals detected through X-ray diffraction analysis are mostly sericite and chlorite with additional kaoline, pyrophyllite. It is difficult to distinguish sericite and biotite by X-ray diffraction analysis. Although diffraction patterns are slightly different between both minerals, this difference does not distinglish two clay minerals. Thus the potassic zone was defined with the help of microscopic observations of thin sections. Among samples of the potassic zone, YY-10, YY-15, KY-23 and HH-26 were identified as belonging in the potassic zone by microscopic observation, and HH-24 and HH-46 were grouped into the potassic zone through consideration of the field evidence in which these samples contained very fine filmy molybdenite-chalcopyrite veinlets are distributed at downstream of the Hasan Dere, and have undergone biotitization in altered porphyritic granite (as detarmined by the geological survey of the initial phase).

Samples located at the periphery of the potassic zone contain chlorite and sericite. In this zone, sericite rich white rock is classified into the phyllic zone, while chlorite rich greenish rock is classified into the propylitic zone. For instance, outcrops distributed along 400 m in extention to the south from the junction of Maden River and Hasan Dere contain chalcopyrite molybdenite as filmy veinlets or with quartz veins in joints and fissures of the andesite of the A1 Member (Zagana Formation), and have mainly undergone sericitization. Thus this zone is defined as phyllic. The outer parts of the phyllic zone, chlorite rich propylitic zone, and further outer zones tend to decrease in chlorite

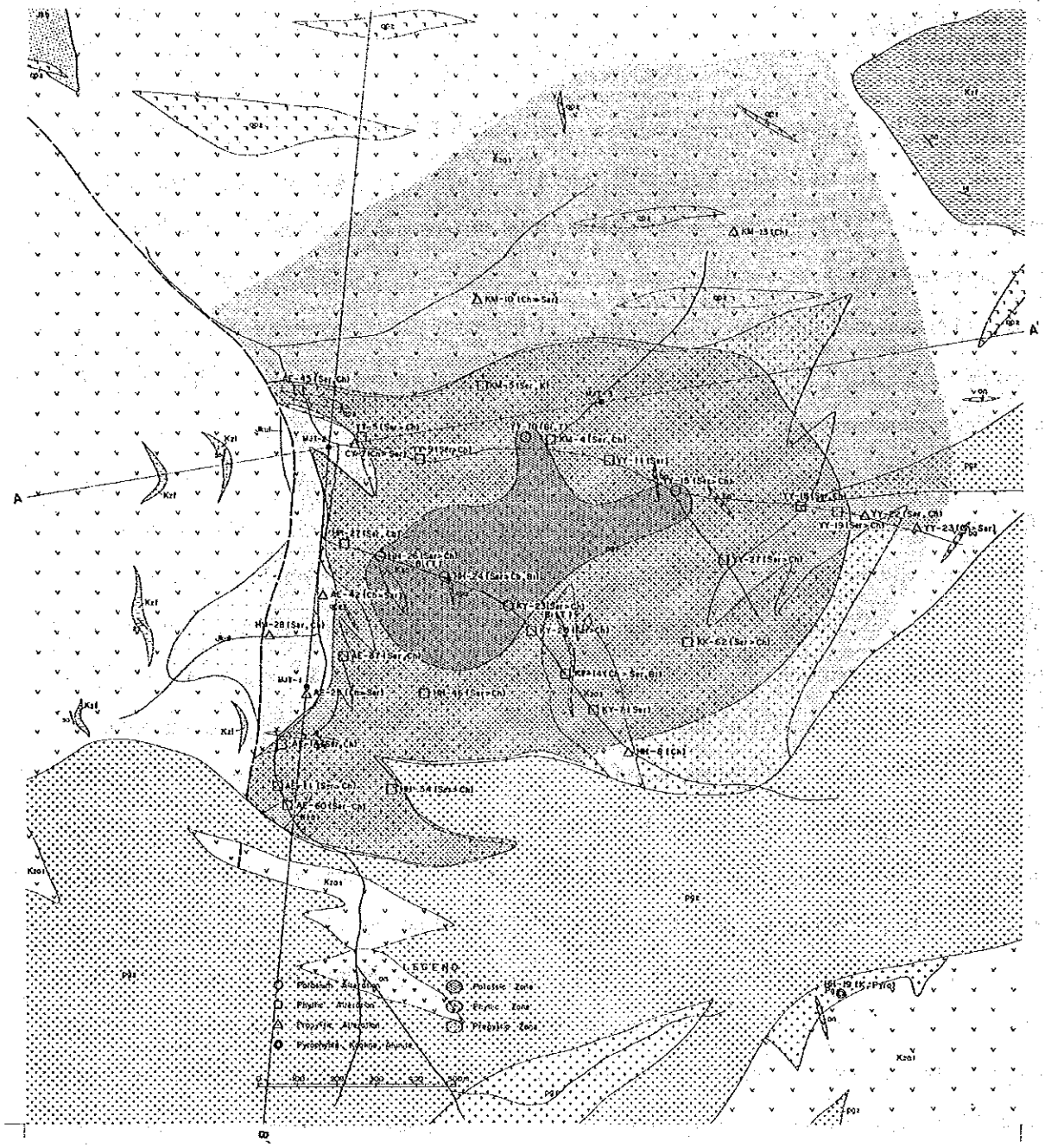

Fig.10 Alteration Zone Map of the Hasandere Area

Table 2 List of X-ray Diffraction Analysis (1)

Hasandere Area

No 1

Sample No.	Name and Description	Mo	Ch	Ser	K	P	Qz	Ep	C	K-f	An	Al	Gy	Ah	Ma	Py	Cp	Li	Mo	Ce	Pl	Bi	Ho	Remarks
AE-11	Pgl with Py-Qz vein		□	○			◎									□					○			
AE-14	Andesite with Mo-Py-Qz vein		□	□			◎									□					○			
AE-25	Andesite with Mo-rich Py-Qz vein		◎	□			◎		□	△						□			□					
AE-37	Andesite with Py-(Mo)-Qz vein		○	○			◎			△						□	□				□			Sericite(2M1)
AE-42	Andesite with Py-Qz vein		◎	○			◎			△														Sericite(2M1)
AE-45	Pgl with Qz veinlets		□	□			◎									△					◎			
AE-60	Andesite with Py-dissemination		□	□			◎									△					?			Sericite(2M1)
YY- 5	Andesite with Mo-Qz vein		□	○			◎			△				□	□	△	△		△					
YY- 7	Pgl		○	□			◎														◎			
YY- 9	Pgl with Qz vein		□	○			◎									△					◎			
YY-11	Qz vein, limonitization			□			◎														○			
YY-15	Pgl with limonite-Py-Qz vein		□	○			◎									△					◎			
YY-18	Unaltered pgl		□	□			◎									△					◎	□		
YY-19	Pgl, silicified and limonitized		□	○			◎														□			
YY-22	Andesite with Py-dissemination		□	□			◎		□							□					○			
YY-23	Unaltered pgl		○	□			○	?						□					◎					
YY-27	Pgl with Py-Qz vein		□	○			◎									□					○			
HH- 8	Andesite with Py-dissemination		○				◎									□					□		□	
HH-19	White altered pgl (sili.and li)			□	◎		◎					□												
HH-24	Biotite-altered pgl with Qz vein		□	○			◎														◎	□		
HH-26	Pgl with Mo-Py-Qz vein		□	○			◎									△					○			
HH-27	Altered pgl with Qz vein		○	○			◎														◎			
HH-28	Andesite with strong Py-diss.		□	△			□	□	□					□		◎								
HH-46	White pgl with Qz vein		△	○			◎																	Sericite(2M1)
HH-54	Pgl with limonite-Qz vein		△	○			◎																	Sericite(2M1)
KK-62	Altered pgl		□	△			◎														○			
KY- 7	Andesite with Py-Qz vein			◎			◎	□	□	□						□					□			
KY-14	Andesite with Py-dissemination		□	△			□									□					○		○	
KY-20	Pgl with Mo-Py-Qz vein		□	○			◎		□							△		□			□			
KY-23	Pgl with Mo-Qz vein		□	○			◎									△		□			◎			
KM- 4	Pgl with cp-diss. and Qz veinlets		□	□			◎									△					◎			
KM- 5	White altered pgl		?	□	□		◎																	
KM-10	Altered rock (Andesite)		◎	□			◎			□														
KM-13	Magnetite-actinolite skarn		□																				○	Actinolite

Table 2 List of X-ray Diffraction Analysis (2)

Hasandere Area

No 2

Sample No.	Name and Description	Mo	Ch	Ser	K	P	Qz	Ep	C	K-f	An	Al	Gy	Ah	Ma	Py	Mag	Li	Mo	Ce	Pl	Bi	Ho	Remarks
MJT-1 20.5m	Chloritized andesite (Ch,Ep,Mag)		◎	□			◎			△						□	□							
MJT-1 87m	Silicified andesite (Ser,Ch)		◎	○			◎			□						□								Sericite (2M1)
MJT-1 108m	Silicified qpl (Ser,Ch)		□	○			◎									□								Sericite (2M1)
MJT-1 189m	Basaltic andesite (Ch,Ser,Ep,Mag)		◎	○	?		◎	△		△						□								Sericite (2M1)
MJT-1 259m	Andesite (Ch,Ep,Mag)		◎	△	?	□	◎	△								□								
MJT-2 29m	Andesite (Ch,Ser)		◎	□			◎			□												□		
MJT-2 89m	Silicified andesite (Ch,Ep,Ser)		○	◎			◎									□						○		
MJT-2 132m	Brecciated basaltic andesite (Ch)		○	○			◎									□						○		
MJT-2 176m	Basaltic andesite (Ch,Ser)		◎	○			◎			□				○		△						○		
MJT-2 299m	Basaltic andesite (Ch,Ep,Mag)		◎	○			◎	△		□				□		□	□					○	□	
MJT-3 23m	White pgl (Ser)		□	○			◎			□						□				□		○		
MJT-3 56m	White pgl (Ser)		□	○			◎			□						△	□			△		○	△	
MJT-3 119m	Strongly altered pgl (Ser)		□	○			◎			□						△						○		
MJT-3 167m	Strongly silicified pgl (Ser,Ch,Ep)		△	○			◎			?				□	○	□						□		
MJT-3 233m	Strongly silicified pgl (Ser,Ch,Ep)		□	○			◎			?	□			□	○	△						○		
MJT-3 308m	Quartz porphyry (Bi,Ser)		□	□			◎			□				□		□						□		

Karadag Area

Table 2 List of X-ray Diffraction Analysis (3)

No 3

Sample No.	Name and Description	Mo	Ch	Ser	K	P	Qz	Ep	C	K-f	An	Al	Gy	Ah	Ma	Py	Cp	Li	He	Ce	Pl	Bi	Ho	Remarks
HH-145	Siliceous garnet skarn with galena and cp.			△			◎				□				△				□	□			△	
HH-154	Oxcp and blackish coloured mineral/s?		△				◎								□				□	○			△	
HH-147	Oxidized garnet skarn						◎		○		○				△									
KK-141	Clay (montmollilonite)				○		△	□		◎														□
MM-124	White clay		△	○			◎			□														Sericite (2M1)

◎: Abundant ○: Common □ : Few △: Rare

Mo: Montmollitonite, Ch: Cholorite, Ser: Sericite, K : Kaoline, P : Pyrophylite, Qz: Quartz

Ep: Epidot, C : Calcite, K-f: Potassium feldspar, An: Andradite, Al: Alunite, Gy: Gypsum

Ah: Anhydrite, Ma: MalaChite, Py: Pyrite, Cp: Chalcopyrite, Li: Limonite, Mo: Molybdenite

He: Hematite, Ce: Cerussite, Pl: Plagioclase, Bi: Biotite, Ho: Hornblende oxcp: oxidized copper

content while increasing in epidote content.

Pyrophyllite and kaoline also occur locally at the southern end of the Pg1 stock which has been intruded by Pg2.

This pattern of alteration zoning is similar to the Lowell-Guilbert model(1970) of potassic zone → phyllic zone → argillic zone→ propylitic zone outwardsfrom the core. In the case of this surveyed area, the outer limit of the propylitic zone was delineated in an area of 1.7 km X 1.4 km, on the basis of the anomalous area of Cu and Mo as found by the soil geochemical survey of the initial phase conducted by MTA, but the alteration area was expanded into an area of 1.8 km X 1.8 km as a result of an extention of the anomalous area to the north and north west subsquent to an additional soil geochemical survey carried out by MTA(Trabzon branch office)

1-4 Fliud Inclusions

1-4-1 Fluid Inclusions in Rocks Exposed on Ground Surface

Samples for measuring fluid inclusions were collected in the Hasandere area in which promising porphyry copper ore deposit is expected. Samples were collected from the following rocks, and their amounts are as follows :

(1) Altered porphyritic granite(Pg1)	39 samples
(2) Unaltered porphyritic granite(Pg2)	7 samples
(3) Andesite(Zigana Formation)	21 samples
Total	67 samples

An additional 33 samples were also collected from drilling cores, and total samples measured number 100 pieces.

Among these samples, quartz veins and quartz phenocrysts were from the altered porphyritic granite(Pg1) (regarded as the ore-bringer intrusion), quartz phenocrysts from the unaltered porphyritic granite(Pg2) (slightly post-intrusion of Pg1) and porphyry (Qp1), and quartz veins in andesite intruded by Pg1, Pg2 and Qp1 were collected for fluid inclusion measurements.

1-4-2 Measurement of Homogenization Temperature

A Leitz microscope and heating stage 1350 were used for heating laboratory work, bichromate kalium (chemical reagent ; melting point : 394 ℃) was used to temperature correlation , and a garvanometer of 20 ℃ scale was used for temperature reading(error: $<\pm 10$ ℃). 116 specimens in total were prepared, but 16 specimens among them could not be measured as they were smaller than 10 μ in size.

After checking reproducibility of temperature measurement, fluid inclusion measurements were carried out 5 or 6 times per a specimen through this check. The error of reproducibility was almost ±10℃. 1,113 fluid inclusions were measured from 68 samples collected. Measured fluid inclusions per sample ranged from 10 to 21 inclusions (average: 17 inclusion per sample). The number of measurements for each rock type and quartz samples are shown as follows:

	Phenocryst	Quartz vein	Total
Altered porphyritic granite(Pg1)	328 pcs	326 pcs	654 pcs
Unaltered porphyritic granite(Pg2)	93 pcs		93 pcs
Andesite(Zigana Formation)		366 pcs	366 pcs
Total	421 pcs	692 pcs	1,113 pcs

Homogenization temperatures measured are shown in Figs.11~13, 15~19 and in Tables 4 and 5.

As a result of the measurements, all homogenization temperatures range broadly between 250 ℃ and 660 ℃, but 90% of these values are included within the range of 350 ℃ to 450 ℃. Over 80 % of the homogenization temperature values per sample are in the temperature range of 50 ℃ to 100 ℃, showing normal distribution. Such a tendency is more predominant in the quartz vein than in the quartz phenocryst.

1-4-3 Result of the Measurement of Fluid Inclusion in Rocks

The measurable diameter of fluid inclusions is 20 μ to 30 μ, but sometimesfluid inclusions 10 μ or several 10's μ in diameter were also measured. Thin sections less than 0.3 mm to 0.4 mm in thickness, with both planes polished were prepared.

Many fluid inclusions are surrounding by transpearent quartz . There are many inclusions less than 10 μ in diameter and are elipsoidal in form. Among these inclusions, negative quartz crystal are also observed, and pseudo secondary or secondary inclusions are of irregular form.

Fluid inclusions of the surveyed area are characterised by a high ratio of the gaseous phase. Thus it is called gaseous phase inclusion.

Fluid inclusions of Hasandere area contain polyphase inclusions, commom in other porphyry copper deposits. They consisit namly of gaseous inclusions, which contain bubbles (over 60 % of inclusion in volume) and little liquid, and is wholly filled by gaseous inclusions owing to the expansion of gaseous after heating, and liquid inclusions, which contain ball-formed gaseous bubbles (10 % ~ 40 % of inclusion in volume) in liquid and is wholly filled by liquid after heating. The 1,115 pieces of fluid inclusions measured are divided into 1,021 pieces of liquid and 132 pieces of gaseous fluid inclusions. Homogenization temperature of the gaseous fluid inclusions is higher than that of liquid fluid inclusions, regardless of whether they are in rock, quartz vein or quartz phenocryst.

Most fluid inclusions in the quartz vein and quartz phenocryst can be described as follows:

① Consisting of two phase inclusions (gaseous and liquid phases)

② Many liquid phase fluid inclusions usually contain carbon dioxide

③ A few solid phase inclusions are observable. Some solid phase inclusions disappear near 260 ℃, and others is disappear at a range of 260 ℃ to 620 ℃. The former may be NaCl crystalized tetrahegonally and the latter aresomewhat round in shape but are of rather irregular form.

④ Minor amounts of polyphase inclusions are present.

⑤ Most fluid inclusions are generally tiny, namely smaller than 20 microns in size.

The mean value of homogenization temperature is 390 ℃ in the quartz vein of Pg1, and 381 ℃ in the quartz vein in andesite. It is 386 ℃ for total samples of both rocks. The mean value of those in quartz phenocrysts is 392 ℃, close to the value for quartz vein of Pg1.

It is made clear as shown in Table 6, that excepting the value from Pg2, the difference between the mean values is stastifically insignificant.

Figs.14 and 15 show that histograms of homogenization temperatures obtained from the respective areas. Homogenization temperatures of quartz phenocrysts from Pgl are highest (427 ℃) at Hasandere Area, 405 ℃ at Mat Dere, and 356 ℃ at Maden Dere, that is, the temperature decreases towards the periphery of the Pgl intrusion. The temperature of fluid inclusions in Pgl at the southern part where it has been intruded by Pg2 drops further to 303 ℃. Here there is no quartz vein and only five quartz phenocrysts were used for the measurment of fluid inclusions, in contrast with 23 quartz phenocrysts of Pgl. Therefore, it is very difficult to compare the results of both rocks. However it is roughly stated that the mean temperature of inclusion in Pg2 (348 ℃) is 50 ℃ lower than that of Pgl (392 ℃). In the case of the difference between the temperatures of gaseous and liquid phases, Pgl shows the largest difference with over 100 ℃, followed by the andesite at Hasan Dere with 100℃, and the andesite at Mat Dere with the smallest differnce of 20℃. The last result indicates that homogenization temperatures of the gaseous and liquid phases are close in value to each other.

Fluid inclusions in the quartz phenocryst of Pg2 is characterized by their small size, while that of Pgl is somewhat larger in size, in comparison with both rocks. Solid-like inclusions which disappear at 590 ℃ and reappear at 390 ℃ such as those in AE-54 of Pg2 as well as those in YY-12 of Pg2 which disappear at 620℃ are recognized among the inclusions in quartz phenocryst. In comparison with homogenization temperatures of fluid inclusions in quartz veins in each part of Pgl, the temperature is highest (408℃) at around Mat Dere, 391℃ at Maden Dere, and tends to decline with a gentle temperature gradient. The temperature of quartz veins in andesite has the same tendency-highest (406℃) at the molybdenum anomalous area of north Mat Dere, 384℃ at Hasan Dere, and 377℃ at Mat Dere. Solid-phase-like fluid inclusions are characteristically observed in samples of AE-39 from Maden Dere, YY-15 from Mat Dere, and HH-47 from Hasan Dere. NaCl in YY-15 disappeared at 260℃, and fluid inclusions in AE-39 and HH-47 contain material like NaCl. Gaseous fluid inclusions are observable in samples from Mat, Maden, and Hasan Deres. Samples from Mat Dere contain many gaseous phase inclusions and thier homogenization temperatures are usually high, as is consistant with the abovementioned pattern.

1-4-4 Homogenization Temperature of Fluid Inclusions in Drilling Cores

Thirty three samples were collected from drilling cores of MJT-1, MJT-2, and MJT-3 analysed by the second phase survey. The amount of samples collected are as follows ;

Andesite (Zigana Formation)	MJT-1	7 samples
	MJT-2	11 samples
Altered porphyritic granite(Pgl)	MJT-1	1 sample
	MJT-2	1 sample
	MJT-3	10 samples
Altered quartz porphyry (Qpl)	MJT-3	1 samples
Total		33 samples

The same method and and conditions were applied in the measument of homogenization tempurature on fluid inclusions in drilling core as were used for the surface rocks. 562 fluid inclusions were detected from 33 samples collected. Fluid inclusions measured ranged from 10 to 20 pieces per sample (average 17 pieces per sample). The number of measurement per each rock and quartz sample is shown as follows;

	Phenocryst(Qtz)	Vein(Qtz)	Total
Quartz vein in andesite		324 pcs	324 pcs
Altered porphyritic granite(Pgl)	92 pcs	91 pcs	183 pcs
Altered quartz porphyry(Qpl)	55 pcs		55 pcs
Total	147 pcs	415 pcs	562 pcs

Results of homogenization temperature measurements are shown in Figures 14 and 15 ,and in Tables 5 and 6. All temperatures range from 290 ℃ to 500 ℃, indicating a narrow range compared with that (250 ℃ ~ 660 ℃) of surface rocks. Ninety percent of the temperature values are in the range from 350 ℃ to 450 ℃, and show normal distribution in the histogram, although the values of some populations are not always well distributed in the histogram. Characteristics of the fluid inclusions in drill core are explained as follows;

① In addition to gaseous and liquid phases, solid inclusions are also included. More solid

inclusions are included in the core than in surface rocks.

② Small size inclusions are common in the quartz vein of andesite collected from MJT-1 and MJT-2. and there are also few gaseous phase inclusions. This tendency is marked at a depth from 200 m to 300 m.

③ Solid inclusions(NaCl) disappear at 260 ℃

④ In the altered porphyritic granite, the content of gaseous inclusions increases.

⑤ In the andesite, gaseous inclusion decreases comparatively, and thier size becomes smaller.

The mean homogenization temperature of all cores is 398 ℃, and this value is 13 ℃ higher than the temperature in surface rocks. Comparing each rock facies, homogenization temperature in core samples of andesite is slightly higher than that in surface andesite, but oppositely, the temperature in core samples of altered porphyritic granite is lower than that in the surface rocks, namely 406 ℃ ~ 410 ℃ in cores, in contrast with 430 ℃ ~ 480 ℃ in ground surface rocks at Mat and Hassan Deres. Mean homogenization temperature of gaseous inclusions in altered quartz porphyry is 416 ℃, higher than that of gaseous inclusions in altered porphyritic granite of MJT-3, but on the contrary lower than that of altered porphyritic granite exposed on the ground surface.

The number of fluid inclusions measured in quartz veins constituted more than 65 percent of total measured inclusions. In order to find the relationship between these fluid inclusions and their mineralization types, the quartz veins were classified into barren quartz, pyrite bearing quartz, chalcopyrite bearing quartz, and molybdenum bearing quartz. The mean homogenization temperature of inclusions was then calculated for each quartz vein type with results, as shown in the following table ;

	F.I.	Pcs	Homogenization Temperature	
			Range(℃)	Average(℃)
Barren quartz	Liq.p	209	300~560	386
	Gas.p	40	370~550	441
Pyrite-quartz	Liq.p	228	280~520	374
	Gas.p	21	380~480	421
Chalcopyrite-quartz	Liq.p	132	320~500	390
	Gas.p	25	380~500	414
Molybdenite-quartz	Liq.p	384	250~580	385
	Gas.p	47	360~560	440

The results indicate that homogenization temperature of gaseous inclusions is generally higher than that of liquid phase inclusions. Although differences between the temperature of gaseous and liquid inclusions of each sulphide mineral type is not especially remarkable, it may be inferred that chalcopyrite was crystalized at the highest temperature conditions in the early stage, and molybdenite was succesively formed at high temperature in the gaseous phase.

Homogenization Temperature of Liquid Inclusions are shown as follows:

Homogenization Temperature of Liquid Inclusions

(Quartz Vein of Andesite in MJT-1)

Depth	Pcs	Homogenization Tempera.	
		Range(℃)	Average(℃)
52.80m	20	330~430	370
99.80m	20	340~400	375
210.50m	14	360~420	392
222.80m	20	370~430	401
290.70m	15	390~470	420

Homogenization Temperature of Liquid Inclusions

(Quartz Vein of Andesite in MJT-2)

Depth	Pcs	Homogenization Tempera.	
		Range(℃)	Average(℃)
58.40m	12	320~430	365
68.50m	12	350~430	371
71.80m	13	360~440	393
129.80m	20	370~410	383
145.30m	19	350~420	398
213.50m	20	350~400	371
248.00m	19	380~430	406
255.30m	15	320~390	357
268.50m	15	380~500	409
272.90m	18	370~420	401
283.40m	19	370~450	410

Homogenization Temperature of Liquid Inclusions

(Quartz Phenocryst of Pg1 in MJT-3)

Depth	Pcs	Homogenization Tempera.	
		Range(℃)	Average(℃)
10.15m	9	350~490	404
59.00m	11	350~450	384
238.90m	6	370~430	397
255.60m	17	390~480	435

As seen in the tables above,the homagenigation temparature in MJT-1 gradually increases with increasing depth. Although some holes irregularities occur, holes MJT-2 and MJT-3 also show an overall increase in temperature with depth.

1-4-5 Salinity in the fluid inclusion

Microscope NE (Nikon) for measurement under low temperature was used to measure salinity

of fluid inclusion. The microscope is able to cool and heat sample between -120 ℃ and +60 ℃ in temperature for freezing and defrosting of solid inclusion. A liquid nitrogen of - 196 ℃ was used for cooling, and thermister thermometer (sensitivity : 0.3 ℃) was instaled for reading temperature.

Amounts of measureble sample were 76 pieces amang 100 samples collected, since there were mostly small inclusions and it was very difficult to observe the phase variation at melting time of frozen inclusion owing to poor liquid phase inclusions. The result of the measurment indicates that their melting range from freezing point were from -7℃ to 17℃, and their NaCl equivalent concentration values were calculated from 4.8 wt% to 20.60 wt % through H_2O - NaCl diagram.

The NaCl concentration values of inclusion and homogenization temperatures are comparatively in definite range from 7 wt % to 15 wt %, and from 310 ℃ to 400 ℃ in quartz veins, while those values in intrusive rocks, especially in pgl, disperses. Relationship between the homogenization temperature and the salinity is shown in Fig. 20. The relationship indicates as follows.

① The homogenization temperatures of most fluid inclusions is higher proportionally in the salinity with higher concentration..

② The fluid inclusion in drilling core contains slightly higher salinity concentration than that in quartz vein of andesite.

③ In the case of Pgl, the salinity is higher concentration in the area of Hasan and Mat Deres, but is comparatively lower concentration in the Maden Dere, corresponding with homogenization temperature.

In a solid phase inclusion, hydrohalite usually occurs, but it is difficult to identify the hydrohalite in this area, because the fluid inclusions are very small in size. In the case of simple crystal solid inclusion accompanying by NaCl and KCl crystals, salinity of the inclusion is detected by volume of solid and liquid in inclusion and calculation of compositions of crystal salt and soluted salt (Takenouchi 1962).

Salinity values calculated by this method are shown as following ;

KY-24(quartz phenocryst in Pgl)	57.0 w%
KY-26(quartz phenocryst in Pgl)	50.3 w%
MJT-2(quartz vein in andesite, 129.8 m)	41.6 w%

MJT-3(quartz phenocryst in Pgl, 80.3 m) 48.9 w%

KCl may be not present because no solid inclusion was disappeared in low temperature.

Salinity values are definitly different between the value of core part in mineralized zone at Maden River and value of marginal part in the mineralized zone around Maden River, namely the former value are 40% ~ 50% detected by salt volume in inclusion and the latter values range from 7 % to 20 % (freezing point ; -4.2 ℃ to 15 ℃) by cooling stage method.

1-4-6 Conclusion of Measurement Results of Fluid Inclusion

Result of fluid inclusions measured from drilling cores and rocks of ground surface is totally summarized in following table.

Rock name	Amount of sample	Qtz vein		Qtz pheno		Qtz vein+Qtz pheno		Total	%
		Liquid	Gaseous	Liquid	Gaseous	Liquid	Gaseous		
Ande	39	631	59			631	59	690	40
Pgl	53	334	83	384	76	718	159	877	51
Pg2	5			87	6	87	93	93	5
Qpl	3			44	11	44	55	55	4
Total	100	965	142	525	93	1,480	235	1,715	100
%	65		35		86	14	100		

(Qtz : quartz, pheno : phenocryst, unit : piece)

The result of fluid inclusion measurement summarises as follows ;

① Homogenization temperatures of gaseous inclusions are generally 30 ℃ ~ 50 ℃ higher than that of liquid inclusion in andesite, on the other hand in the case of andesite of MJT-1, the former is about 10 ℃ higher in the temperature than that of the latter.

② Fluid inclusions in altered porphyritic granite (Pgl) were obtained from quartz veins and quartz phenocrysts. On the surface rock, gaseous inclusions in both quartzs are also about 40 ℃ ~ 50 ℃ higher in the temperature than liquid inclusion's, but on the core sample, gaseous inclusions

are conversely 2 ℃ ~ 10 ℃ lower in the temperature than liquid inclusion's, showing similar tendency to case of andesite. Homogenization temperature of fluid inclusion obtained from quartz phenocryst of altered porphyritic granite (Pg1) around Hasandere on ground surface is highest. The fact presumes that the part is center of intrusive stock body of Pg1. The temperature falls slightly toward deeper part. The fact that the homogenization temperature increases little by little toward deeper part presumes that the altered porphyritic granite (Pg1) rock body inclines.

③ Area where boiling phenomena might take place owing to presence of many gaseous inclusions is located at and around north area of Mat Dere. Fluid inclusions in drilling cores around the center are high salinity because many solid inclusions are observable.

④ Fluid inclusions of Pg2 are higher in homogenization temperature than that of Pg1, also gaseous inclusions in the former are smaller in scale than that of the latter.

⑤ Fluid inclusion has been observed in Pg1 at the southern side intruded by Pg2.

⑥ A dense salinity ore solution was probably supplied to the area of Mat and Hasan Dere.

Table 3 List of Amount of Fluid Inclusion Samples(Rocks 1)

No 1

Sample No.	V/P	Name and Description
AE- 7	V	Qz-vein in andesite,wd:3mm,Qz:crystal,limonite
AE- 8	V	Qz-vein in pg1,wd:1mm,with small amount of Py
AE- 8	P	Qz-phenocryst of pg1,Qz-pheno:2~1mm
AE- 9	P	Qz-pheno,pg1,Qz-pheno.max 4mm,Py-diss
AE-11	P	Qz-pheno of pg1,Qz-pheno:4mm
AE-13	P	Qz-pheno of pg1,Qz-pheno:2mm,diss
AE-15	V	Py-Qz vein in andesite,wd:3mm
AE-16	V	Py-Qz vein andesite,wd:2~3cm,Py:coarse grain.
AE-18	V	Py-Qz vein in andesite,wd:4~5mm,Py-rich
AE-23	V-1	Py-Qz vein andesite,wd:1~1.5cm,Py:coarse,rich
AE-23	V-2	Mo-Py-Qz vein in andesite,wd:1~1.5cm,Py:coarse,rich
AE-24	V	Mo-rich Py-Qz vein in andesite,wd:5mm,max 2cm,Qz:crys
AE-25	V	Mo-rich Py-Qz vein in andesite,wd:5mm
AE-31	V	Mo-Py-Qz vein in sili andesite,wd:8mm,Qz:crystal
AE-33	V	Mo-Py-Qz vein in sili andesite,wd:4mm,Mo:strong
AE-37	V	Py-(Mo)-Qz vein in sili andesite,wd:8mm,max 2mm crystal
AE-39	V	Py-Mo-Cp-Cc ? -Qz vein in chl-rich andesite,wd:1cm
AE-42	V	(Py)-Qz vein in andesite,wd:10-15mm
AE-43	V	Qz-vein in sili-ser pg1,wd:3-4mm,Qz:big crystal
AE-45	P	Qz-phenocryst of pg1,with Qz veinlets
AE-54	P	Unaltered pg2
AE-56	P	Unaltered pg2
YY- 5	V	Mo-Qz vein in andesite,wd:1cm,with ser & chl.
YY- 6	P	Qz-pheno of pg1
YY- 9	V	(Py)-Qz vein of pg1,wd:1cm
YY-12	P	Qz-phenocryst of unaltered pg1 ,no-mineralization
YY-15	V	Py-Qz-vein of pg1,wd:2cm
YY-15	P	Qz-phenocryst of pg1
YY-18	P	Qz-pheno of pg1(pinkish,unaltered,glassy)
YY-33	P	Unaltered pg2

Table 3 List of Amount of Fluid Inclusion Samples(Rocks 2)

No 2

Sample No	V/P	Description & Remarks
YY-26	V	Py-Qz vein pgl, wd: 4mm
YY-26	P	Qz-pheno of pgl
YY-27	V	Py-Qz vein of pgl, wd: 10mm
YY-27	P	Qz-pheno of pgl
YY-29	P	Qz-pheno of pgl
HY- 1	V	Mo-Qz vein in andesite, wd: 3mm, Qz: crystal, limonitized
HH- 9	V	Pgl with little Mo.Py, Qz, vein, limonitization, wd: 1cm
HH-13	P	Qz-pheno of pgl, Py-diss
HH-19	P	Qz-pheno of wht-alt pgl, sili-limonitized
HH-21	P	Pgl with Py diss
HH-24	V	Qz-vein of biotite-alt pgl, wd: 4-5mm, Py-poor, Qz: crystal
HH-24	P	Qz-pheno of biotite-alt pgl
HH-27	V	Qz-vein of alt pgl, wd: 1cm, Py-poor, limonitized
HH-36	P	Qz-pheno of greenish-pink pg2
HH-37	P	Qz-pheno of gry glassy pg2
HH-46	P	Qz-vein wht pgl
HH-46	V	ditto
HH-47	V	Qz-veinlets of pgl, wd: 1mm, limonitized
HH-53	V	Qz-veinlets of pgl, wd: 1-2mm, limonitized
HH-53	P	Qz-pheno of sili-limo.pgl
KY- 1	V	Py-Qz vein in andesite, wd: 10mm, with Mo, Cc
KY- 9	V	Py-Qz vein in andesite, wd: 6mm
KY-12	V	Mag-Py-Qz vein in andesite, wd.10mm, limo-Ep-Ch: strong
KY-18	V	Mo-Py-Qz vein in andesite, wd: 5mm, Qz: coarse
KY-19	V	Mo-Py-Qz vein of pgl, wd: 3-4mm, with small amount Cp
KY-19	P	Qz-pheno of pgl
KY-20	P	Qz-pheno of pgl
KY-21	V	Mo-Qz vein of pgl, wd;5mm
KY-21	P	Qz-pheno of pgl
KY-23	V	Mo-Qz vein of pgl, wd: 4mm, biotite-rich
KY-24	V	Mo-Qz vein of biotite pgl, wd: 6mm
KY-24	P	Qz-pheno of biotite pgl
KY-25	P	Pg with Mo-Qz vein
KY-25	V	Pg with Mo-Qz vein
KM- 4	V	Qz-veinlets of dark grey glassy pgl, wd: 1mm
KM-21	V	Qz-vein(float) from andesite wd: 3cm, no pyritization
KM-25	V	Qz-vein of andesite, wd: 7mm, no pyritization

Table 3 List of Amount of Fluid Inclusion Samples(Cores 1)

MJT-1 No 3

Depth(m)	V/P	Name and Description
52.8	V	Py-Cp-Qz vein in andesite, wd:5mm
99.8	V	Py-Mo-Cp vein in andesite, wd:3mm
138.0	V	Py-Mo-Qz vein in pgl, sericite along the Qz vein wd:15mm
183.3	V	(Mo-Py)-Qz vein in pgl,wd:10mm,Qz:huhedral crystal
183.3	P	ditto
210.5	V	Magnetite-Py-Qz vein in andesite,wd:3mm
222.8	V	Py-Cp-Mo-Qz vein in andesite,wd:10m
290.7	V	Mo-Py-Qz vein in andesite,Qz:huhedral crystal in druse,wd:10mm

Table 3 List of Amount of Fluid Inclusion Samples(Cores 2)

MJT-2 No 4

Depth(m)	V/P	Name and Description
58.4	V	Mo-Qz vein in andesite,wd:3mm
68.5	V	Cp-Qz vein in andesite, wd:10mm
71.8	V	Cp-Mo-Qz vein in andesite,wd:6mm,Qz:huhedral crystal
129.8	V	Qz vein in andesite,wd:2mm, Qz:coarse.
145.3	V	Magnetite-Cp-Qz vein in andesite,wd:4mm
213.5	V	Mo-Qz vein in andesite,wd:4mm,Cutting Cp-Py vein
248.0	V	Mo-Qz vein in andesite,wd:10mm
255.3	V	Py-Mo-Qz vein in andesite,wd:3mm
268.5	V	Magnetite-Cp-Qz vein in andesite,wd:12mm
272.9	V	Mo-Qz vein in andesite,wd:6mm
278.0	P	Porphyritic granite(pgl) with Py-Cp diss.
283.4	V	Py-Cp-Qz vein in andesite,with Py-Cp diss. wd:3mm

Table 3 List of Amount of Fluid Inclusion Samples(Cores 3)

MJT- 3 No 5

Depth(m)	V/P	Name and Description
10.15	P	Qz-pheno of pgl
59.0	V	Cp-(Mo)-Py-Qz vein in pgl, wd:10mm
59.0	P	ditto
80.3	V	(Mo)-Py-Qz vein in pgl, wd:18mm
118.7	V	Mo-Qz vein in pgl, wd:3mm
196.0	V	Cp-Py vein in pgl
238.9	P	Pgl with disseminated Cp-Py.
255.6	P	Pl-rich pgl
258.0	A	Qz-anhydrite vein in pgl, wd:20mm
312.5	P	Quartz porphyry
328.1	P	Quartz porphyry with Cp-Py diss.
378.0	V	Py-Mo-Qz vein in pgl, wd:6mm
400.6	P	Quartz porphyry with Cp-Py diss.

Table 4 List of Fluid Inclusion Samples on Sampling Items

Rock/Core	V/P	Rock Name	Locality of sample	No of Sample	Sample Name
Rock	V	Andesite (Zigana F)	Maden dere(A)※	15	AE-7,15,16,18,23(V1),23(V2),24,25,31,33,37,39,42,YY-5,HY-1
			Hasan dere(B)	4	KY-1,9,12,18,
			North Mat dere(C)	2	KM-21,25
		Porphyritic granite (pg1)	Maden dere(D)	4	AE-8,43,YY-26,27
			Hasan dere(E)	11	HH-9,24,27,46,47,53,KY-19,21,23,24,25
			Mat dere(F)	3	YY-9,15,KM-4
	P	Porphyritic granite (pg1)	Maden dere(G)	6	AE-8,9,11,13,45,YY-6
			Hasan dere(H)	9	HH-13,24,46,53,KY-19,20,21,24,25
			Mat dere(I)	6	YY-12,15,18,26,27,29
			South Hasan(J)	2	HH-19,21
		Porphyritic granite (pg2)	South Hasan(K)	5	HH-36,37,AE-54,56,YY-33
Core	V	Andesite (Zigana F)	MJT-1(L)	7	52.8m,99.8m,138m,183.3m,210.5m,222.8m,290.7m
			MJT-2(M)	11	58.4m,68.5m,71.8m,129.8m,145.3m,213.5m,248m,255.3m,268.5m,272.9m,283.4m
		Porphyritic granite (pg1)	MJT-1	-	
			MJT-2	-	
			MJT-3(N)	6	59m,80.3m,118.7m,196m,258m,378m
	P	Porphyritic granite (pg1)	MJT-1(O)	1	183.3m
			MJT-2(O)	1	278m
			MJT-3(P)	4	10.15m,59m,238.9m,255.6m
		Quartz porphyry(qp1)	MJT-3(Q)	3	312.5m,328.1m,400.6m

※ : (A)～(K) correspond to Fig. 11～15

AE-23(1) Maden dere

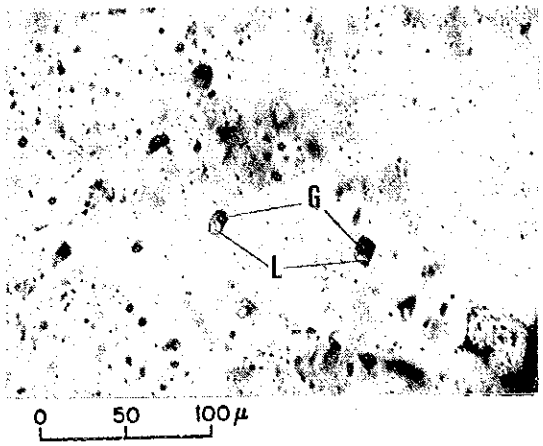

AE-23(2) Maden dere

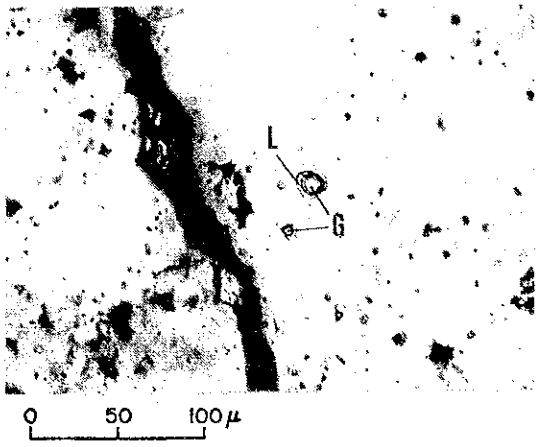

KM-25 North Mat

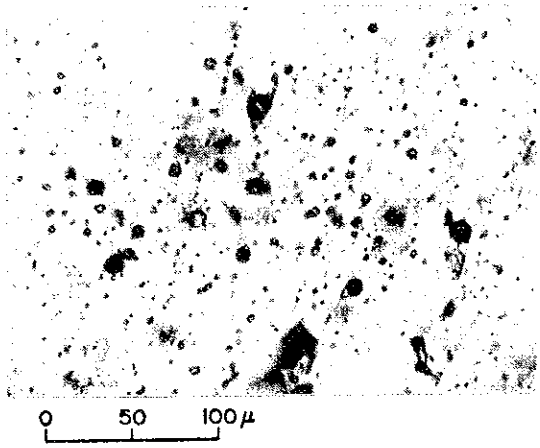

MJT-2 71.8m

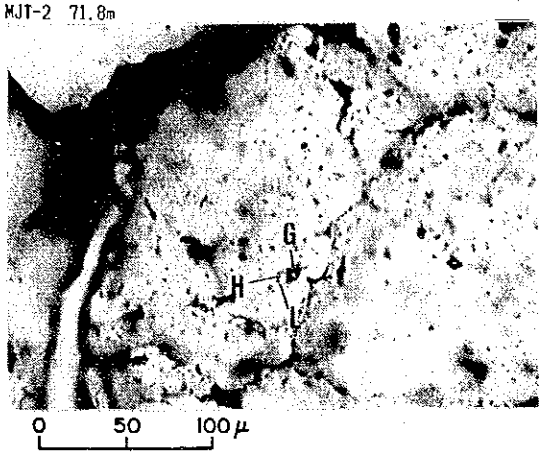

MJT-2 248m

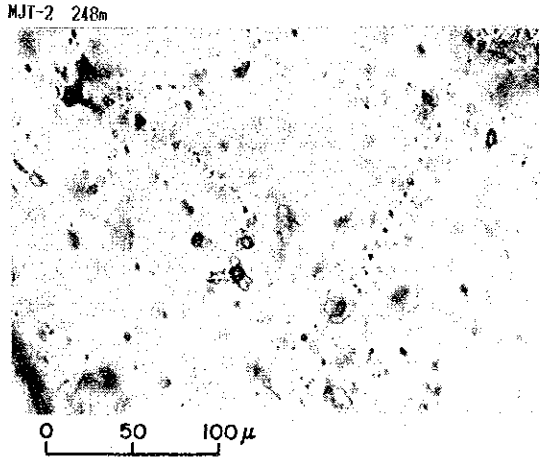

MJT-2 255.3m

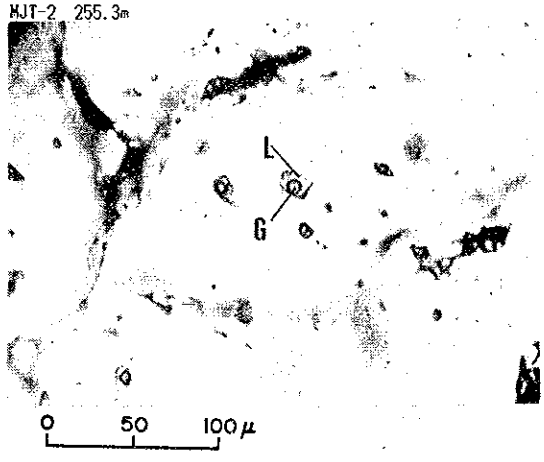

L: Liquid G: Gaseous H: Halite

Photograph Microscopic Photographs of Fluid Inclusions(1)

AE-45 Maden dere

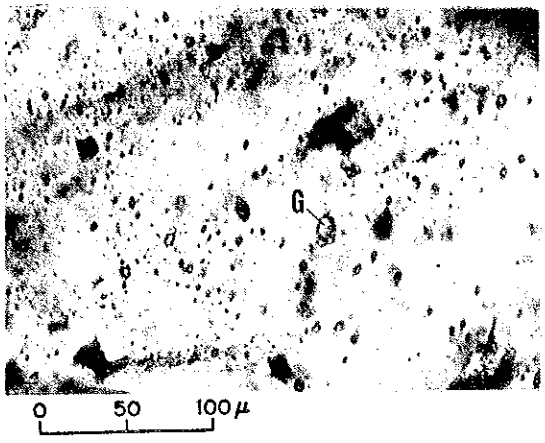

AE-8 Maden dere

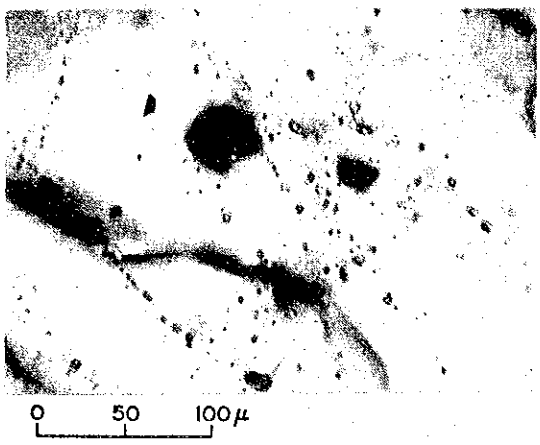

AE-8 Maden dere

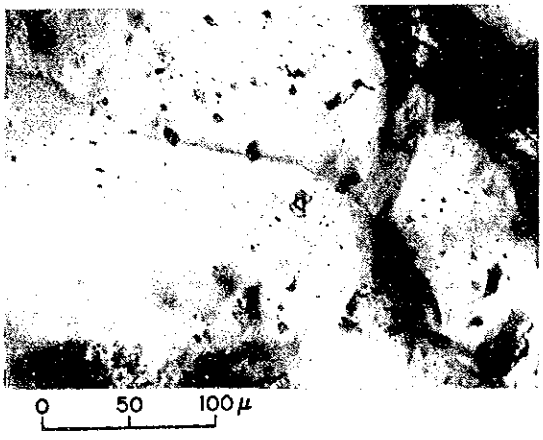

YY-26 Mat dere

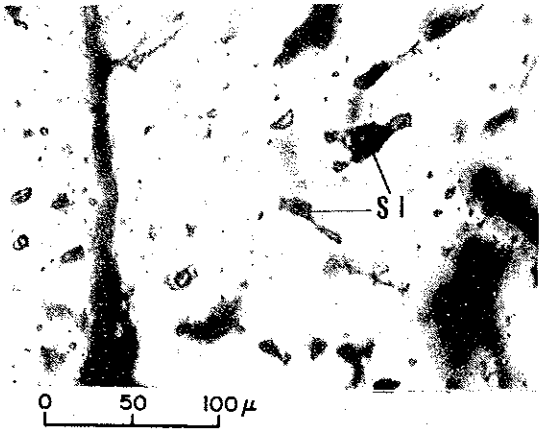

BH-46 South Hasan

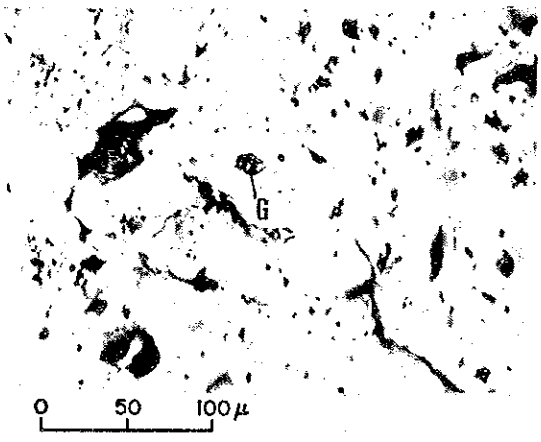

KY-25 Hasan dere

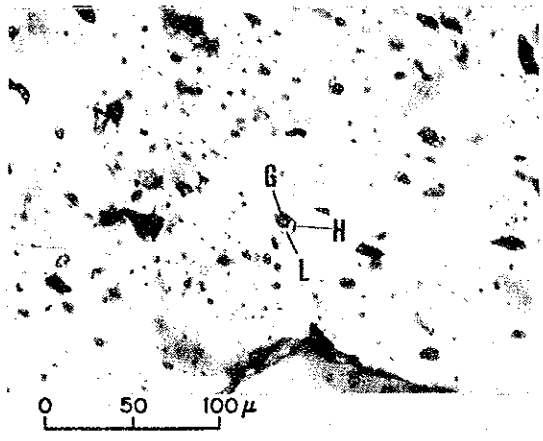

L: Liquid G: Gaseous H: Halite

Photograph Microscopic Photographs of Fluid Inclusions(2)

AE-9 Maden dere

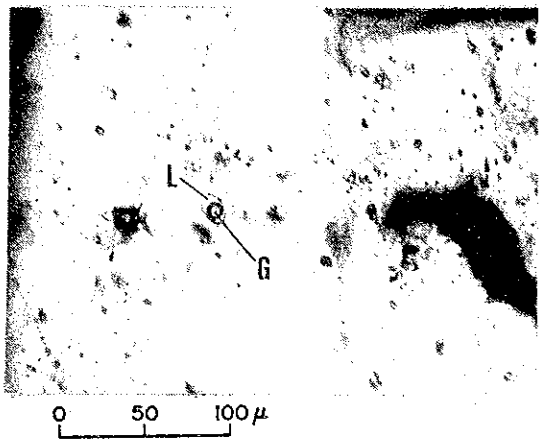

YY-12 Hasan dere

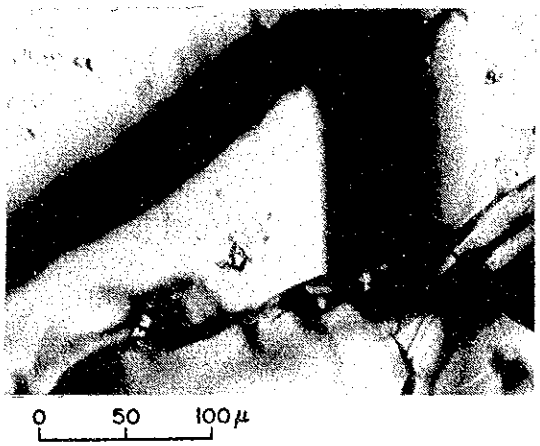

YY-15 Hasan dere

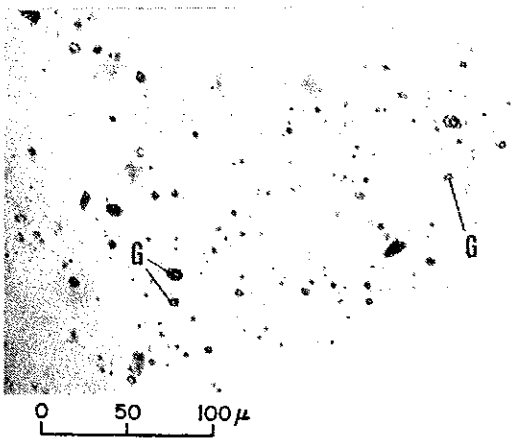

YY-29 Mat dere

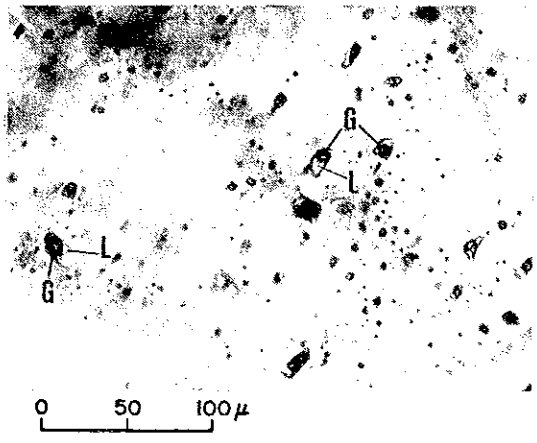

MIT-3 59.0m

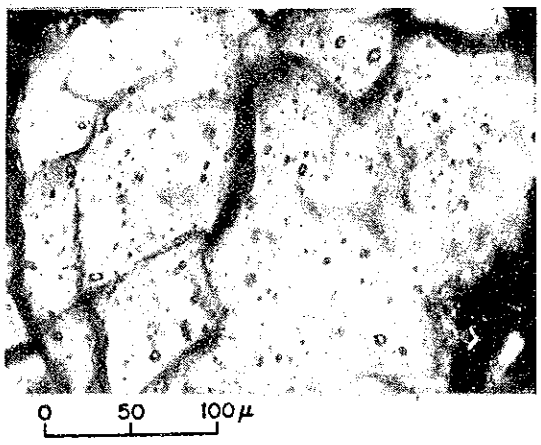

MJT-3 196.0m

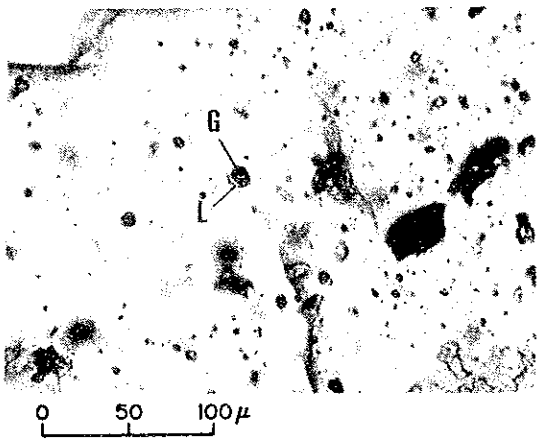

L: Liquid G: Gaseous H: Halite

Photograph Microscopic Photographs of Fluid Inclusions(3)

Quartz Phenocryst in pgl (KY-24)

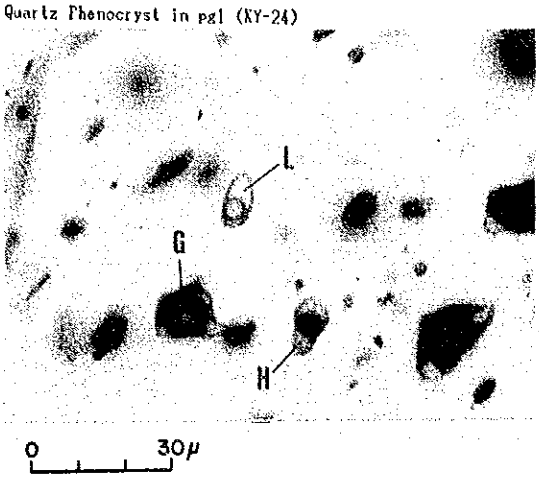

Quartz Phenocryst in pgl (KY-24)

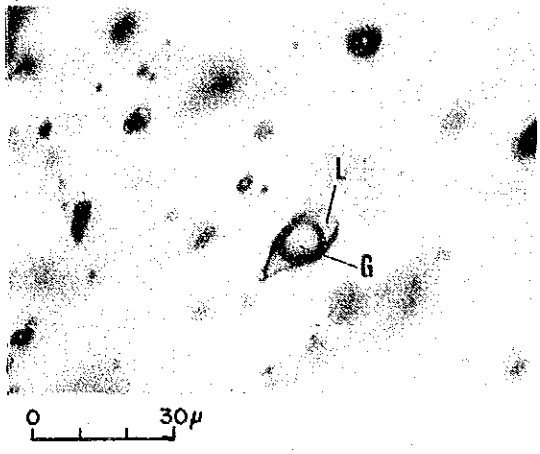

Quartz Phenocryst in pgl (YY-26)

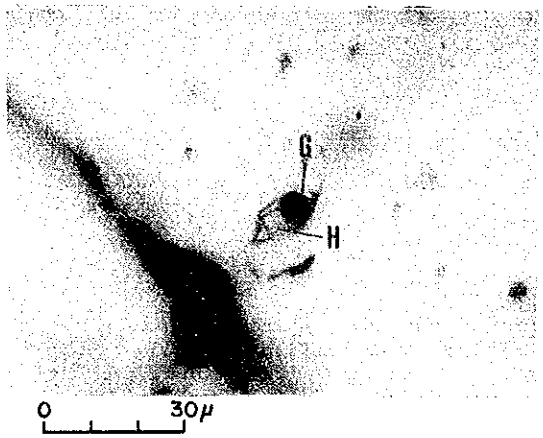

Quartz Vein in Andesite (AE-39)

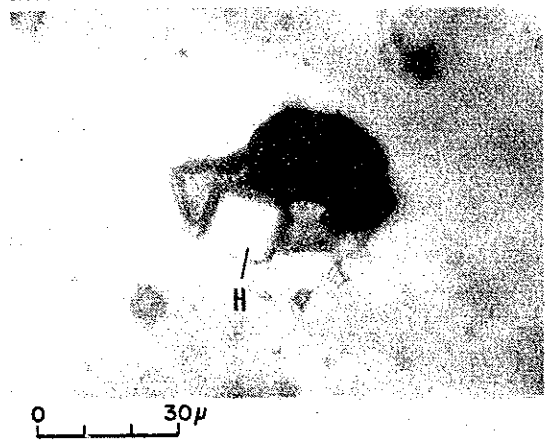

Quartz Vein in Andesite (MJT-2, 129.8m)

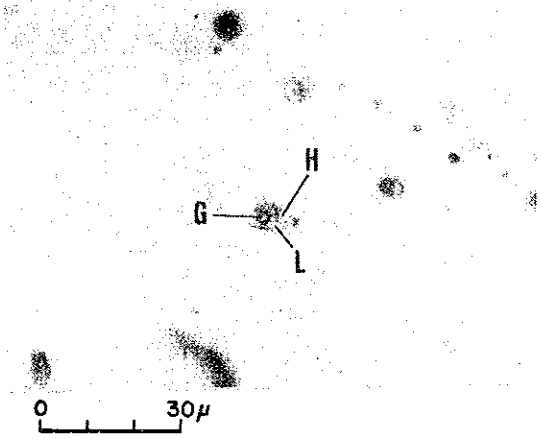

Quartz Vein in pgl (MJT-3, 80.3m)

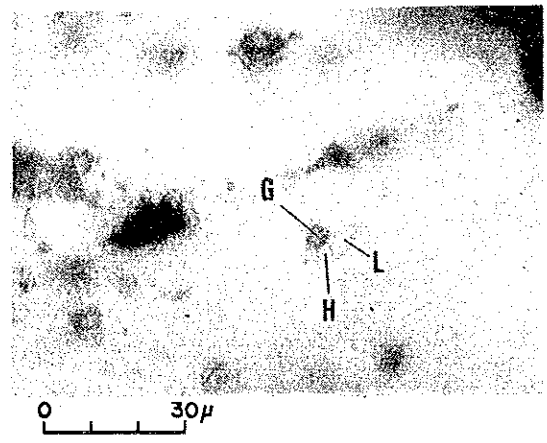

L: Liquid C: Gaseous H: Halite

Photograph Microscopic Photographs of Fluid Inclusions(4)

Table 5 List of Homogenization Temperatures and Gaseous and Liquid Phases Fluid Inclusions

Rock/Core	V/P	Rock Name	Locality of sample	Liquid Inclusion		Gaseous Inclusion	
				No of M.I	Homogenization T.	No of M.I	Homogenization T.
Rock	V	Andesite (Zigana F)	Maden dere	232	369℃	22	465℃
			Hasan dere	58	363	17	457
			North Mat dere	30	403	7	421
		Porphyritic granite (pgl)	Maden dere	67	372	4	422
			Hasan dere	189	387	17	441
			Mat dere	42	401	7	447
	V			618	378	74	450
	P	Porphyritic granite (pgl)	Maden dere	82	352	5	450
			Hasan dere	127	410	33	482
			Mat dere	75	389	12	430
			South Hasan	32	303	-	-
		Pophyritic granite (pg2)	South Hasan	87	339	6	478
P			403	370	58	466	
V+P			1,021	375	132	457	
Core	V	Andesite (Zigana F)	MJT-1	129	391	1	380
			MJT-2	182	389	12	423
		Porphyritic granite (Pgl)	MJT-3	36	416	55	406
	P	Porphyritic granite (Pgl)	MJT-1	15			
			MJT-2	10	364		
			MJT-3	43	412	24	410
		Qz por (Qpl)	MJT-3	44	426	11	416
V+P			459	396	103	410	

Table 6 List of Homogenization Temperatures of Fluid Inclusions

Rock/Core	V/P	Rock Name	Locality of sample	No of Sample	No of Inclusims	Range of Temperature(℃)	Mean value(℃)
Rock	V	Andesite (Zigana F)	Maden dere	15	254	250~550	377
			Hasan dere	4	75	280~560	384
			North Mat dere	2	37	340~460	406
		Porphyritic granite (pgl)	Maden dere	4	71	280~450	375
			Hasan dere	11	206	300~580	391
			Mat dere	3	49	330~560	408
	V			39	692	250~580	386
	P	Porphyritic granite (pgl)	Maden dere	6	87	300~570	358
			Hasan dere	9	160	320~660	427
			Mat dere	6	89	290~620	405
			South Hasan	2	32	260~350	303
		Pophyritic granite (pg2)	South Hasan	5	93	380~540	348
	P			28	461	260~660	382
	V+P			67	1,153	250~660	385
Core	V	Andesite (Zigana F)	MJT-1	7	130	330~470	391
			MJT-2	11	194	320~500	392
		Porphyritic granite (Pgl)	MJT-3	6	91	360~490	410
	P	Porphyritic granite (Pgl)	MJT-1	1	15	290~420	364
			MJT-2	1	10		
			MJT-3	4	67	350~490	411
		Qz por (Qpl)	MJT-3	3	55	350~490	424
	V+P			33	562	290~500	398
Rock &Core V+P				100	1,715	250~660	389

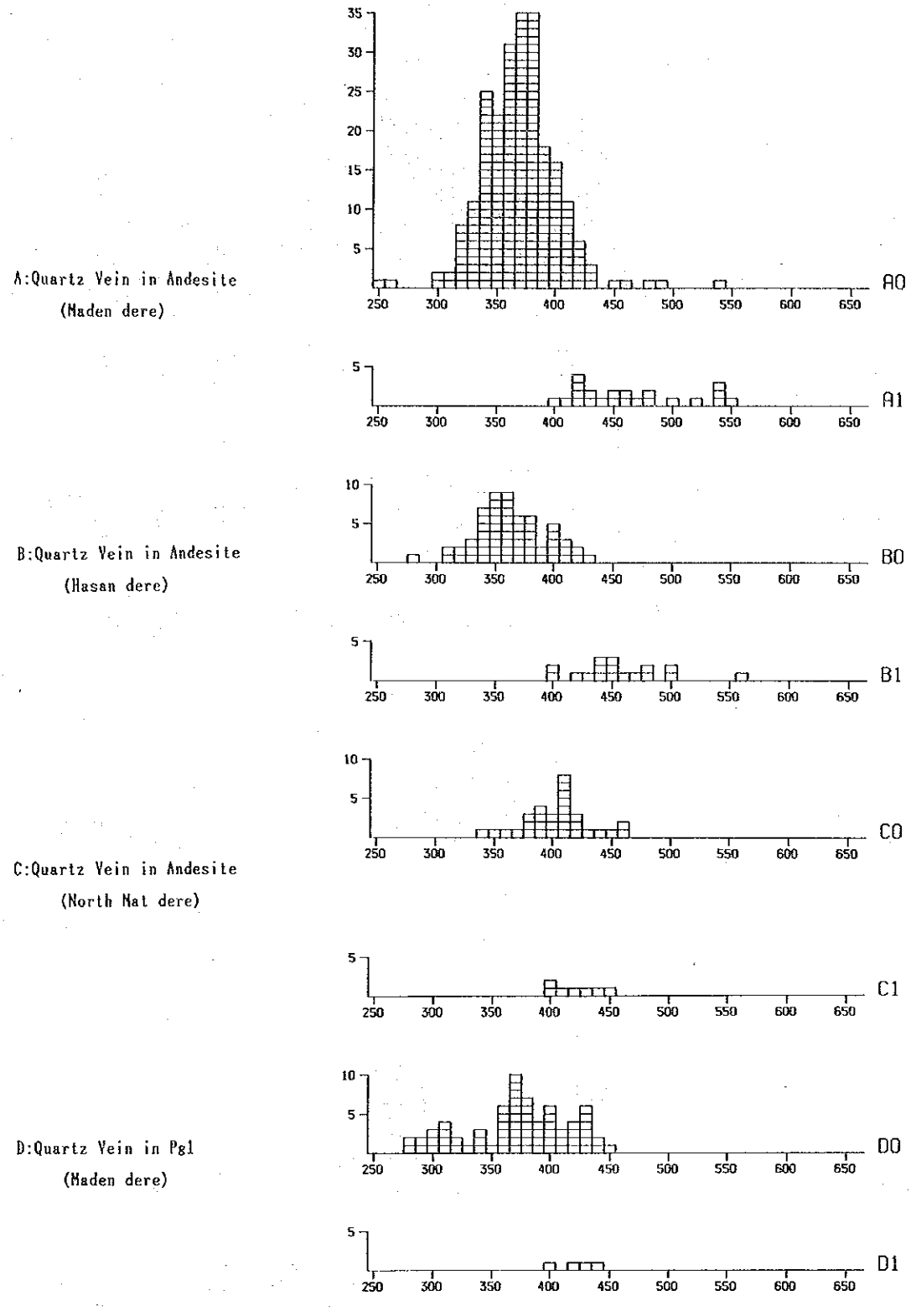

Fig.11 Histogram of Homogenization Temperature (Rock 1)

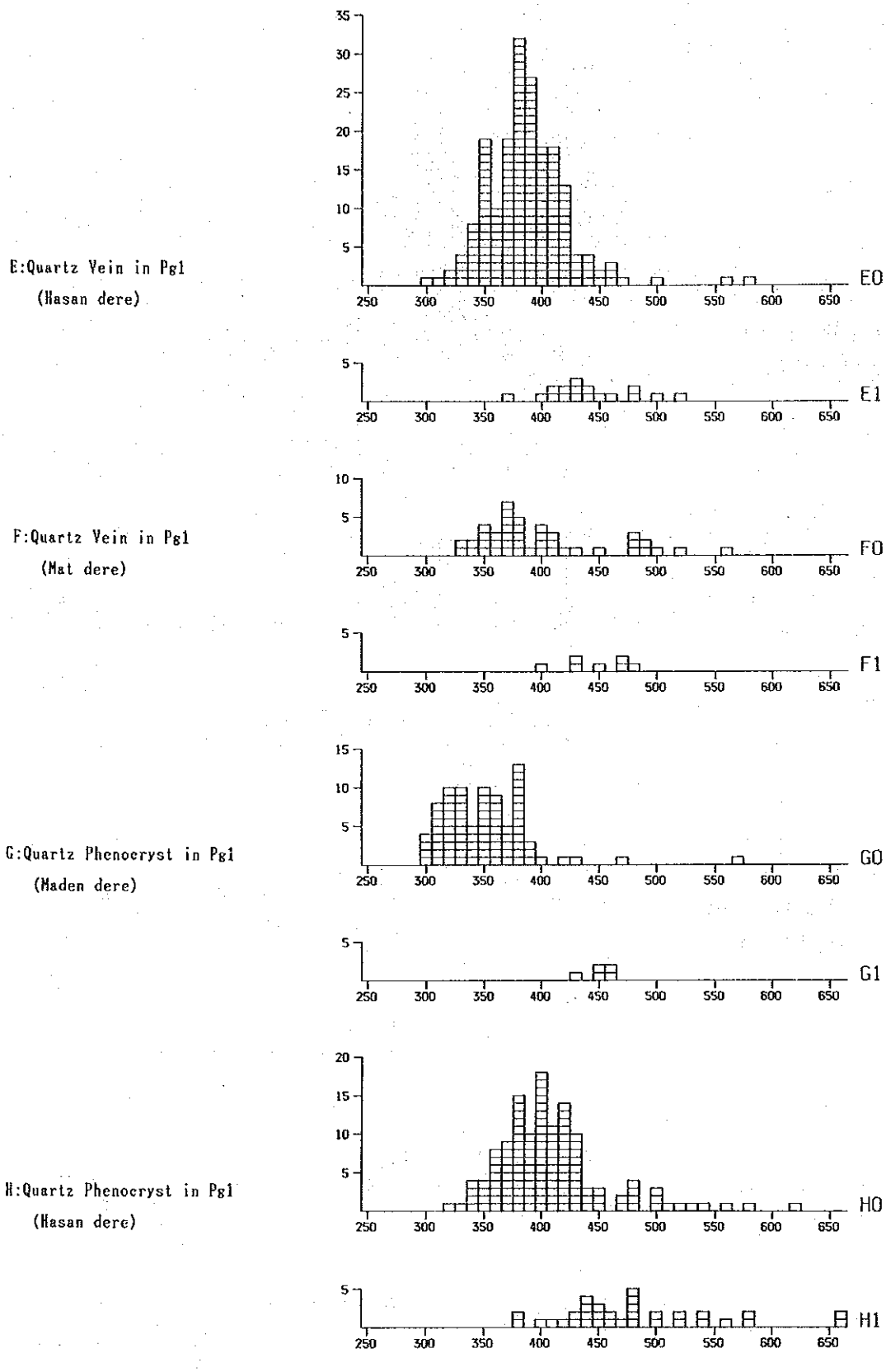

Fig.12 Histogram of Homogenization Temperature (Rock 2)

I:Quartz Phenocryst in Pg1
(Mat dere)

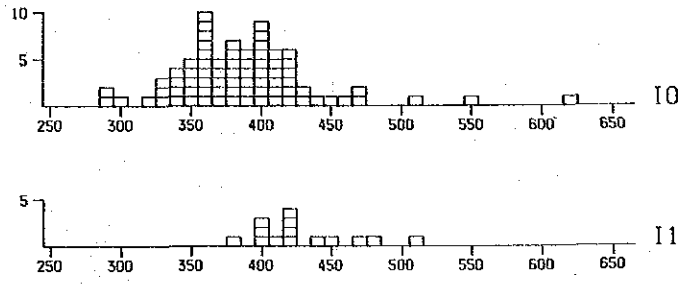

J:Quartz Phenocryst in Pg1
(South Hasan)

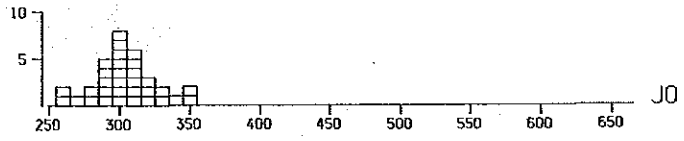

K:Quartz Phenocryst in pg2

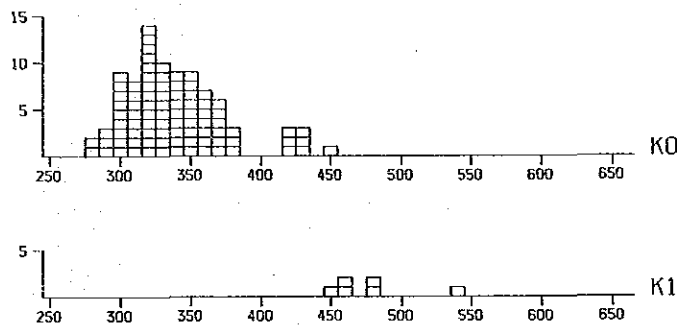

0:Liquid Inclusion(Upper Histogram)
1:Gaseous Inclusion(Lower Histogram)

Fig.13 Histogram of Homogenization Temperature (Rock 3)

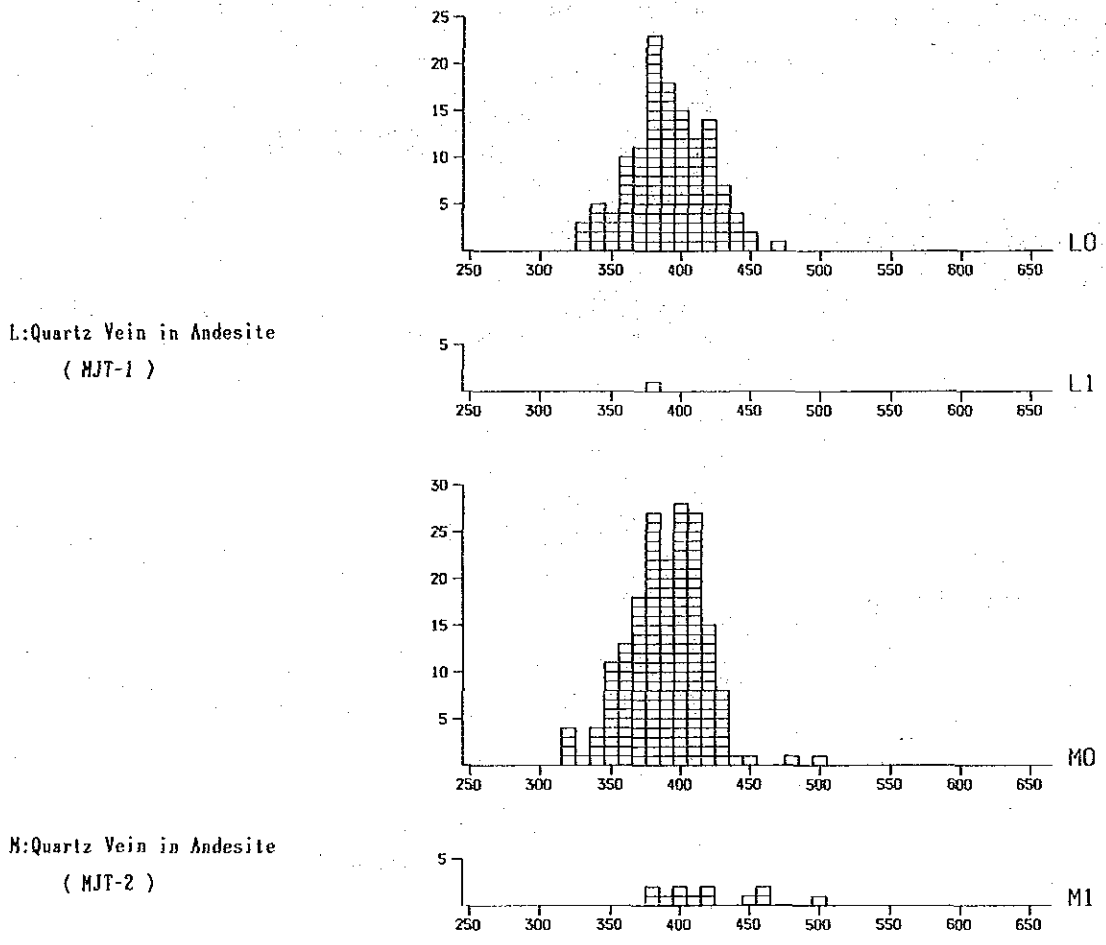

Fig.14 Histogram of Homogenization Temperature (Core 1)

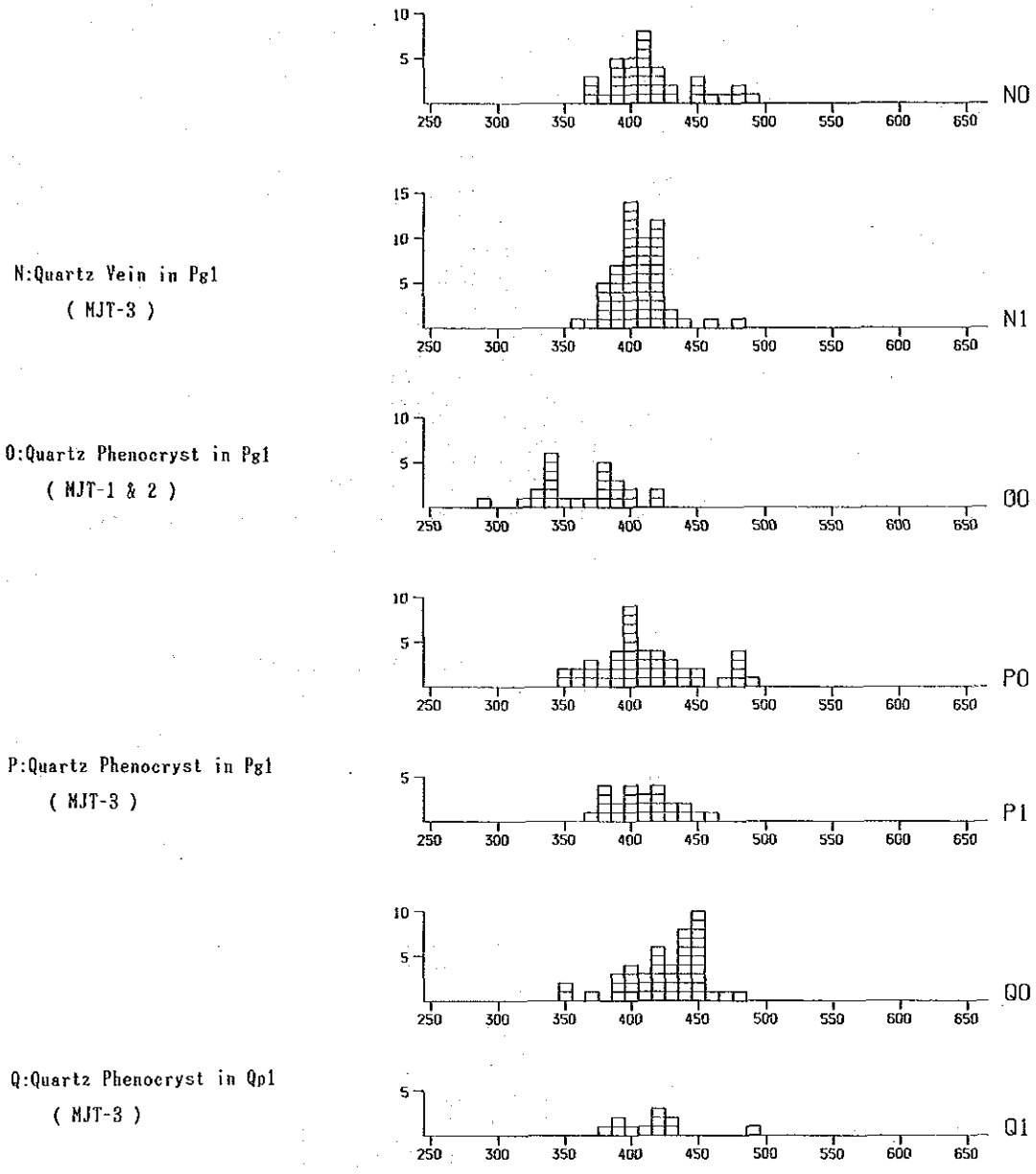

Fig.15 Histogram of Homogenization Temperature (Core 2)

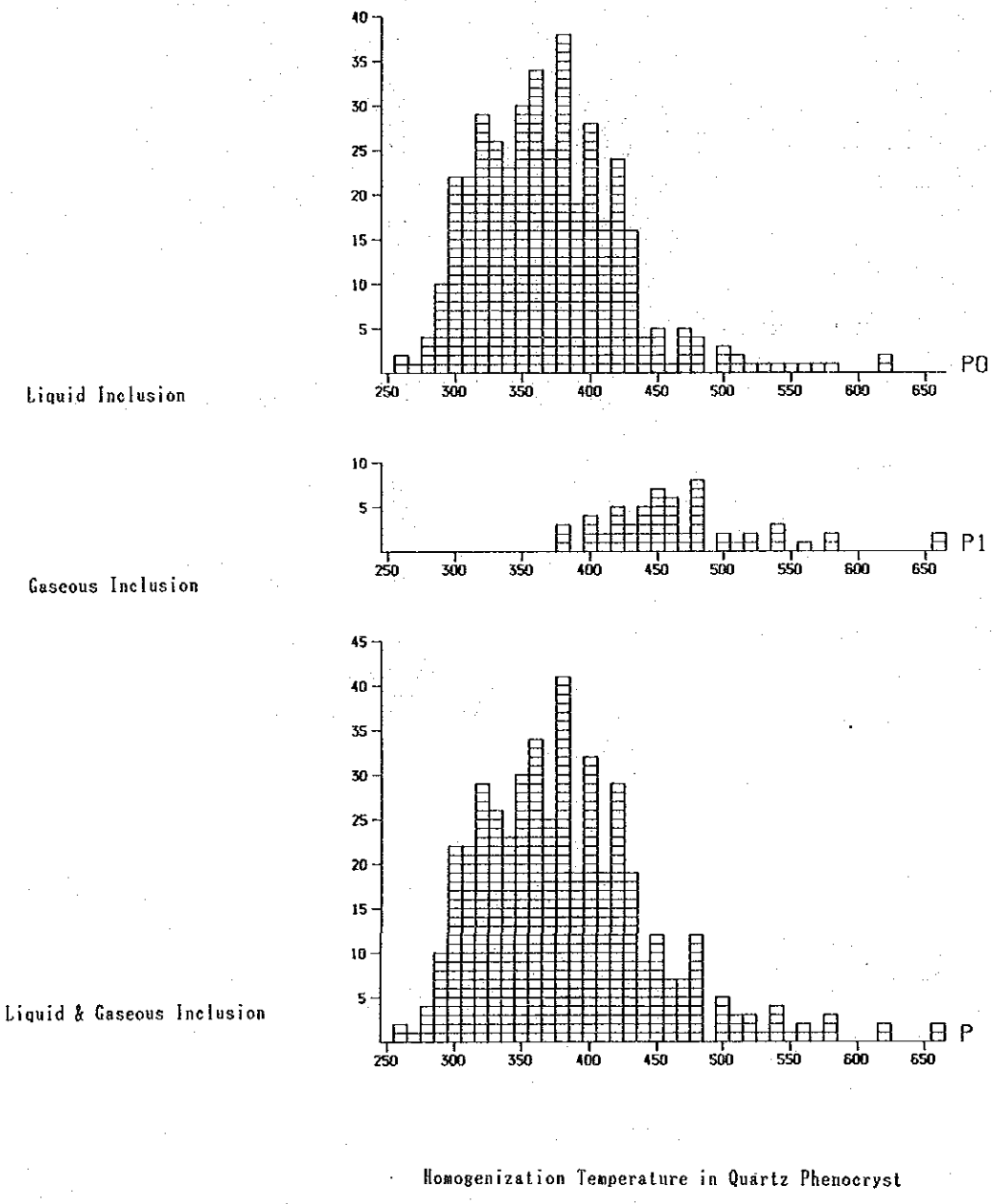

Fig.16 Histogram of Homogenization Temperature (Quartz Phenocryst in Rock)

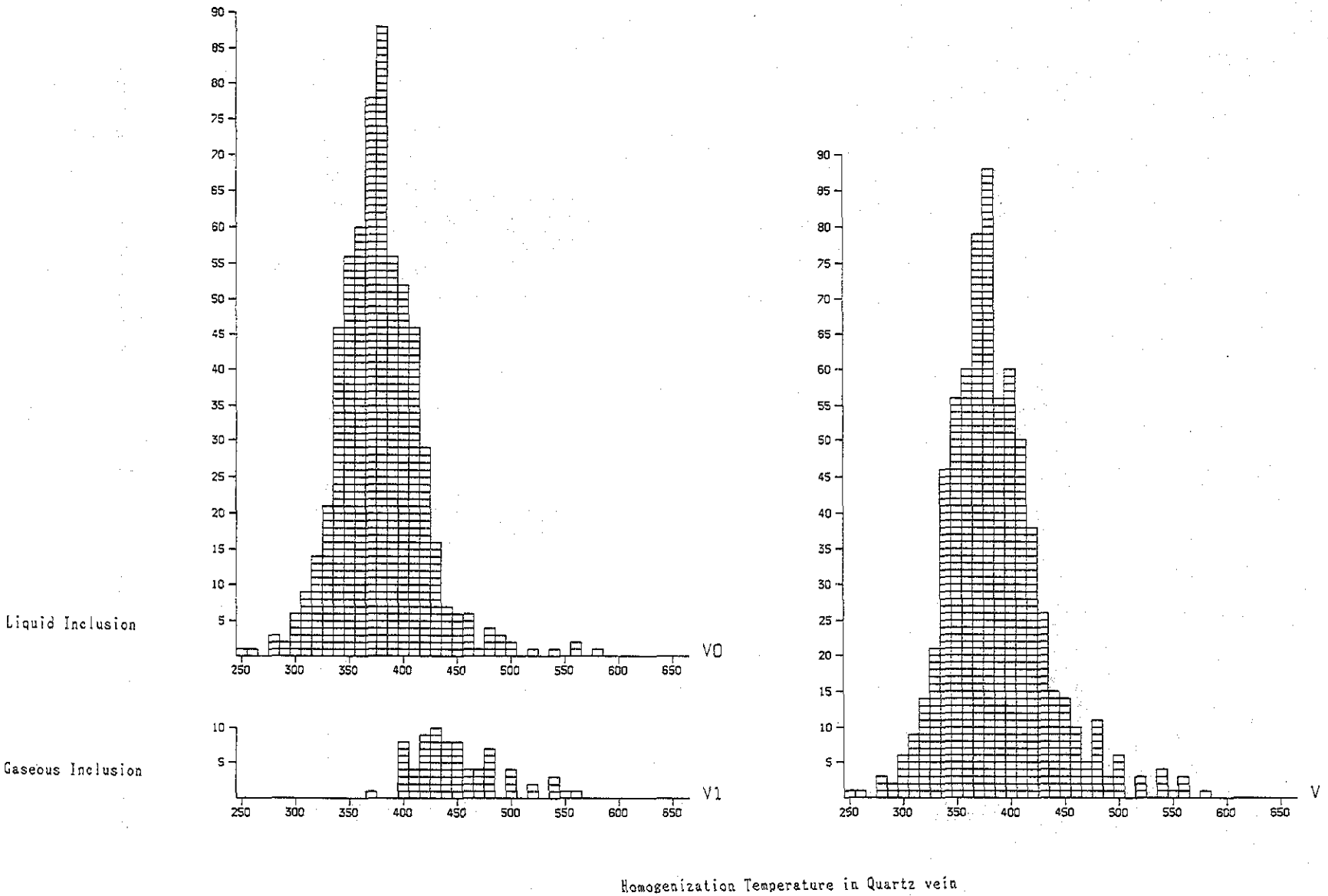

Fig.17 Histogram of Homogenization Temperature (Quartz Vein in Rock)

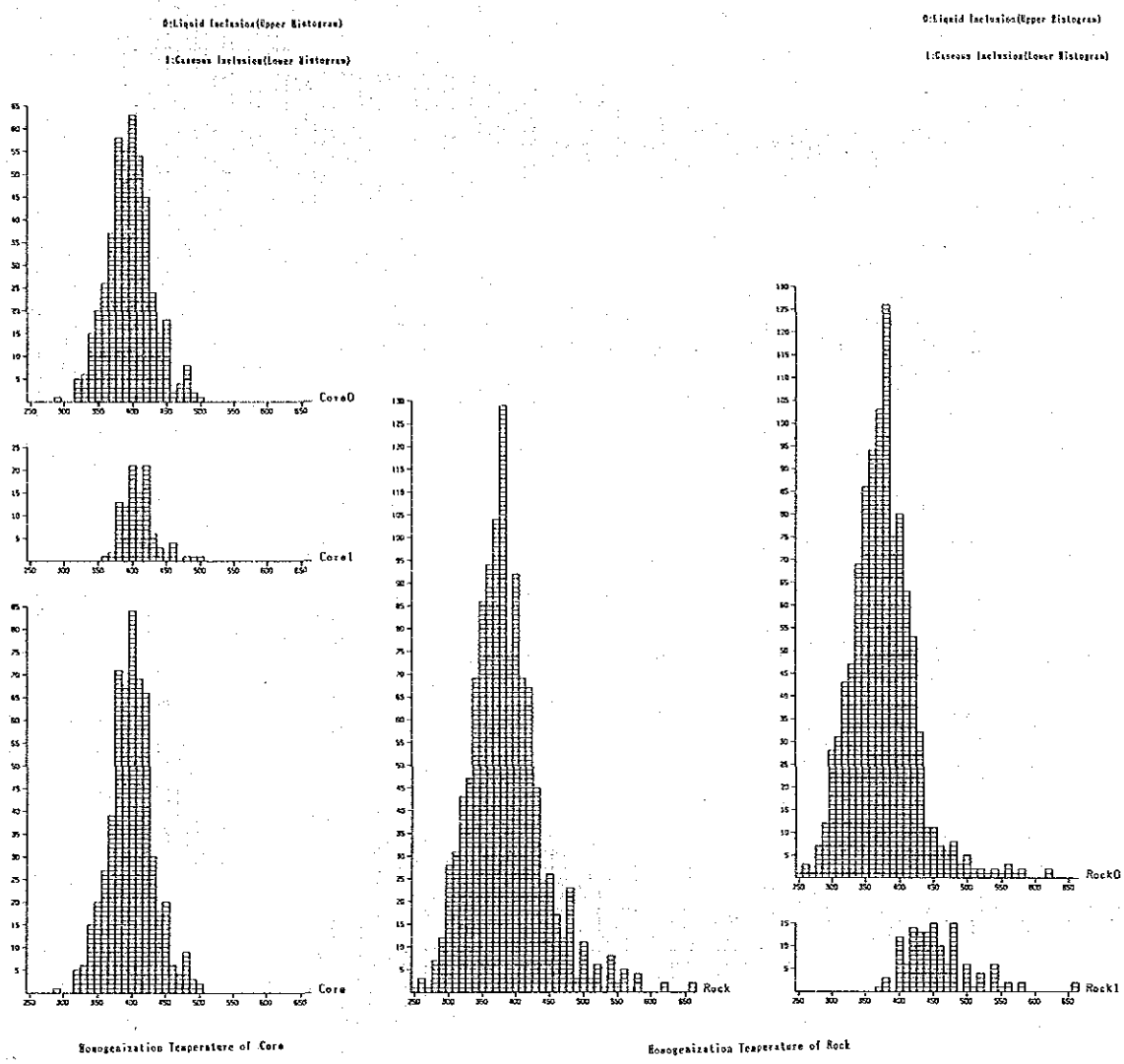

Fig.18 Histogram of Homogenization Temperature (Gaseous Phase in Rock and Core)

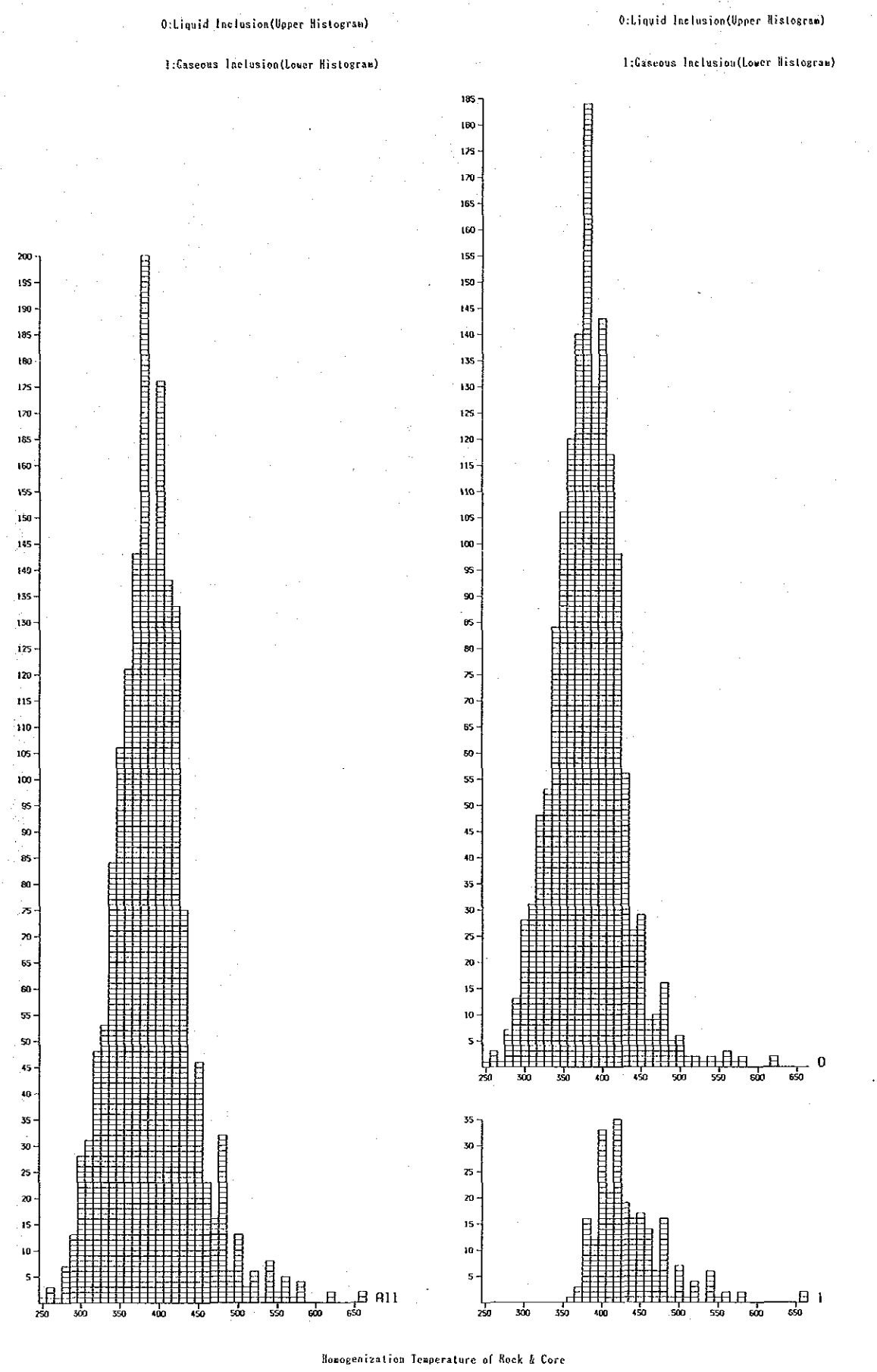

Fig.19 Histogram of Homogenization Temperature (Gaseous Phase in All Samples)

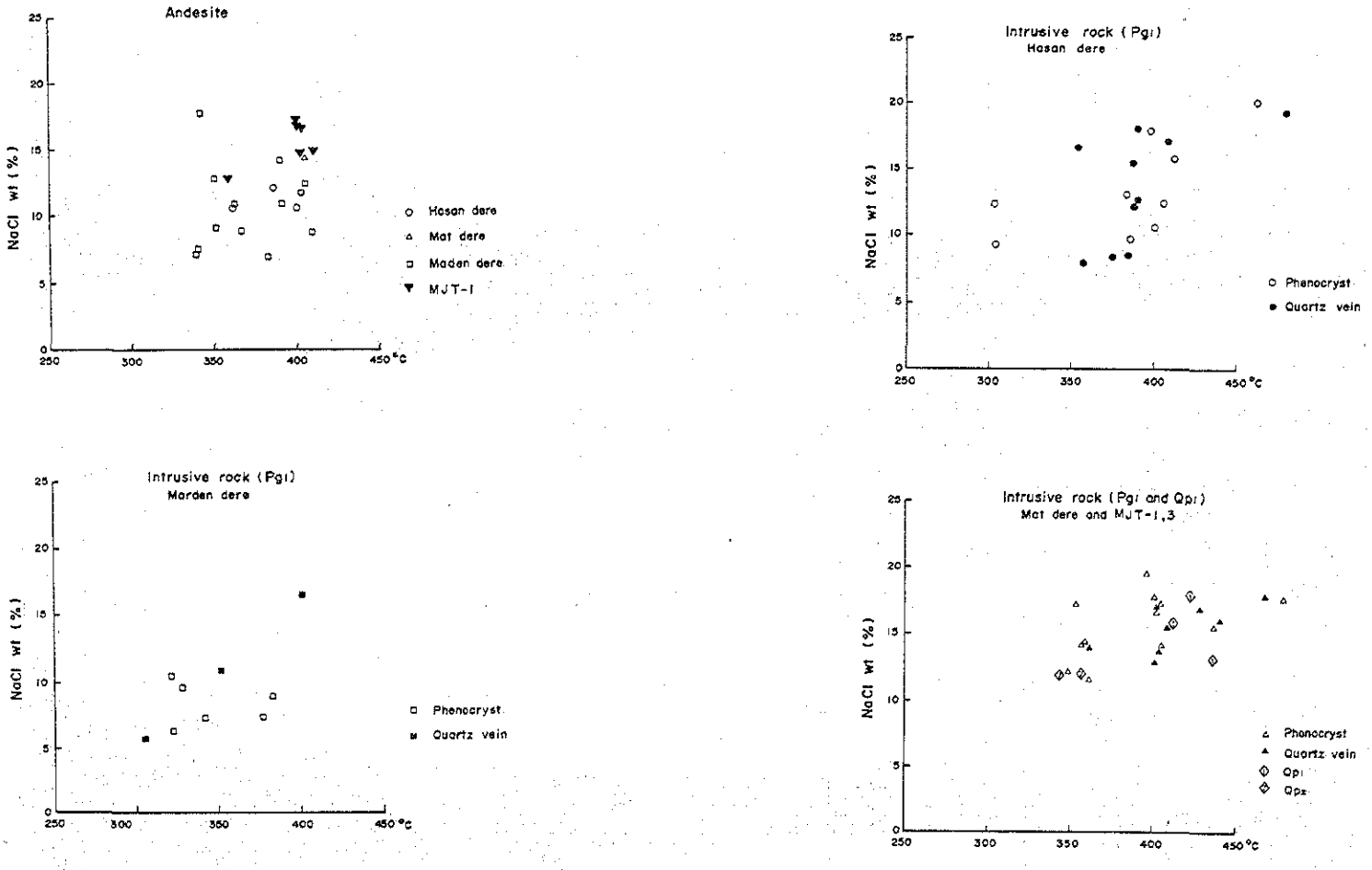

Fig 20 Relationship between Homogenization Temperature and Salinity

1-5 Soil Geochemical Survey

1-5-1 Outline

In 1984, soil geochemical survey was carried out at the Hasandere area over an area covering about 3.63 km^2 from Mat Dere to Hasan Dere by MTA. Geochemical anomalies of Cu and Mo reaching 3,820 ppm Cu and 272 ppm Mo in maximum value were discovered. An anomolous area based on a threshold value of 236 ppm Cu was open to the northern area, and the result pointed out the possibility that the area may extend further to the north of the geochemically surveyed area.

Taking this into consideration, MTA continued the soil geochemical survey in the north area. Soil samples were collected from the B or C soil horizon at 50m intervals along each 50 m contour level following the same specifications as the 1984 survey. These samples were analysed for the two elements, Cu and Mo.

1-5-2 Data Processing

Total assay results for 1331 samples,(942 samples of the 1984 survey combine,d with 389 samples from the 1985 survey) were processed through the computer applying the Lepertier method (1969). The data processing method was introduced in detail in the report by the cooperative mineral exploration of the initial phase.

Statistic parameters obtained through the data processing are shown in the table described below. Histogams cumulative frequency and correlation diagrams are shown in Fig. 13.

Element	N	Mean(M)	M+α	M+2α	Min valu	Max value	γ
Cu	1311	66.3	200	602	4	3,820	0.56
Mo	1331	4.4	18	71	<1	272	

1-5-3 Data Examination

Cu consists of one unit since its cumulative curve is a straight line, shown in Fig. 13. On the contrary, the cumulative distribution curve of Mo has two inflection points, t1 (11 ppm) and t2 (27 ppm). The form of the histogram and the two inflection points in the cumulative distribution curve indicate that Mo consists of an anomalous population (larger than t2), a background population (less than t1) and on overlaping population (between t1 and t2).

As shown in the correlation diagram in Fig 13, the coefficiency of correlation between Cu and Mo (γ) is 0.56, a slight correlation. Investigation of the distribution tendency of high values delineated on the equi-contour value map indicates that anomalous zones of Cu and Mo are discordantly distributed. Cu anomalous zones are located on the outer side of Mo anomalous areas, backing up the weak correlation between both elements.

A high Mo anomalous zone was distinct in the area from Mat Dere to Hasan Dere. An especially anomalous area of higher than ($M+2\sigma$) is found north of MJT-3 drill site located on the north side of Mat Dere. Areas with Cu high anomalies larger than ($M+\sigma$) are indistinctly concentrated, and the distribution is dispersed.

The initial phase survey predicted that the Cu anomalous zone of greater than $M+\sigma$ might extend to the northern area. This survey proved that the Cu anomalous zone of morethan 200 ppm extended to the northern area, in accord with the expectation. Comparative investigation beween geological and geochemical surveys resulted as follows.

There is no geochemically anomalous area of Mo located downstream of Mat Dere and Hasan Dere. This area coincides with the potassic alteration zone identified by geological and alteration surveys, and is regarded as a barren zone, namely core of mineralization of the porphyry copper ore deposit.

A post-mineralization fault on the west side of Maden Dere is inferred by geological survey. Anomalous areas of both elements , Cu and Mo,was not found on the west side of the inferred fault, and the west end of the detected anomalous area extends harmoniously along the inferred fault. This fact consequently reveals the existence of the fault.

Contrary to the fact that the Cu anomalous zone is distributed centering around the stream, the

Mo anomalous area is not influenced by topographic conditions. In the case of the forming of the oxide and leached zone in the ore deposit, copper and sulpher are completely leachable by acidic water produced from sulphide minerals such as pyrite through oxidation, and is easily movable, but on the other hand, contrary gold and molybdenum in general are scarecely moved (Bloom, 1966; Shanon Jr.,1971 ; Asami and Britten, 1980) in general. When molybdenite is oxidized, and molybdic acid (MoO_4^{2+}) is produced, the molybdenum is extremely soluble, but if Fe^{3+} ion (low Eh) exists in acid water or if Ca^{2+} ion exists in neutral water, ferrimolybdenite ($Fe_2O_3MoO_3 \cdot 8H_2O$) and powellite ($CaMoO_4$) are precipitated and fixed as mineral phase (Garrels and Christ, 1965).

It is presumed that such a difference in the secondary dispersion between copper and molybdenum controls the distribution of the Cu and Mo anomalies. It is expected from the characteristic of Mo for difficult dispersion that the geochemical anomaly of Mo will indicate precisely the mineralization condition (such as grade), and the area with a concentration of high Mo anomalies on the north side of Mat Dere is expected to be the most promising area for emplacement of the ore deposit.

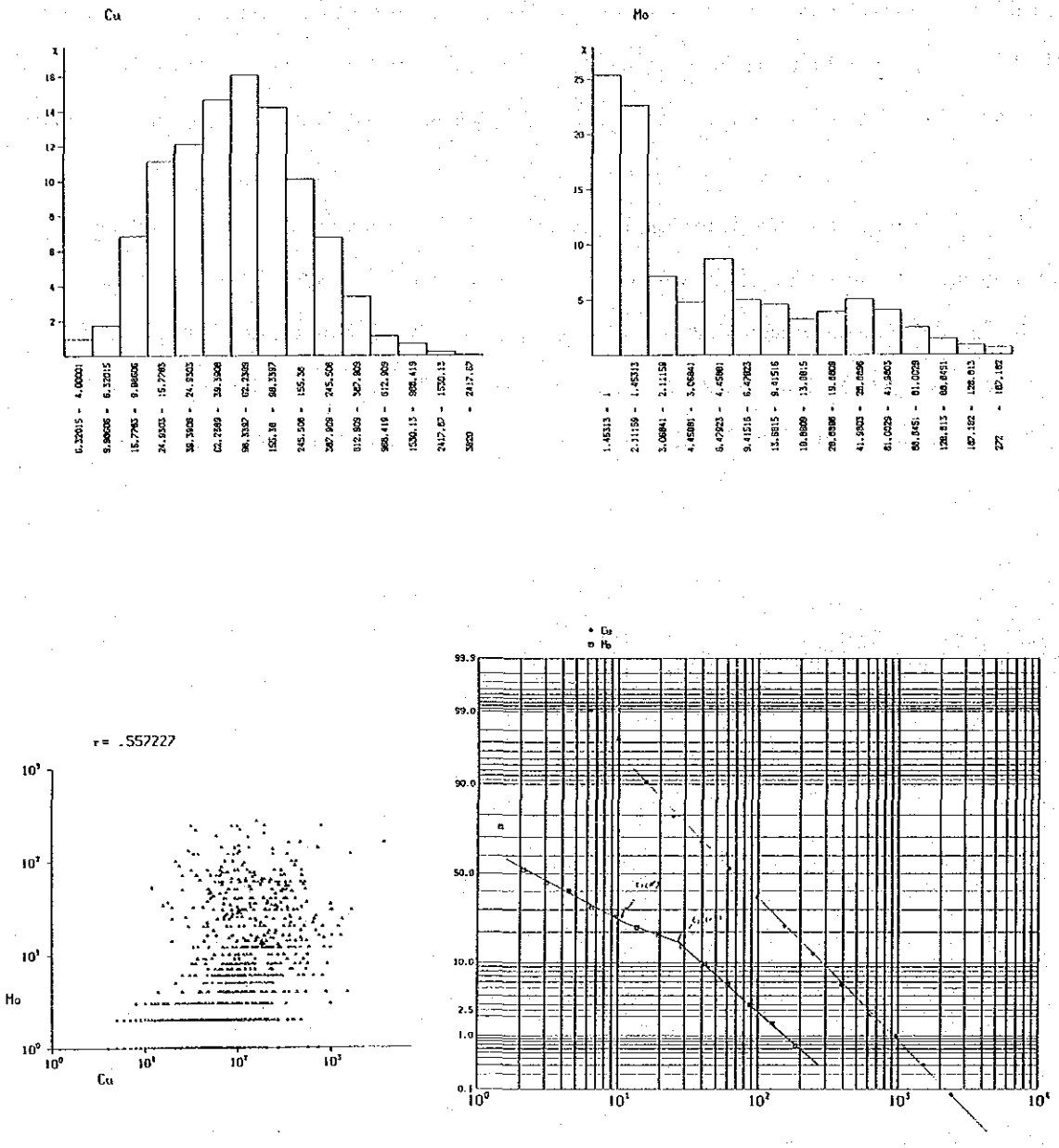

Fig 21 Histogram, Cumulative Frequency Distribution Curve, and Correlation Diagram of Soil Geochemical Survey, Hasandere Area

Cu

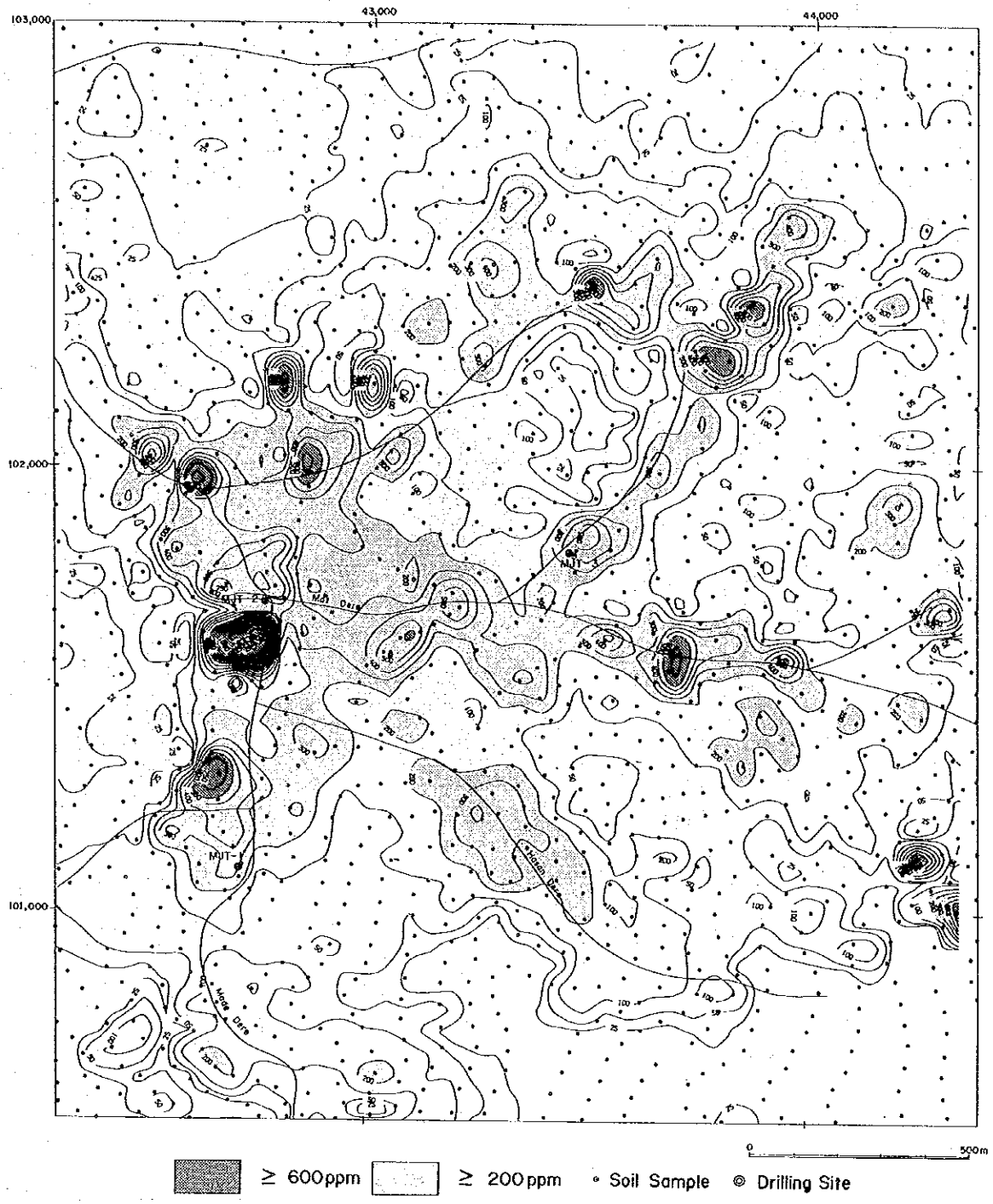

Fig.22 Soil Geochemical Contour Map of Cu Anomaly in Hasandere Area

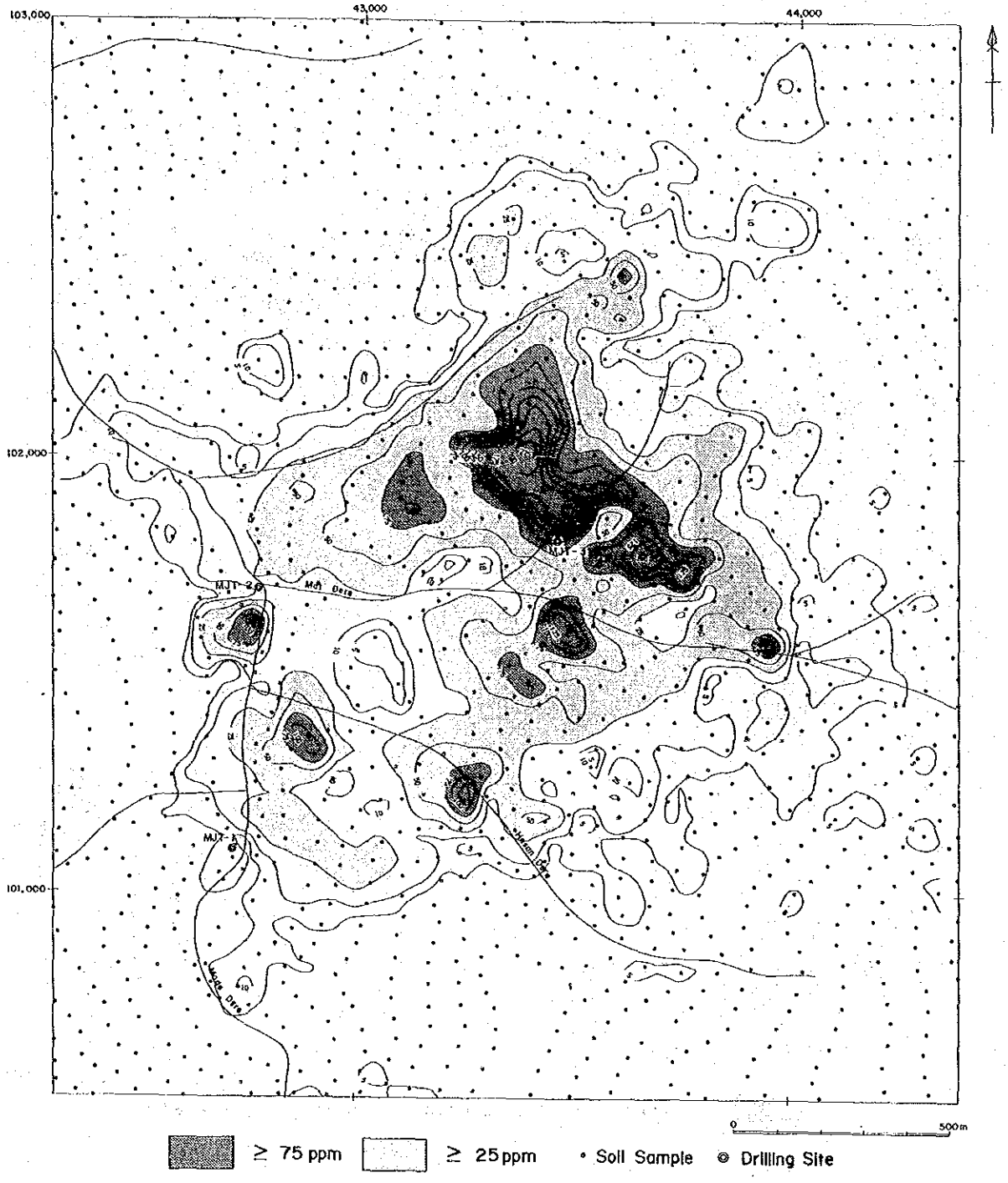

92

Fig.23 Soil Geochemical Contour Map of Mo Anomaly in Hasandere Area

Mo-Py Ore

(AE-34: Maden Dore)

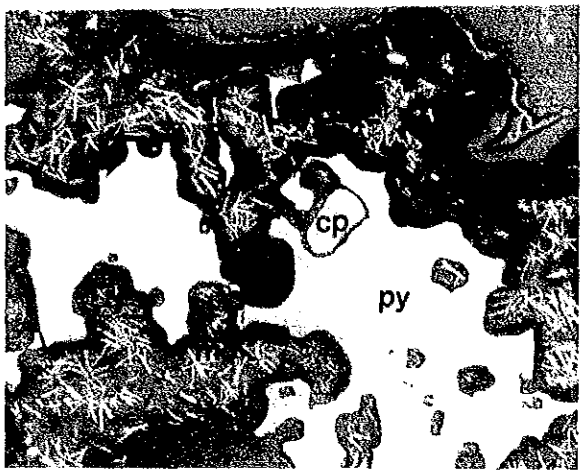

Cc-Cp Ore

(MJT-1: 196.2m)

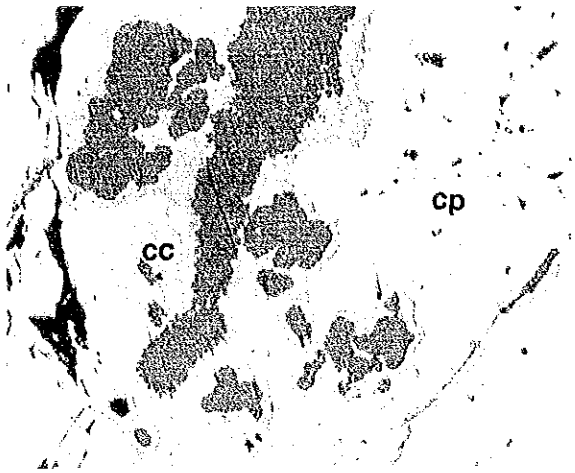

Cp-Sp Ore

(MJT-2: 193.45m)

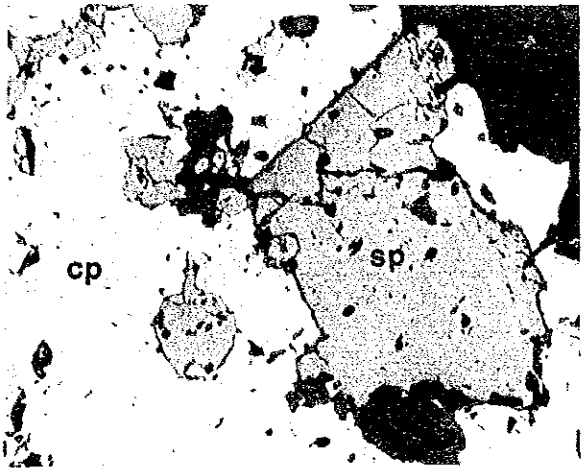

Mag-Cp Ore

(MJT-2: 268.5m)

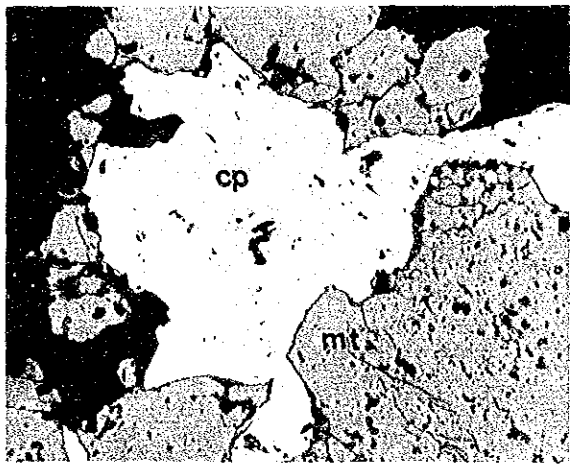

Cc-Cp Ore

(MM-120: Karadag)

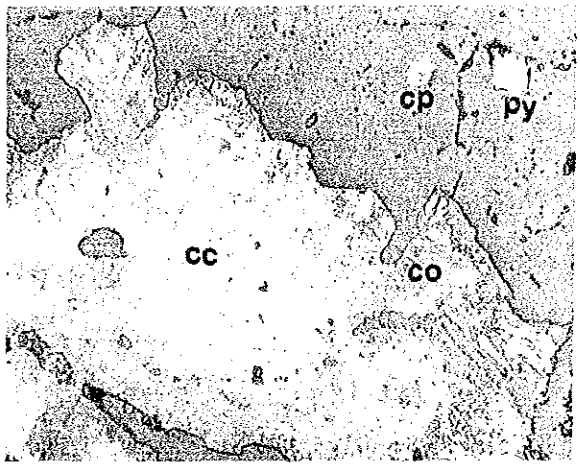

Cp-Co Ore

(YY-132: Karadag)

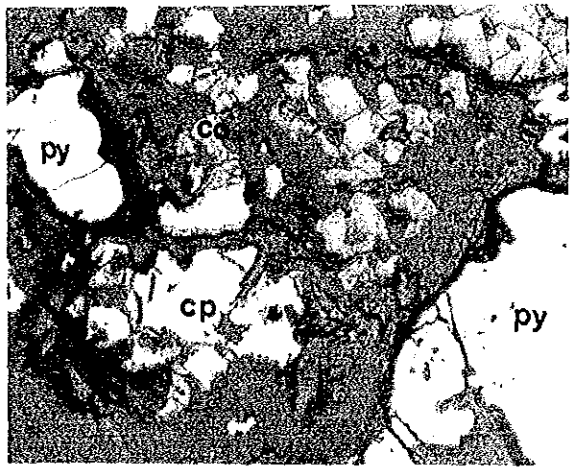

0 0.2mm

Mo: Molybdenite CC: Chalcocite Co: Covolline Cp: Chalcopyrite

Sp: Sphalerite Mag: Magnetite Py: Pyrite

Photograph Microscopic Photographs of Polished Ore Specimens(5)

Quartz-diorite pophyry (pgl)

(AE-10: Hasandere)

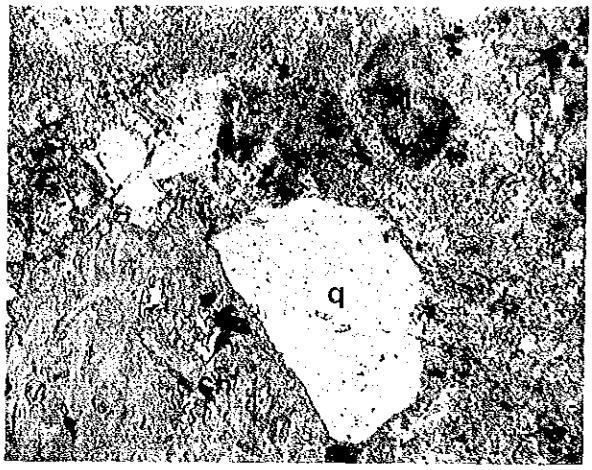

Porphyritic granite (pgl)

(MJT-3: 177.2m)

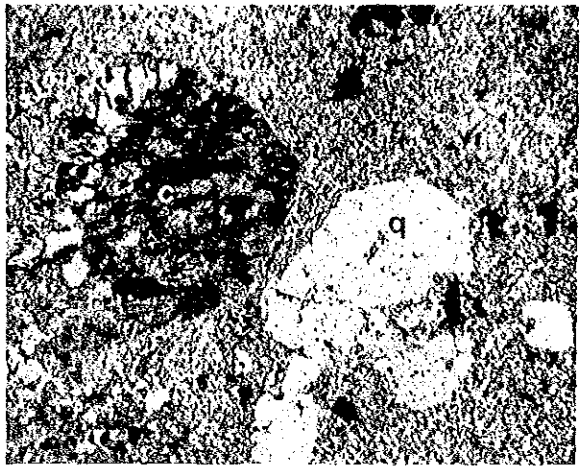

Quartz Porphyly (Qp1)

(MJT-3: 323.3m)

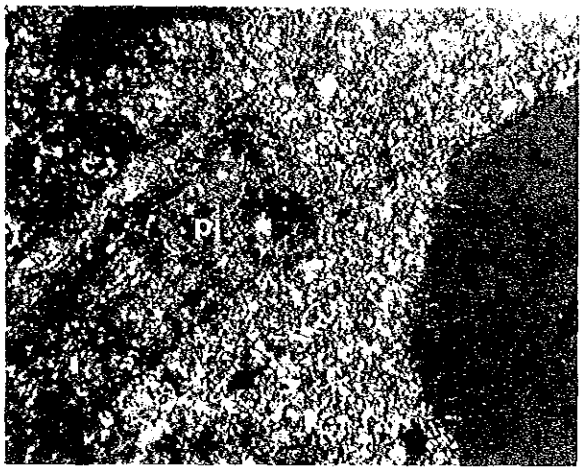

Quartz porphyry (Qp2)

(KM-20: Hasandere)

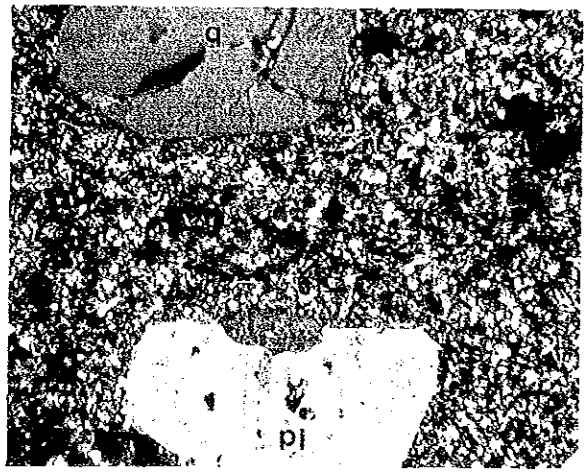

Hornblende Andesite

(EE 101: Karadag)

Quartz-diorite porphyry

(EE-129: Karadag)

0 0.5 mm

q: quartz ho: hornblende pl: plagioclase C: calcite

bi: biotite ep: epiodote

Photograph Microscopic Photographs of Thin Sections (6)

Table 7 list of Microscopic Observations of Thin Sections

Sample No.	Rock Name	Rock unit	Texture	Phenocryst								Groundmass								Alteration
				Q	Kf	Pl	Bi	Ho	Au	Hy	Mf	Op	Q	Pl	Bi	Ho	Au	Hy	Mf	Op	Kf	
AE- 2	Bre Andesite	Kz	Crush., Amy			◎					□	□	◎	○	○				?	□		Ho, Bi →Ch., Qz, C, Ah
AE-10	Tonalite	Pg1	Porp	○	?	◎		□				□										Pl→Ser, Ch, Ep
AE-25	Altered R	Kz	Porp			?					□	□	◎						?	□		Pl→Ser, Ch., Qz,
AE-50	Basalt	Kk	Amy									□	□	◎			□			□		Pl→C, Ch
AE-53	Tonalite	Pg1	Porp	○	?	◎	△															Pl→Ch, Ser, Ep
AE-55	Qz bearing A	(dyke)	Porp	△		○		△	△	?		□	○	○		□				□		P, Ho→Ch, C
AE-56	Grano P	PG 2	Porp	○	?	○					□	□	○	○					□	□		Pl→Ch, Ser, Qz
EE-11	Grano P	Pg1	Porp	○							?		◎							□		Qz, Ser
YY-10	Tonalitic P	Pg1	Porp	○		◎	△	△				□	◎	□	□	?				□		Pl→Ch, Ser, Ep
YY-14	Basalt	(dyke)	Inters			□	□	○	□					◎	□	□	?	?		□		Pl→Ch, C
YY-30	A	Kz	Crush			◎					□	□	□	◎					?	○		Pl→Ch, Ser, Ep, C
HH-26	Grano P	pg1	Porp	◎	?	□	□					□	◎	□	□				□	□		Pl, Bio→Ser, Ch, Qz
HH-37	Grano P	Pg2	Porp	○	?	○		□				□	◎	○		□				□		Pl, Ho →Ch, Ser, Ep, C, Ah
KY-23	Grano P	Pg1	Porp	△		○	△					□	◎	□	□					□		Pl, Bi →Ser
KH-20	Qp	Qp2	Porp	○	?	○					□	□	◎	○					□	□		Pl, Gm →Ch, Ser, Ep., Qz
MJT-1	Qp1	115.8m	Porp	○		?						□	◎	?					?	○		Pl, Gm →Ser, Ch
MJT-1	Grano P (pg1)	139.9m	Porp	?		○					?		◎	?					□	□		Pl, Gm →Ser, Ch, Qz
MJT-2	Grano P (pg1)	49.0m	Porp	○	?	?							◎	?						□		Pl, Gm →Ser
MJT-2	Altered R. (Kz)	299.8m	Porp																			Gm→Ch, Ep, C., Ah, Qz
MJT-3	Grano P(pg1)	177.2m	Porp	△		○	△				□		◎	□					□	□		Pl, Bi →Ser, Ch, Ah
MJT-3	Grano P(pg1)	209.8m	Porp	□	?	□					?	□	◎	□					?	□		Pl, Gm →Ser, Ch, C, Ah
MJT-3	Qp1	323.2m	Porp	○		○	?					□	◎	□						□		Pl, Gm →C, Ah, Qz
MJT-3	Qp1	324.7m	Porp	○		○	□						◎	□	□	?	?	?		□		Pl, Gm →Ser, Ch, C, Ah, Qz
HH106	Pyroxene A	Kz	Crush			◎	□		□			□	○	◎					□	□		Pl→Ep
HH129	Qz dio porphyry	Porp		○		◎	□	□				□	◎	□	□	□				□		Pl→Ch
HH145	Skarn	Kz																				Galena, Sphalerite
KK115	Qp	—	Porp	○		?							◎							□		Gm→Ser, Ep., Qz
KK120	Qp	—	Porp	○		?							◎							□		Gm→Ser , Qz
KK124	Qp	—	Porp	○									○							○		Gm→Ser, Ep., Qz
MH108	Dacitic tuff	Kz	Pyro	Pyroclastic texture						Fragment: Qz, Pl, Bi			Mataix: Qz, Fl, Mf, Op									Pl, Gm →Ch, Ser, Ep, C
MH118	Qp		Porp																			, Ser, Ep
EE101	Hornblende A	Kz	Amy			◎		○				□	□	○		□				○		Pl, Ho →Ch, Ep
EE114	Altered R	Kz	—																			Qz, Ser
EE129	Qz dio porphyry		Porp	○		◎	□	□				□	◎	○	□	□				□	□	Pl, Ho →Ch, Ser
EE130	Micro-diorite			□		◎		□				□										Pl→Ch
YY119	Diorite	—				◎	?	?	○	?		□										Pl→Ch, Ep

Abbreviations of Rock Unit
same as in the geological maps

◎:Abundant
○:Common
□:Few
△:Rare

Grano:Granodioritic

Qp:Quartz porphyry
Altered R:Altered Rock

A:Andesite

Bre:Brecciated
Amy:Amygdaloidal
Porp:Porphyritic
Pyro:Pyroclastic

Pheno:Phenocryst
Gm:Groundmass
Qz:Quartz
Pl:Plagioclase
Kf:Potassium feldspar
Bi:Biotite
Fd:Feldspar
Py:Pyrpxene
Au:Augite
Hy:Hyperthene
Ho:Hornblende
Mf:Mafic mineral
Op:Opaque minerals
Ser:Sericite
Ch:Chlorite
Ep:Epidote
C:Calcite
Ah:Anhydrite

Table 8 List of Microscopic Observations of Ore Polished Specimens

No.	Ore	Cp	Co	Cc	Bo	Ma	Cu	Sp	St	Mo	Mt	He	Po	Py	Su-m	H-Fe	Q	Pl	Bi	Se	Ch	Ep	Ca	Ah
AE- 25	Cu-Mo ore ※※	□								○				○			◎			□	□			
AE- 34	Cu-Mo ore	□								○				○										
AE- 39	Cu-ore			□	○	△									◎									
EE- 6	Cu-ore				□	○		◎							△									
HH- 28	Cu-ore			○											◎									
KY-23	Zn-Mo-Cu ore※	□	△	△				△		□				□			◎	○	□	○				
KM-18	Cu-Fe ore	△									◎	□		○										
MJT-1	Cu-Fe ore(115.8m) ※	□												○			◎			◎	?			
MJT-1	Cu-Fe(196.2m)	○	□	□	?									◎										
MJT-2	Cu-Fe ore(22.3m)	□									◎			◎										
MJT-2	Mo-Cu ore(49.0m) ※	△								△				□			◎	?		○				
MJT-2	Cu-ore(193.45m)	○						□		△				○										
MJT-2	Mo-Cu ore(231.3m)	○								△				○										
MJT-2	Cu-Fe ore (268.5m)	□																○			□			
MJT-2	Cu-Mo ore(299.8m) ※	□								□				□	◎				○	□	□	○		
MJT-3	Cu-ore(12.8m)	◎			□			△						○										
MJT-3	Cu-ore(147.5m)	□												□										
MJT-3	Cu-ore(177.2m) ※	□												□			◎	○	□	□			□	○
MJT-3	Cu-Zn ore (206.9m) ※	△						○						△			◎			□			□	□
MJT-3	Cu ore(248.5m)	□												○										
MJT-3	Mo-Cu ore(323.3m) ※	□								?				□			◎	○	□				○	□
HH-143	Slag (?)		□												△									
HH-149	Cu-ore														□								△	
HH-151	Py-ore																			△				
HH-154	Cu-ore	△	□	□										□										
EE-134	Sb-ore										◎													
MM-119	Slag(?)															△	□					○	□	
MM-120	Cu-ore	△	□	□		◎								△										
MM-126	Cu-ore	○												◎										
YY-132	Cu-ore	□	□											◎										

Cp :Chalcopyrite Co :Covelline Cc :Chalcocite Bo :Bornite
Ma :Malachite Cu :Copper Sp :Sphalerite St :Stibnite
Mo :Molybdenite He :Hematite Po :Pyrrhotite Py :Pyrite
Su-m :Sulphide mineral
H-Fe :Hydroxide iron
Mt :Magnetite Qz :Quartz Pl :Plagioclase Bi :Biotite
Se :Sericite Ch :Chlorite Ep :Epidote Ca :Calcite
Ah :Anhydrite

※ :Polished-thin section
※※ :Polished section and thin section

1-6 Geophysical Survey (SIP Method)

1-6-1 Outline

(1) Purpose of the Survey

The survey refers to an area where a mineralized zone of porphyry copper type has been found through geological and geochemical surveys in the initial phase. In the second phase, semi-detailed geological, geophysical and drilling surveys were successively carried out aiming at exploration of the mineralized zone. A geophysical method of spectral induced polarization (SIP) was used to unravel emplacement condition and continuity of the mineralized zone. Geophysical responses were passed through drill holes and combined with results of the drilling.

(2) Area of the Survey

The area of SIP survey is situated around the confluence of Maden Stream and Hasan Stream, some 4 km southeast of Hamsiköy village. Two survey lines were laid down, namely Line A connecting holes MJT-1 and MJT-2, and Line B connecting holes MJT-2 and MJT-3. All holes were drilled in the second phase survey. The area and arrangement of survey lines are illustrated in Figs. 2 and 24.

(3) Survey Specifications

Field work specifications were set as follows :

a. Electrode Configuration	dipole-dipole array
b. Electrode Separation	100 m
c. Electrode Separation coefficient	n = 1 ~ 5
d. Measurement Method	Frequency domain
e. Frequencies	0.125 ~ 88 Hz(18 frequencies)

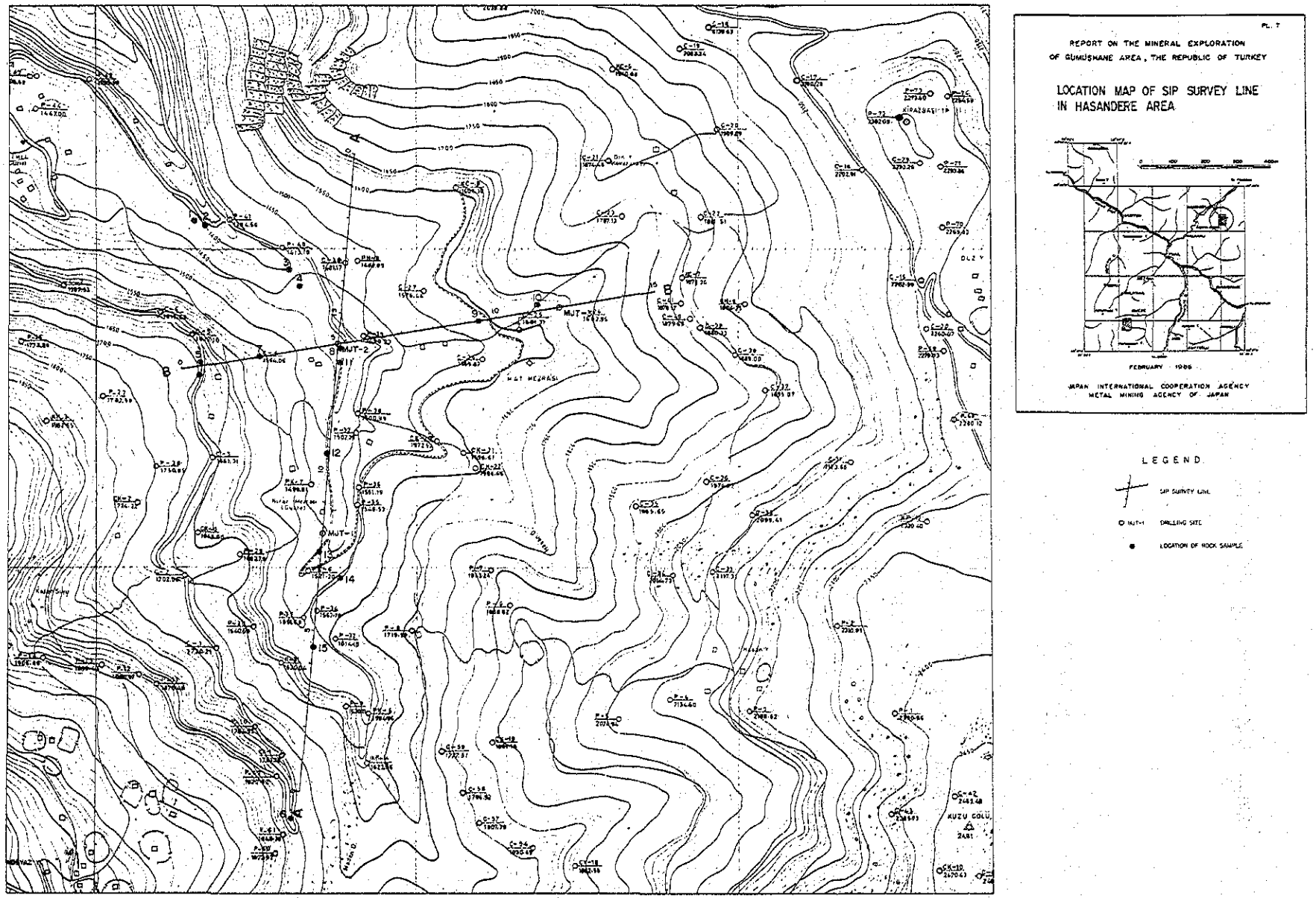

Fig.24 Location Map of SIP Survey Line in the Hasandere Area

f. Length of Survey Line		3.5 km in two lines
Line A	2.0 km	80 stations
Line B	1.5 km	55 stations

(4) Survey Method

The SIP method is the abbreviated name of spectral induced polarization and operates on the same principal as the conventional IP method. SIP method measures apparent resistivity and phase difference over a frequency range from 0.01 Hz to 100 Hz, while conventional IP method measures a difference in apparent resistivity expressed in percentage of two frequencies. The measurement data are expressed in spectral diagrams of phase and magnitude, and in Cole-Cole diagram. Analyses of these responses gives discrimination of minerals or types of mineralization and eliminates electromagnetic coupling which occurs at low resistivity in the ground, at wide electrode separations, and with a large number of electrode coefficients.

In this survey, the Harmonic System of Zonge(USA) was applied. The IP responses over a range of 0.125 Hz to 88 Hz are measured through calculation and extraction of high frequency, using the Fast Fourier Transform of 3rd, 5th, 7th, 9th and 11th harmonics from three basic frequencies of 0.125 Hz, 1.0 Hz and 8.0 Hz.

Observation of a wave form is necessary for measurement of phase , and a communication cable which connects transmiter with receiver was laid down parallel with the survey line separated by 25 m to 30 m The layout of these lines is shown in Fig.25a. At the receiving station, response is amplified through three porous pot-electrodes in copper saturated solution with a copper rod(Fig. 25 b). Amplified sesponses are transmitted through communication cable to the receiver(GDP-12/2GB). Data is processed and printed out.

(5) Measuring Equipment

The equipment used in this survey are listed in Table 9. An illustrated diagram of the equipment is shown in Fig. 26.

Table 9 Measuring Equipment for SIP and IP Survey

Item	Specification		Quantity
Zonge GGT-5 Transmitter	Output Voltage	: 250, 500, 750, 1,000 V	1
	Output Ampere	: 1.2 - 20 A	
	Wave Form	: Square wave	
	Frequency	: 1/8 - 2,048 Hz	
	Weight	: 61 Kg	
Zonge XMT-12 Transmitter controller	Frequency	: 1/8 - 2,048 Hz	2
	Weight	: 58 Kg	
	Power Supply	: 12 V Battery	
Zonge ZMR-5 Engine generator	Output Power	: 5 Kw	1
	Output Voltage	: 115 V	
	Frequency	: 400 Hz	
Honda G-400 Engine		: 10 hp 4 cycles	
Zonge GDP-12/2GB Receiver	Input	: 2-Channel	2
	Frequency	: 1/8 - 2,048 Hz	
	Senstivity	: 0.2 μV	
	Weight	: 15 Kg	
	Power Supply	: 12 V Battery	
Zonge CAP-12 Mini Cassette Recorder	Weight	: 6.2 Kg	2
	Power Supply	: 12 V Battery	
Tektronic 212 Oscilloscope			1
Zonge ISO/1 Isolation Amp.	Weight	: 1 Kg	3
Zonge FP-1 Feild Preamp.	Gain	: 1, 10	3
Electrode	Current Electrode	: Stainless steel	200 rods
	Potencial Electrode	: Cu-$CuSO_4$ non-polarizable Porous Pots	10 pcs.
Cable	Current	:	10 Km
	Communication	: 640 m length	3 rolls

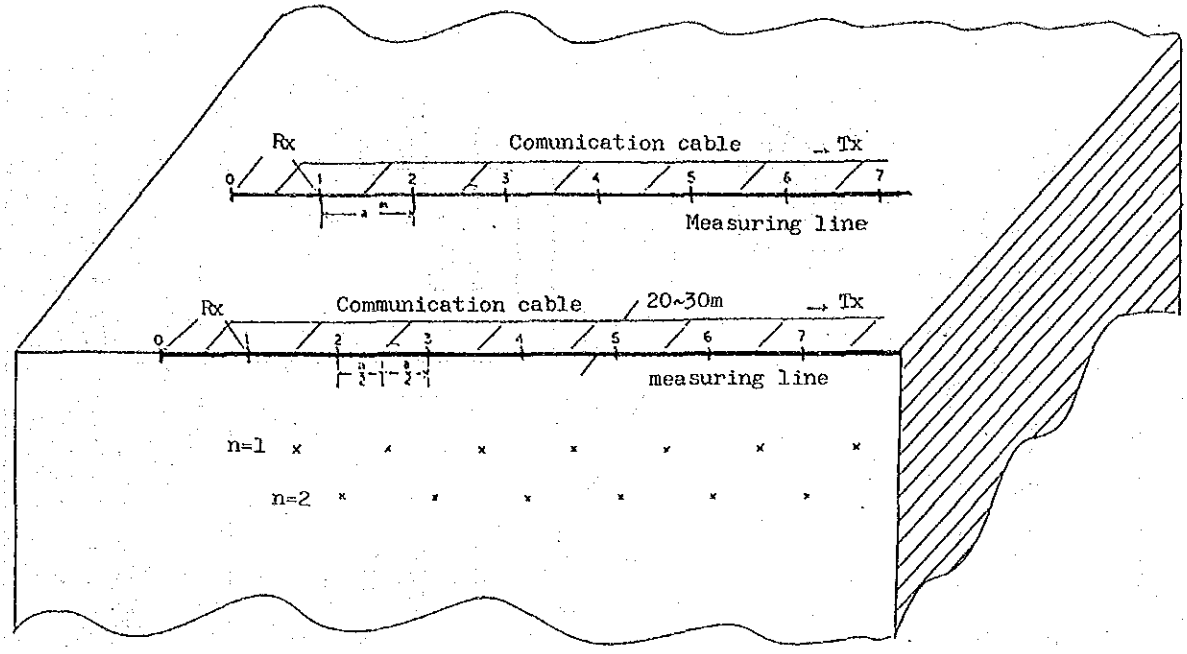

(a) SIP measuring line

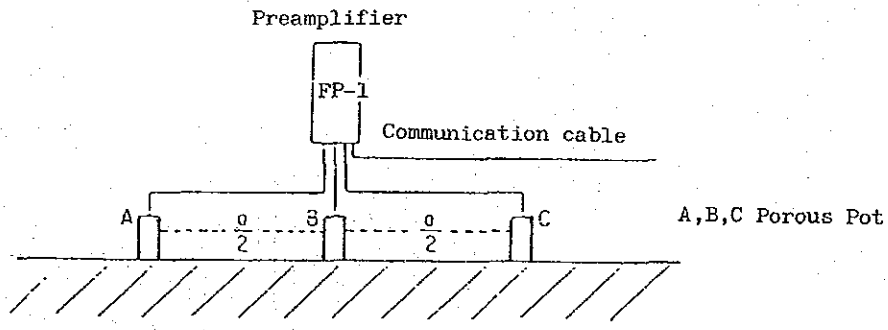

(b) Receiver station

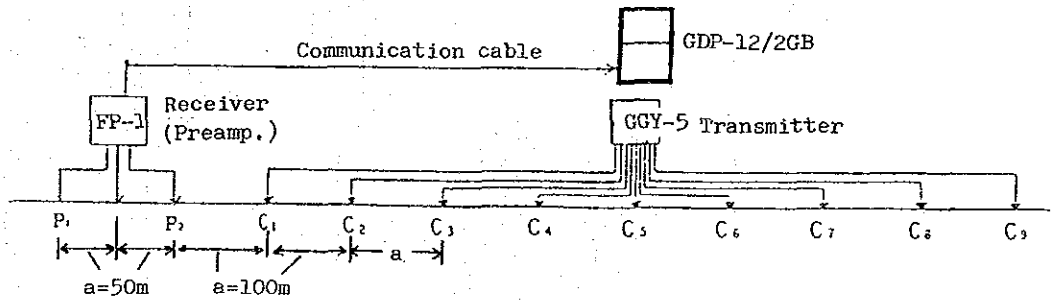

(c) Extention of electrode

Fig.25 Field Work for SIP Measurement

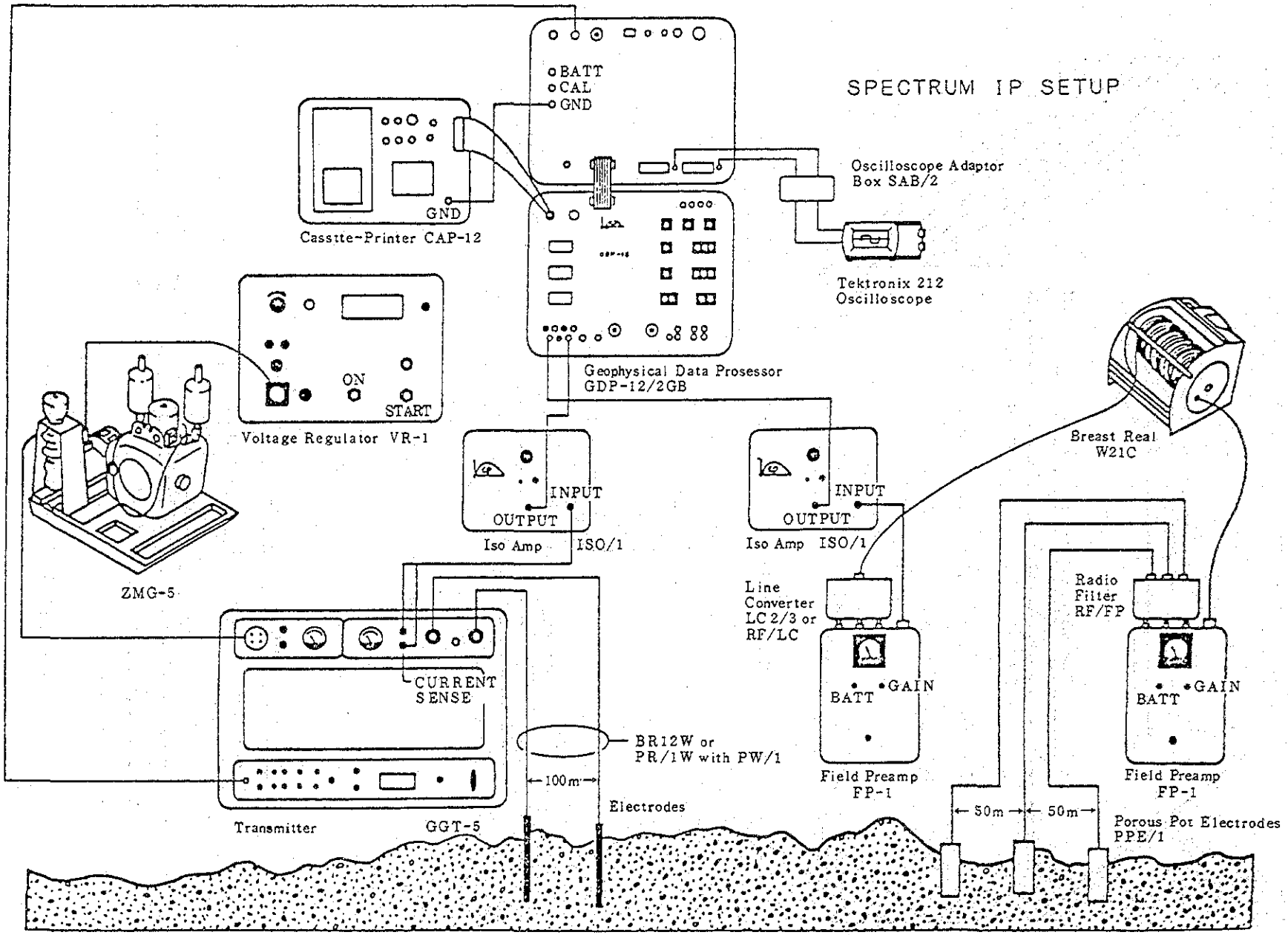

Fig.26 Illustrated Diagram for SIP Equipments

1-6-2 Data Processing and Rock Sample Measurement

(1) SIP Data Processing

Data obtained in a field consist of real and imaginary parts of complex resistivity response at each frequency, and apparent resistivity, phase and magnitude of received basic frequency and so on. The following figures are made from these data :

① Cole-Cole Diagram

② Magnitude Spectrum

③ Phase Spectrum

④ Raw Phase at five freqencies

⑤ PFE Pseudo-section

⑥ Apparent Resistivity Pseudo-section

Data processing and method of analysis are given as follows :

A) Cole-Cole Diagram

In a Cole-Cole diagram, print-out data for each frequency are plotted on a coordinate by setting the negative imaginary part on the vertical axis and the positive real part on the horizontal axis. An example is shown in Fig.27. θi and Mi on the figure are respectively called phase angle and magnitude. The Cole-Cole diagram is known to display a special spectrum depending on the kind of mineral or rock.

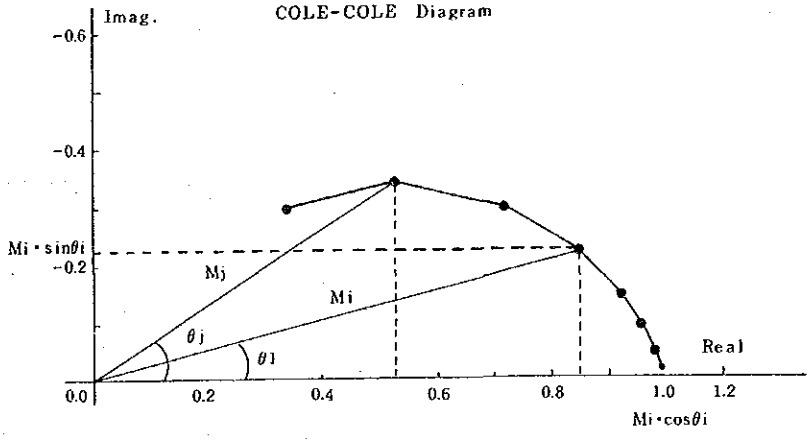

Fig.27 Cole-Cole Diagram

According to Zonge et al, there are three types of spectra as illustrated in the right figure. Type A showing a pattern of ascent to the right indicates existence of sulphide minerals, graphite or strong alteration. The flat line pattern of Type B indicates moderate alteration, and the Type C pattern of descent to the right indicates weak alteration, alluvium sediment, fresh igneousrock or limestone. Discrimination of Cole-Cole diagrams of this survey was based on this classification of the three types.

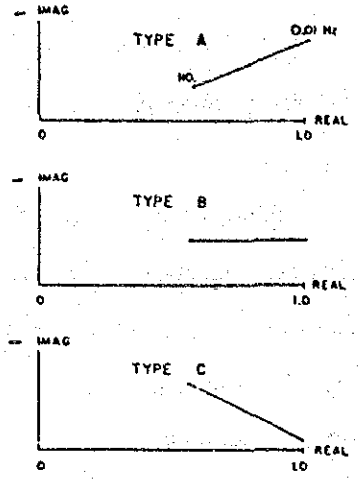

B) Magnitude Spectrum

The magnitude refers to Mi and Mj of Fig. 27, and is easily obtained from positive real and negative imaginary components of field data. The values are normalized by dividing by Magnitude M_0 of minimum frequency (0.125 Hz). A magnitude spectrum figure is plotted by setting the magnitude value on the vertical axis and frequency on the horizontal axis. (Fig. 28)

In the figure, a flat line indicates fresh rock without mineralization or alteration, whereas the spectrum line descending to high frequency indicatesstrong alteration, sulphide minerals and graphite.

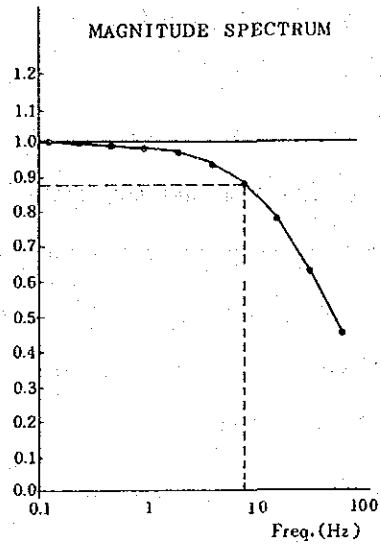

Fig.28 Magnitude Spectrum

C) Phase Spectrum

In a phase spectrum, the vertical axis is phase angle θ of Fig. 27, and the horizontal axis is frequency. (Fig. 29 a). Data obtained in the field survey are a combination of original IP responses (solid line A in Fig. 29 b) and pseudo-IP responses (dotted line B in Fig. 29 b) derived from electromagnetic coupling. Line C (-x---x-) in Fig. 29 b shows the combined IP responses. Phase spectrum indicated in Fig. 29 a was obtained through measurement.

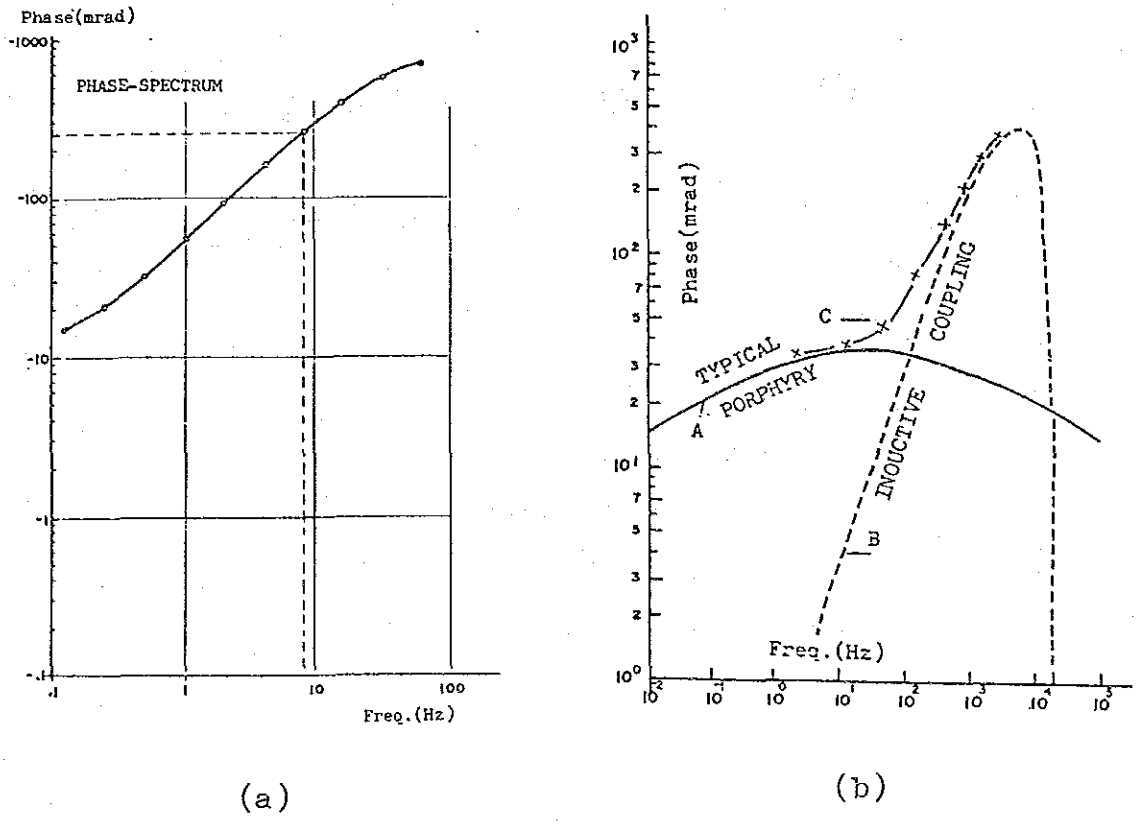

Fig.29 Phase Spectrum

(2) Decoupling Manipulation

Decoupling denotes the removal of a false component in IP responses originating from electromagnetic coupling. The decoupling process was conducted on data over the whole lines of A and B. The decoupling procedure on the SIP measurement in this area was based on the method provided by P.G.Hallof and W.H.Pelton. The analytical method is summarized below. A complex impedance ZA(f) obtained from the SIP survey is approximated by the following equation.

$$ZA(f) = Ro\left[1 - m_1\left\{1 - \frac{1}{1+(i\,2\pi f\tau_1)^{c_1}}\right\} - m_2\left\{1 - \frac{1}{1+(i\,2\pi f\tau_2)^{c_2}}\right\} + m_3\left\{1 - \frac{1}{1+(i\,2\pi f\tau_3)^{c_3}}\right\}\right]$$

where, m : chargeability

τ: time-constant

c : frequency dependence

f : frequency

The equation can be separated into three parts as follows ;

$$1 - m_1\left\{1 - \frac{1}{1+(i\,2\pi f\tau_1)^{c_1}}\right\} \qquad (1)$$

$$-m_2\left\{1 - \frac{1}{1+(i\,2\pi f\tau_2)^{c_2}}\right\} \qquad (2)$$

$$+m_3\left\{1 - \frac{1}{1+(i\,2\pi f\tau_3)^{c_3}}\right\} \qquad (3)$$

The first nominal refers to an IP response, the second indicates electromagnetic coupling derived from a homogenous earth and the third represents the value of electromagnetic coupling in a

conductor. Ten parameters (Ro , m_1 , τ_1 , c_1 , m_2 , τ_2 , c_2 , m_3 , τ_3 , c_3) of the equation above are determined from the SIP measurement using the least squares method of a non linear type. The nominal (2) and (3), being the values of electromagnetic coupling, are removed from the equation , and only the complex impedance Zco(f) of the IP response is obtained.

$$Zco(f) = [1 - m_1 \{1 - \frac{1}{1 + (i\,2\,\pi f \tau_1) c_1}\}]$$

(3) Rock Sample Measurement

In the analysis and interpretation of the survey results, it is essential to understand the SIP features of main rocks and ores distributed in the surveyed area. The measurement of SIP was conducted over samples totaling 35 pieces - 16 pieces of rock and 19 pieces of drilling core - to investigate spectra of phase and magnitude, Cole-Cole property, percent frequency effects and resistivities. A location map of samples is shown in Fig.24. The procedure of measurement is as follows :

① Sample preparation : A cube of 3 cm is prepaired.

② Saturation with water : The samples are soaked in distillied water for 24 hours.

③ Measurement : Instruments used are illustrated in Fig. 30.
Except for the laboratory transmitter, all instru ments and measuring methods are the same as those used in the field.
Standerd value of current was set at 50 μA.

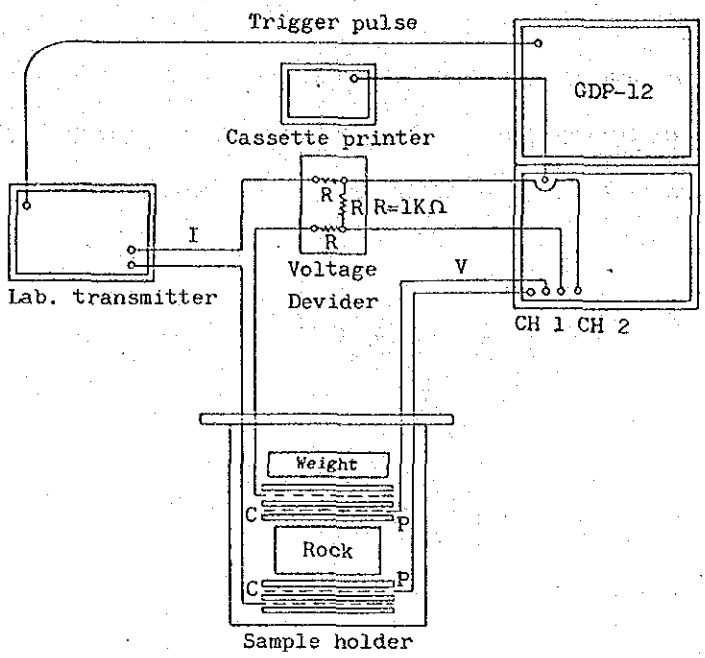

Fig.30 Laboratory Equipment for Rock Sample

Results of Rock Sample Measurements

Results of the laboratory measurements are shown in Table 10 for total samples, and in Table 11-1 for each rock type. The results from these samples can be categorized by their phase spectra which fall into six types as A, B, C, D, X, Y. In comparison, types in the Cole-Cole diagram are divided into two groups; one belonging to type C in the Cole-Cole diagram contains A,B,C and D types of phase spectrum, and the other belonging to type A in the Cole-Cole diagram contains X and Y types of phase spectrum.

The result indicates the following :

① *Phase and PFE of andesite and porphyritic granite are 7 to 10 times hi ger than those* of other rocks. In the same rock, these values vary exten sively in range depending on condition of alteration and pyrite dissemination.

② Phase and PFE are proportionately Correlated.

③ Resistivity values are in a wide range from 126 ohm-m to 12,650 ohm-m. the most

Table10 Results of Rock Sample Meassurement(Hasandere Area)

SampleNo.	Rock	Phase (-mrad)	PFE (%)	Resis. (ohm-m)	Spectrum type	Remarks
6	Calcareous mudstone	10.1	1.16	4,322	C	
5	Siltstone	1.9	0.32	12,649	A	Compact
7	Siltstone	2.4	0.34	3.273	A	Siliceous
8	And.pyroclast	4.1	0.59	4,996	A	Propyliza.Epidote-quart,diss.pyrite
10	And.pyroclast	5.1	0.73	1.819	A	
12	And.pyroclast	3.9	0.58	4,669	A	Magnetite-diss.pyrite
1	Andesite	7.6	1.22	639	X	Propylization.
2	Andesite	0.8	0.09	290	D	Epidote-hematite
3	Andesite	12.6	1.94	2,236	A	Propylization.
27	Andesite	8.8	1.43	1.299	A	Filmy pyrite
21	Alt. andesite	-2.2	0.50	162	D	Sericite-chlorite
22	Alt. andesite	-4.3	-0.19	126	D	Diss.pyrite
24.	Alt..andesite	561.6	134.17	449	Y	Epidote,pyrite along fissures
32	Alt. andesite	6.7	1.49	824	D	Propylization.diss.pyrite
33	Alt. andesite	541.2	144.57	550	X	Diss.pyrite along fissures
34	Alt. andesite	221.2	37.22	2,035	Y	ditto
35	Alt. andesite	21.2	3.30	10,068	A	ditto
4	Basaltic andesite	7.5	1.22	7,164	A	Propyliza.,magnetite-diss.pyrite
26	Basaltic andesite	3.5	0.45	4,757	A	Propyliza.
28	Basaltic andesite	117.8	18.20	547	X	Propyliza.,diss.pyrite
29	Basaltic andesite	376.2	88.31	1,361	X	ditto
36	Basaltic andesite	32.1	4.91	4,303	B	Diss.pyrite along fissures
11	Andesite(Qz.vein)	1.4	0.19	2,544	A	Molybdenite
13	Andesite(Qz.vein)	49.3	7.92	1,579	X	Diss.pyrite
	(Average 21 pcs)	94.1	21.37	2,496		
16	Por.granite(pg2)	7.8	0.88	6,551	A	
9	Alt.por.gr(pgl)	9.2	1.48	3,846	A	Filmy pyrite
14	Alt.por.gr(pgl)	40.0	6.19	7,041	A	Biotite,filmy pyrite
23	Alt.por.gr(pgl)	21.8	4.56	219	D	Pyrite-quartz vein
25	Alt.por.gr(pgl)	208.8	38.71	1,795	X	Diss.pyrite
31	Alt.por.gr(pgl)	7.8	1.60	294	D	Diss.pyrite,sericite-chlorite
41	Alt.por.gr(pgl)	36.7	5.53	849	A	Sil.,sericite,molybdenite-qz
42	Alt.por.gr(pgl)	32.4	4.69	3,754	B	Sil.,sericite,diss.pyrite
43	Alt.por.gr(pgl)	19.4	3.08	6,253	B	Sil.,sericite,molybdenite
44	Alt.por.gr(pgl)	38.6	0.83	1,694	X	Sil.,sericite,diss.pyrite
	(Average 9 pcs)	46.0	7.41	2.861		
15	Qz.porphyry	6.5	0.84	5,207	C	Diss.pyrite

Table11 SIP Responce in the classification of Rock (Hasandere Area)

Rock	No. of samples	Phase (-mrad)	PFE (%)	Resistivity (ohm-m)	Phase spectrum type					
					A	B	C	D	X	Y
Andesite	21	-4.3 ~ 561.6 (94.1)	-0.19 ~ 144.57 (21.37)	126 ~ 10,068 (2,496)	9	1		4	5	2
Por.Granite	10	7.8 ~ 208.2 (42.2)	0.83 ~ 38.71 (6.76)	219 ~ 7,041 (3,230)	4	2		2	2	
Qz.porphyry	1	6.5	0.84	5,207				1		
Cal. mudstone	1	10.1	1.16	4,322				1		
Siltstone	2	1.9 ~ 2.4	0.32 ~ 0.34	3,273 ~12,649	2					
Total No.	44				15	3	2	6	7	2

( ): Average value

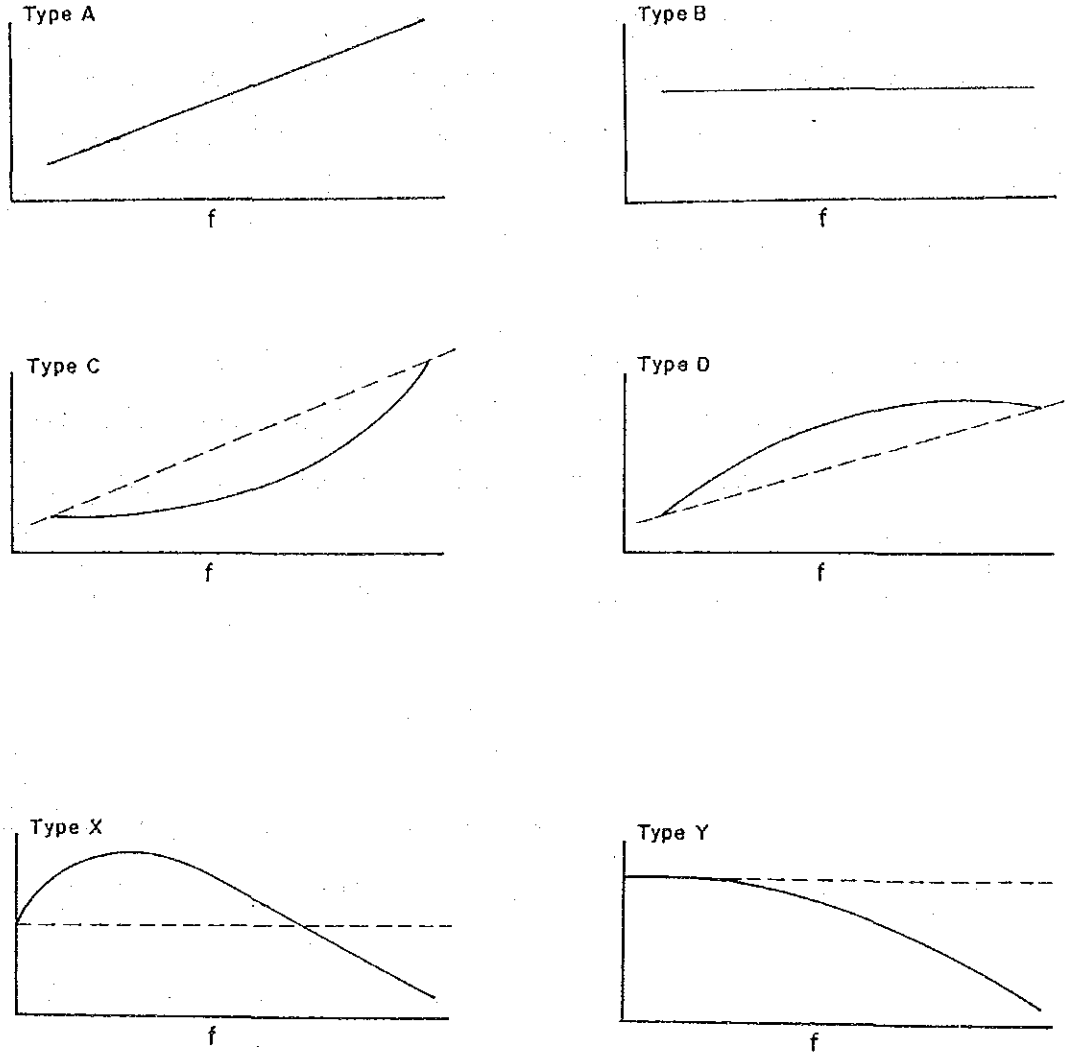

Fig.31 Phase Spectrum Types of Rock Sample

values are generally high, but only 6 samples (17 % of the all samples) are below 500 ohm-m.

④ In the case of the phase spectrum, samples of high phase and PFE belong to X and Y types, and resistivity is not correlated with the phase spectrum.

⑤ On the other hand, weakly mineralized or fresh rock samples are higher than 2,000 ohm-m in resistivity, and mostly belong to A and D types of the phase spectrum.

1-6-3 Results of Interpretation

Three plan maps of apparent resistivity and PFE were drawn for each electrode coefficient of n = 1, 3, 5. On the SIP response, phase variation among 5 frequencies between 0.125 Hz to 3 Hz, phase spectrum, magnitude spectrum and Cole-Cole diagrams were drawn for the pseudo-section of each Line.

Interpretation results are summerized as follows on the basis of these figures.

(1) Plan Map and Pseudo-Section of Apparent Resistivity

Resistivity in the surveyed area shows values ranging from 4.4 ohm-m to 1,094 ohm-m, and the arithmetic mean value (M) is 83 ohm-m. The standard deviation (σ) is 0.400 after conversion through common logarithms, and values of $M+\sigma$ and $M-\sigma$ are calculated as 207 ohm-m and 33 ohm-m respectively. 200 ohm-m and 50 ohm-m are regarded as basic values of high and low resistivity zones with respect to the above values.

The following facts are presumable, taking into consideration the distribution of resistivity obtained from the right-angle arrangement of the survey lines .

Plan Map of Apparent Resistivity (Fig.32, 33 and 34)

Two low resistivity zones were detected at the MJT-1 site and in the area south of the MJT-2 site. The latter was also detected up to the deep plan of n = 5. On the other hand, high resistivity zones are distributed at the west side of the MJT-3 site and the south end of Line A on plans of n = 1 and n = 3. On the plan of n = 1, two high resistivity zones were found at the

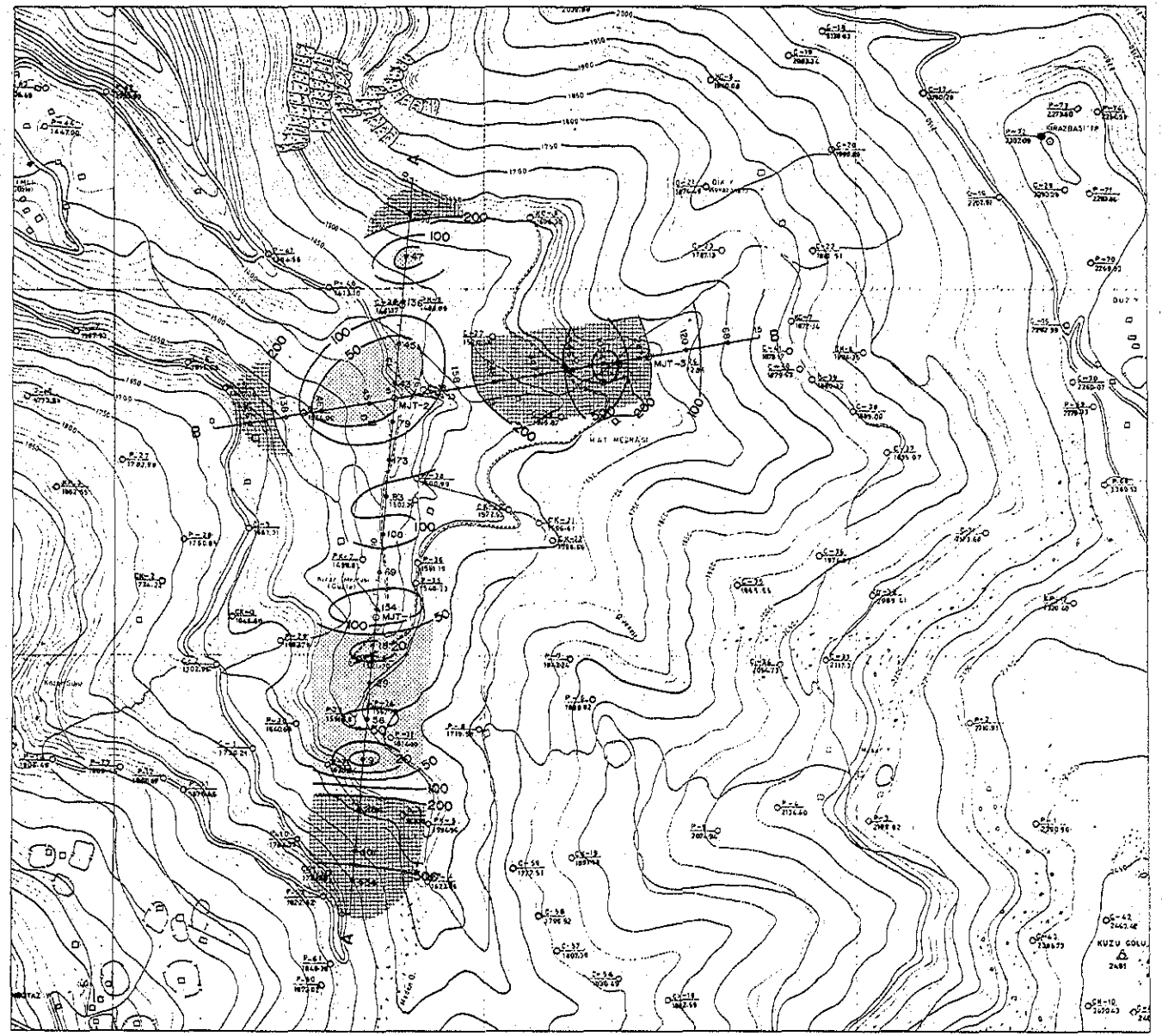

REPORT ON THE MINERAL EXPLORATION
OF GUMÜŞHANE AREA, THE REPUBLIC OF TURKEY

PLAN MAP OF APPARENT RESISTIVITY
(0.125 Hz) (n = 1)

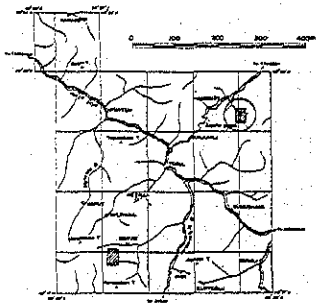

FEBRUARY 1984

JAPAN INTERNATIONAL COOPERATION AGENCY
METAL MINING AGENCY OF JAPAN

LEGEND

SIP SURVEY LINE

MJT-1 DRILLING SITE

LOW RESISTIVITY ZONE

HIGH RESISTIVITY ZONE

(UNIT : ohm-m)

Fig.32 Plan Map of Aparent Resistivity [0.125 Hz] (n = 1)

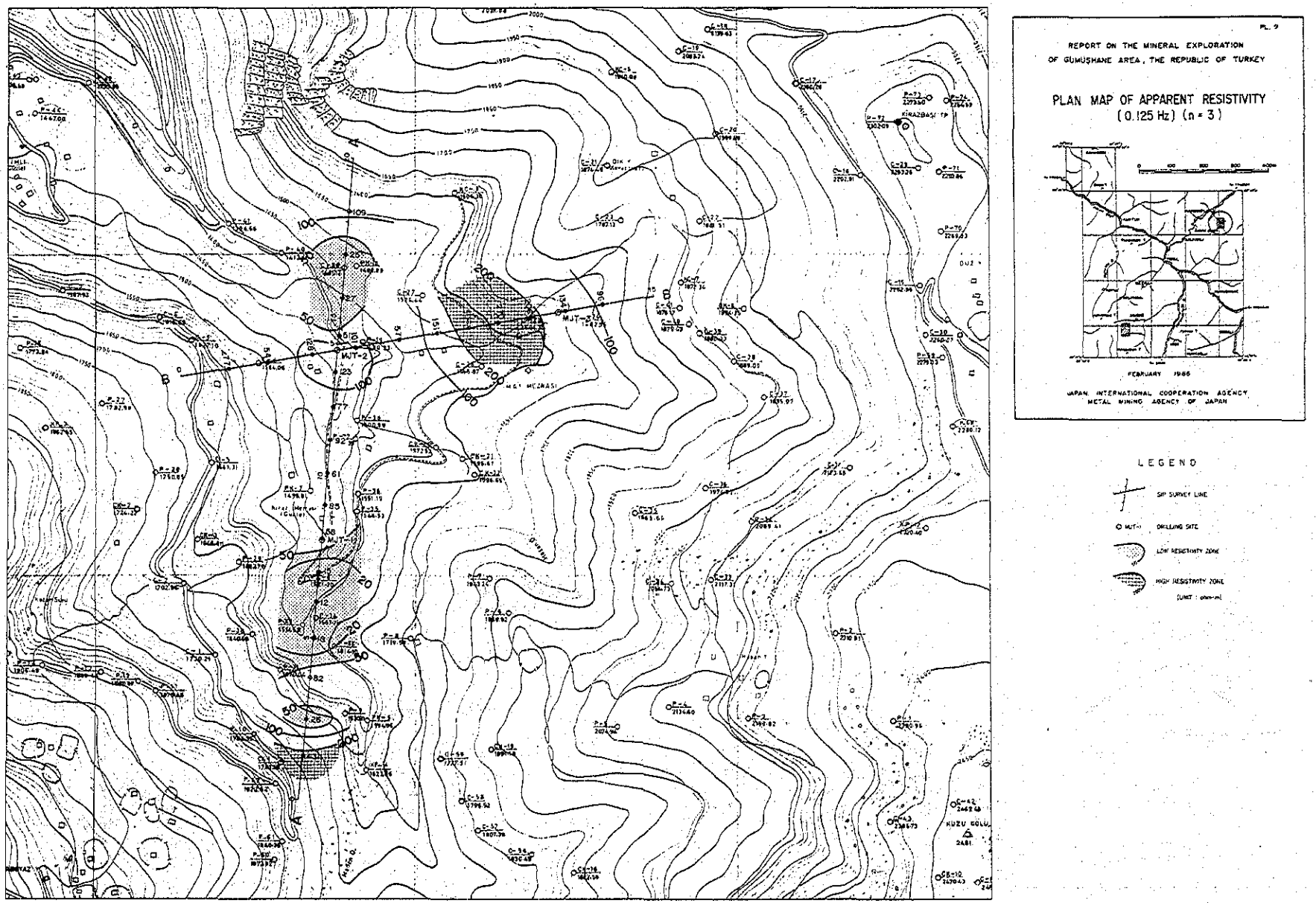

Fig.33 Plan Map of Aparent Resistivity [0.125 Hz] (n = 3)

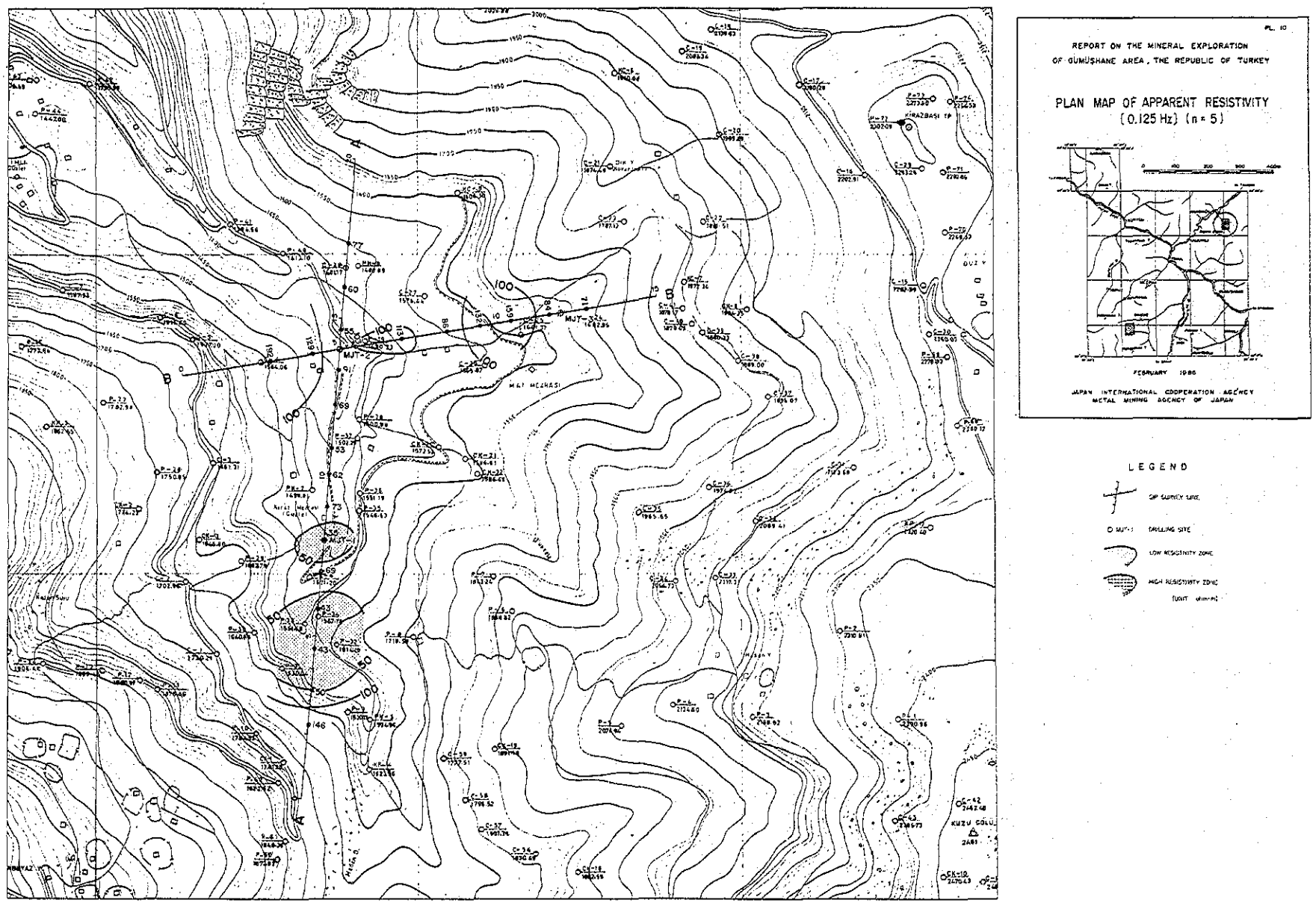

Fig.34 Plan Map of Aparent Resistivity [0.125 Hz] (n = 5)

northern end of Line A and at the western end of Line B, but their extentions are still undelineated owing to the termination of the Lines. Medium to low resistivity zones (less than 200 ohm-m) are predominant on the plan n = 5.

Pseudo-Section of Apparent Resistivity

These sections are shown together with geologic and PFE sections on each survey line.

Line A (Fig. 35 AR)

Low resistivity zones are extensively distributed at the southern part of the MJT-1 site and at the northern part of the MJT-2 site covering the area of porphyritic granite (Pg1) and andesite lava (Zigana Formation). High resistivity zones are present in an extensive distribution on the southern site of this line (unaltered porphyritic granite Pg2), and in small scale at the northern part (Andesite of Zigana Formation).

Line B (Fig. 36 AR)

A small-scale low resistivity zone of less than 50 ohm-m is located on the west side of MJT-2, while a high resistivity zone is present in the porphyritic granite area distributed in the deep part between stations No.7 to No.12. The center of the high resistivity zone, showing over 1,000 ohm-m, is present at the shallow part of station No.10 .

As above mentioned, plan and pseudo-section of apparent resistivity reveal that resistivity values obtained by survey are lower than values of rock samples tested, and most of them are in intermediate values of around 100 ohm-m. A low resistivity zone of smaller than 50 ohm-m is centered on Line A, and it may be caused by emplacement of mineralization and water permiating from Maden Stream. A high resistivity zone is located at both ends of Line A and at the western end of Line B. The relationship between apparent resistivity and alteration by mineralization is described in paragraph 1-6-4.

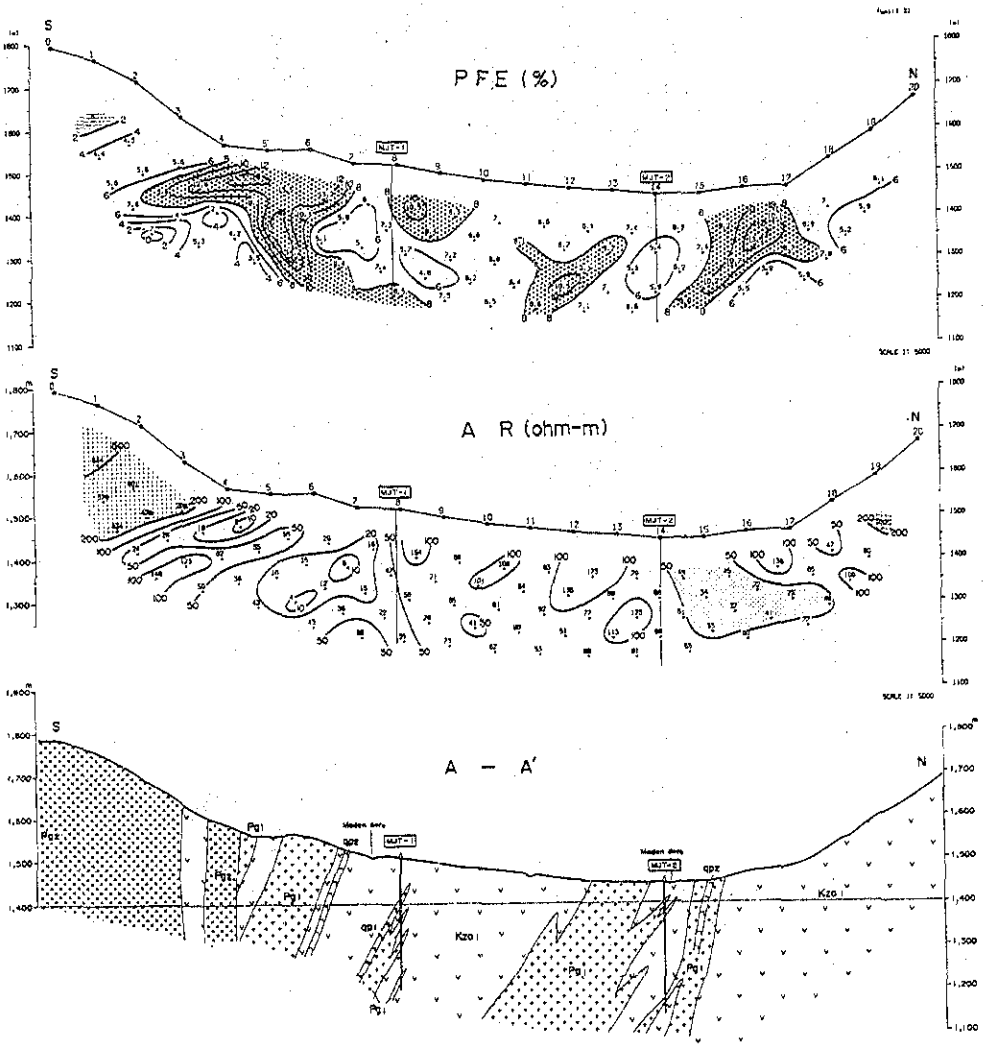

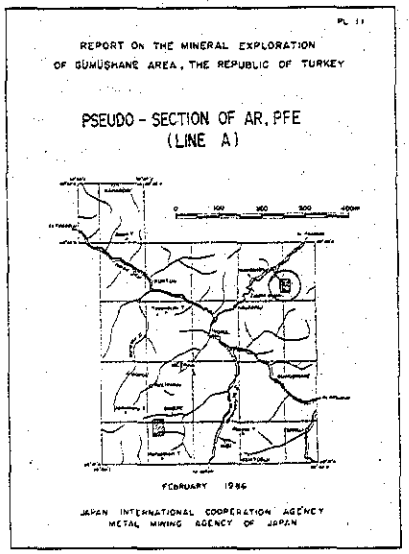

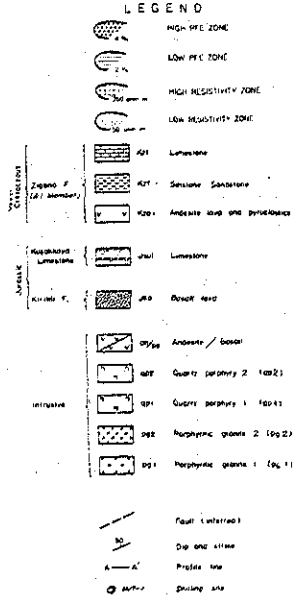

Fig.35 Pseudo-section of AR, PFE (Line A)

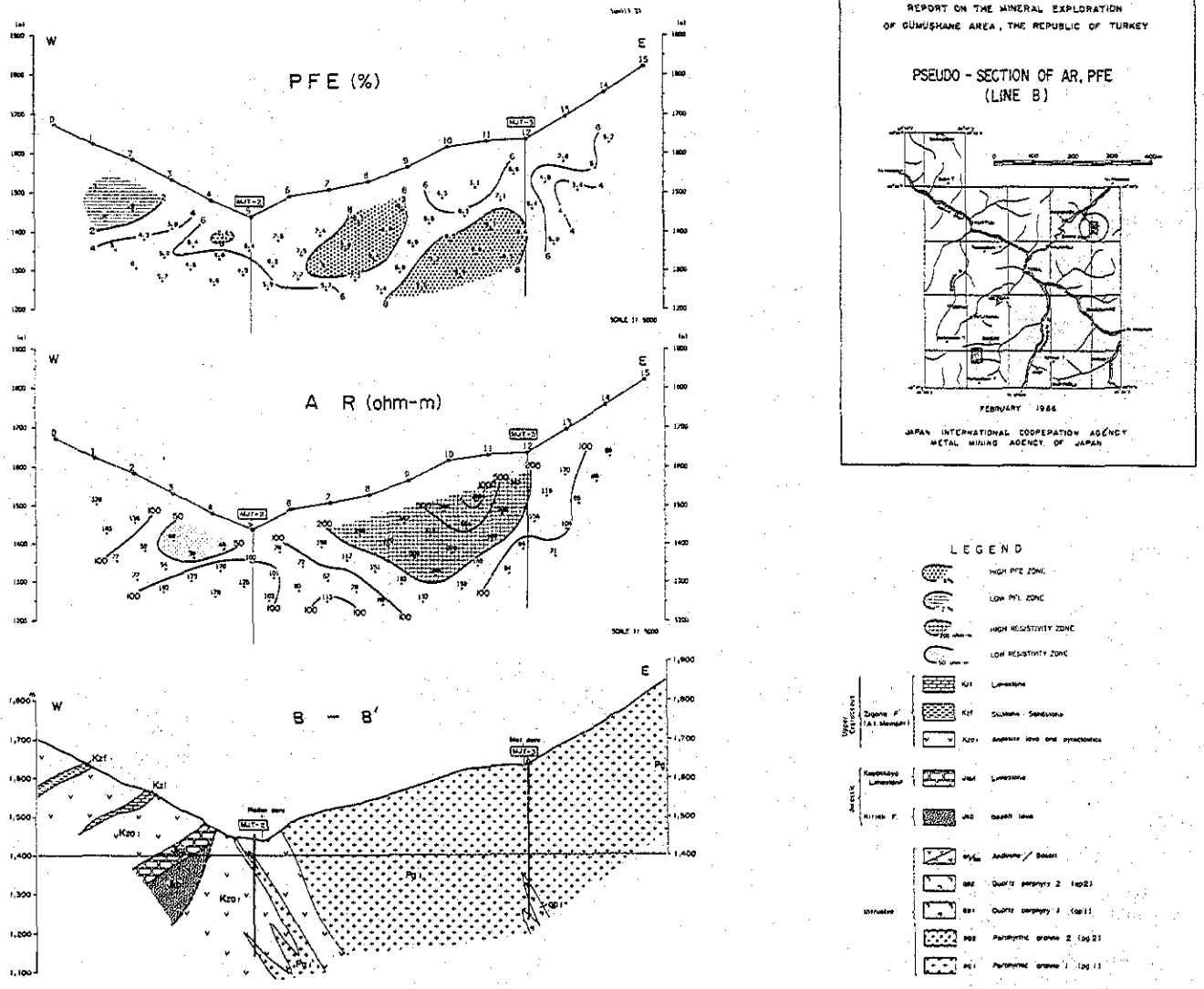

Fig.36 Pseudo-section of AR, PFE (Line B)

(2) Plan Map and Pseudo-Section of Percent Frequency Effect

The values of Percent Frequency Effect(PFE) range from -0.7 % to 15.5 % in the area, and an arithmetic mean value (M) of 6.99 %, 2.704 for standard deviation (σ), and 9.68 % for M+σ, 4.29 % for M-σ were calculated. These PFE values are grouped into three populations based on a histgram made with 1 % intervals. PFE larger than 4 % is regarded as anomalous, considering the measurement result of rock samples. Namely, the area is mostly in an anomalous area because 95.6 percent of all the values are larger than 4 %. The following is revealed when a strong anomalous area of over 8 % PFE is delineated .

Plan Map of Percent Frequency Effect

n = 1 plan (Fig. 37)

High PFE zones are observable at the MJT-1 site to the south, and in the northern to eastern area of the MJT-2 site. Two non-mineralized areas on the basis of PFE less than 2% are pointed out at the southern part of Line A and in the western part of No.3 at Line B.

n = 3 plan (Fig. 38)

It is pointed out on this plan that the high PFE area indicated at No.5 of Line A on the n= 1 plan becomes smaller, that the MJT-2 site extends south in a doughnut shape, and that a new, small-scale, high PFE is newly found.

n = 5 plan (Fig. 39)

High PFE anomalies at No.7 of Line A and No.10 of Line B extend on the plan, and a non-mineralized zone (less than 2 % PFE)is found at the south end of Line A.

Pseudo-Section of PFE

The Line A (Fig. 35 PFE)

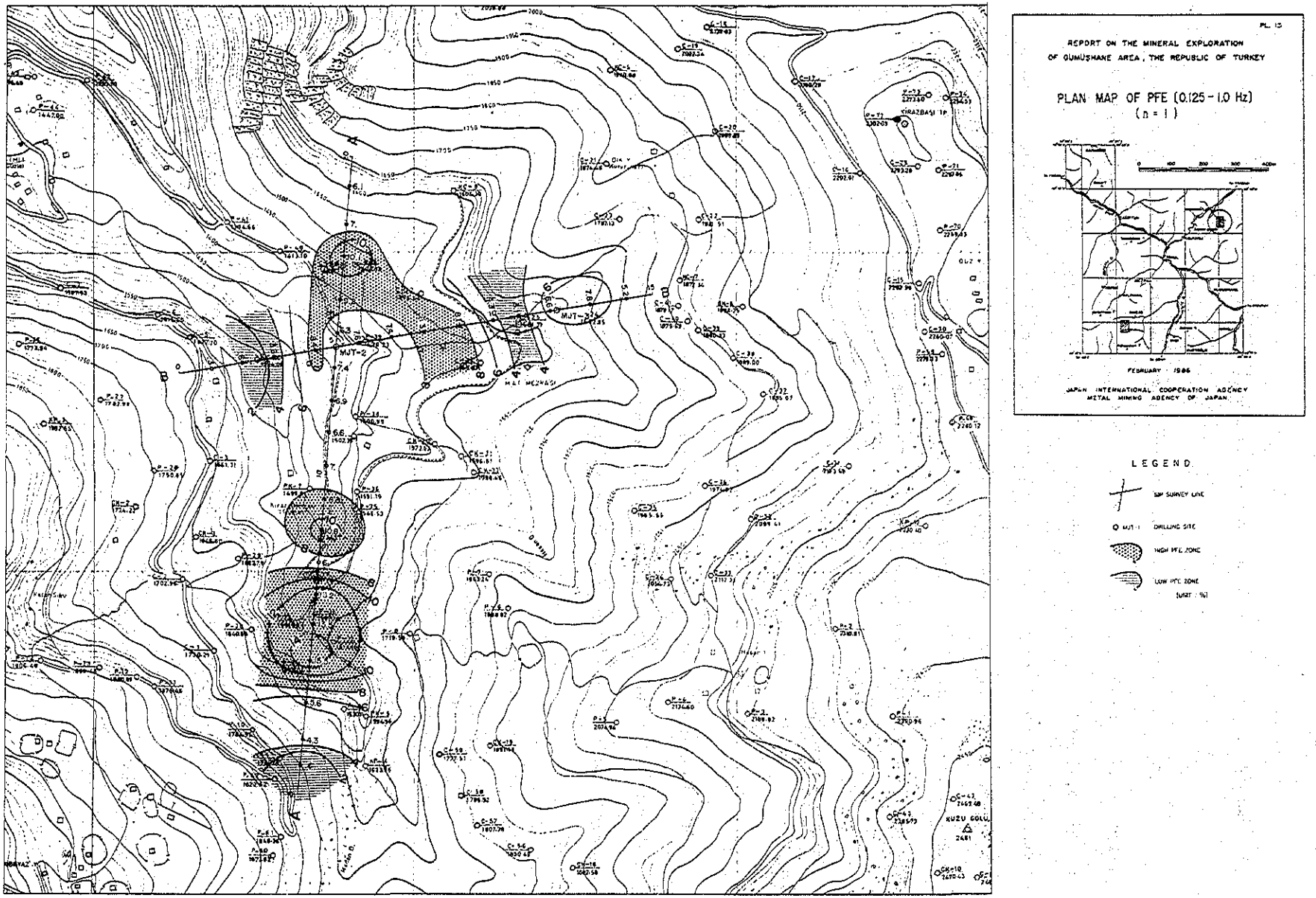

Fig.37 Plan Map of PFE [0.125 - 1.0 Hz] (n = 1)

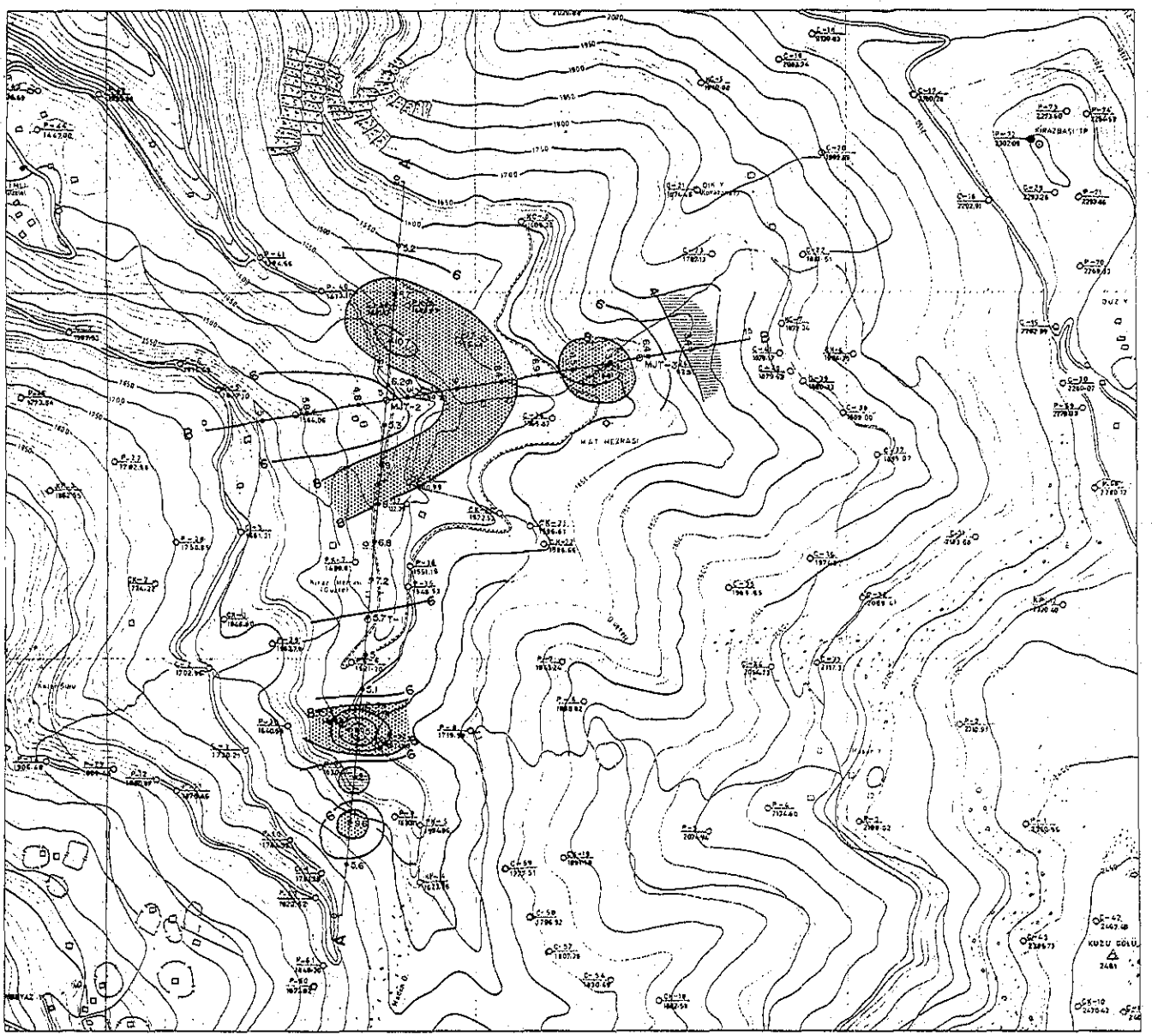

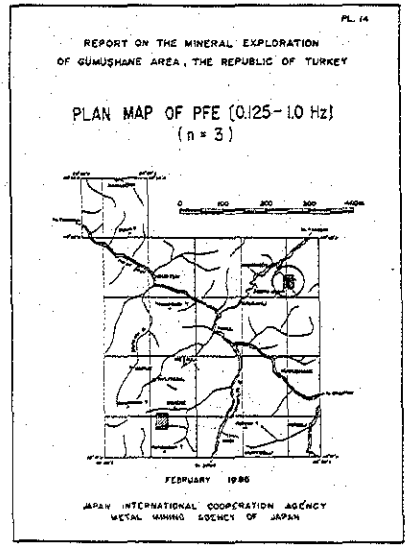

Fig.38 Plan Map of PFE [0.125 - 1.0 Hz] (n = 3)

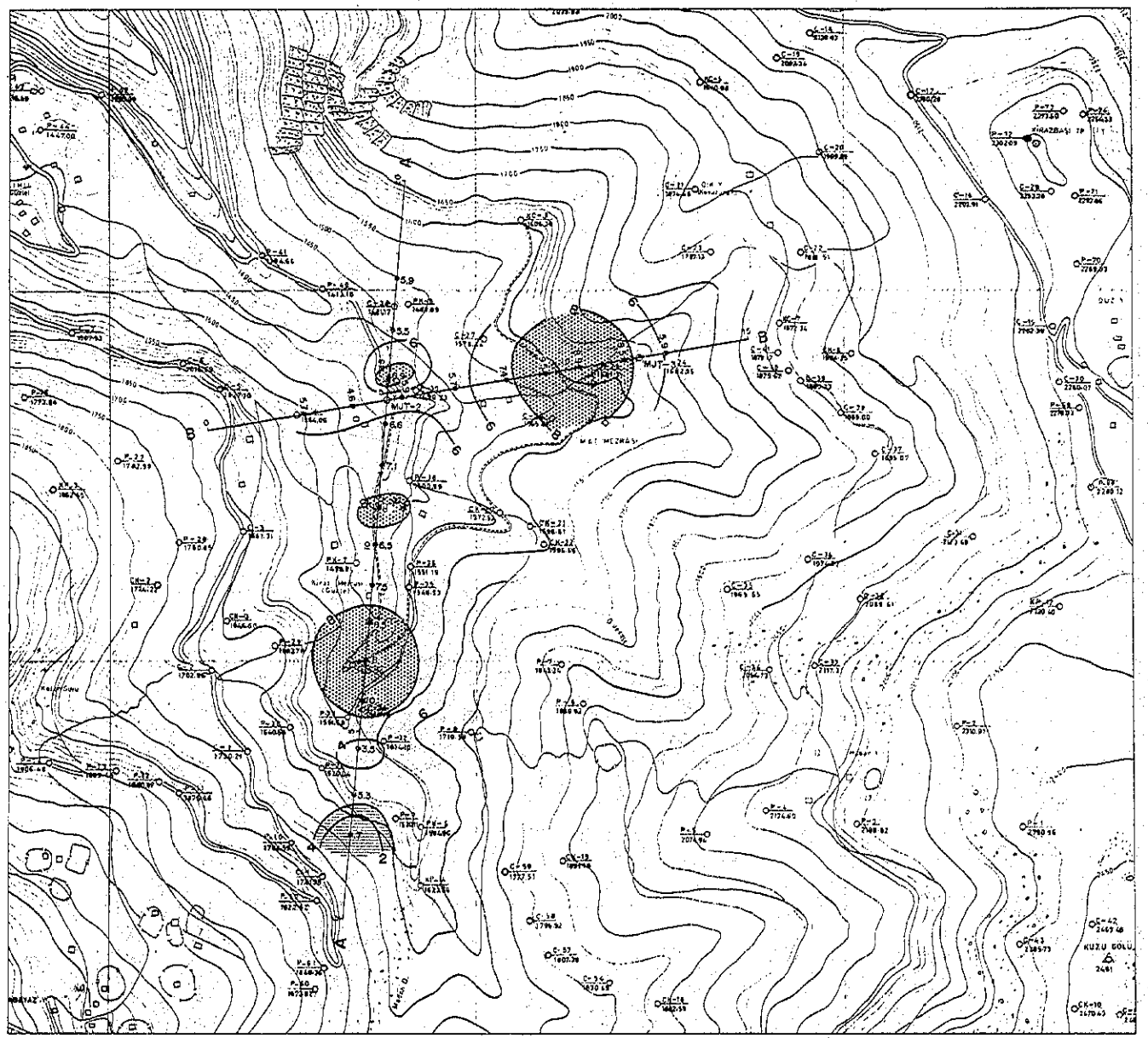

PL. 13

REPORT ON THE MINERAL EXPLORATION
OF GUMUSHANE AREA, THE REPUBLIC OF TURKEY

PLAN MAP OF PFE (0.125 - 1.0 Hz)
(n = 5)

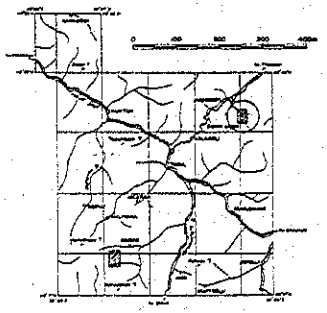

FEBRUARY 1986

JAPAN INTERNATIONAL COOPERATION AGENCY
METAL MINING AGENCY OF JAPAN

LEGEND

- SIP SURVEY LINE
- MUT-1 DRILLING SITE
- HIGH PFE ZONE
- LOW PFE ZONE

(UNIT : %)

Fig.39 Plan Map of PFE [0.125 - 1.0 Hz] (n = 5)

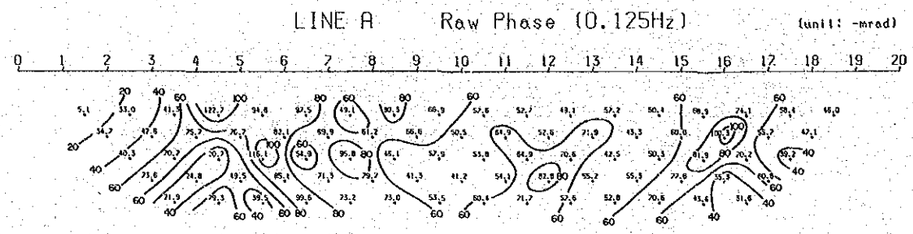

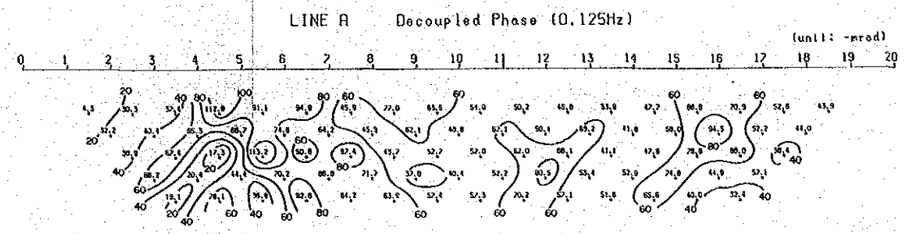

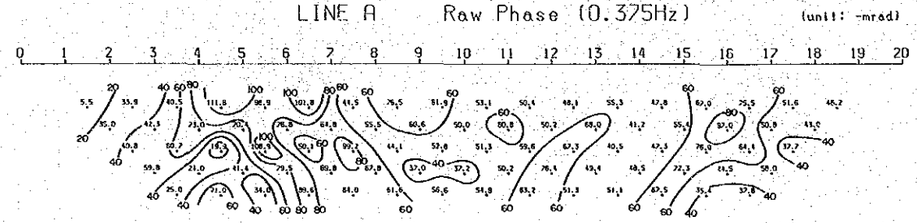

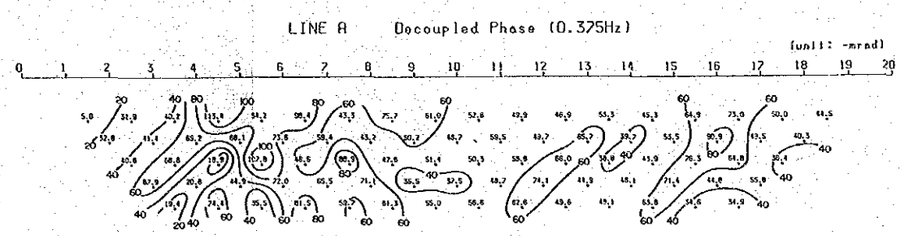

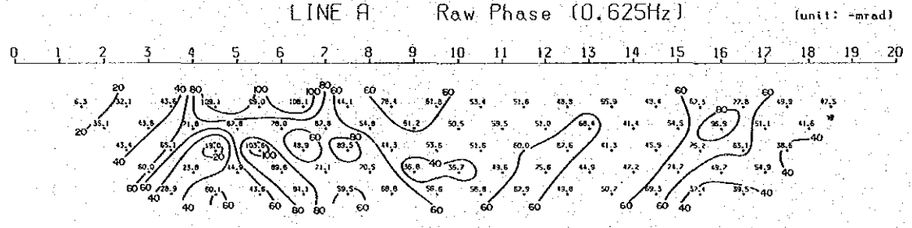

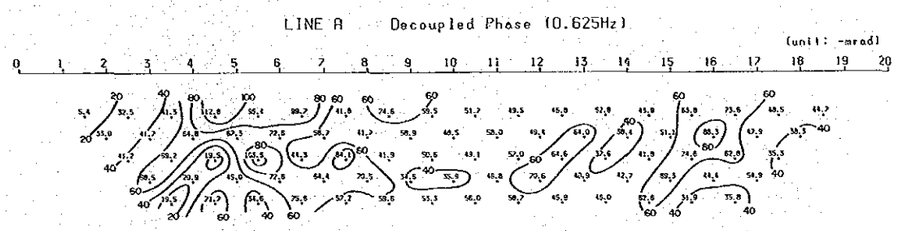

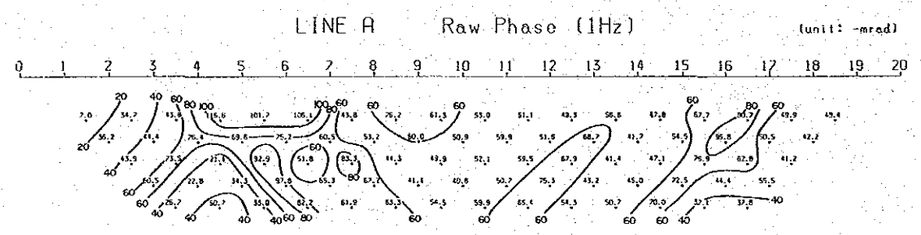

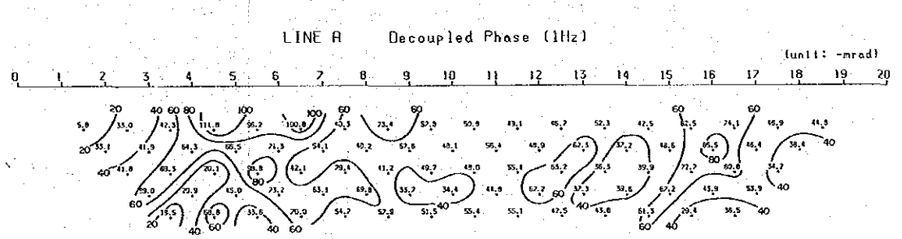

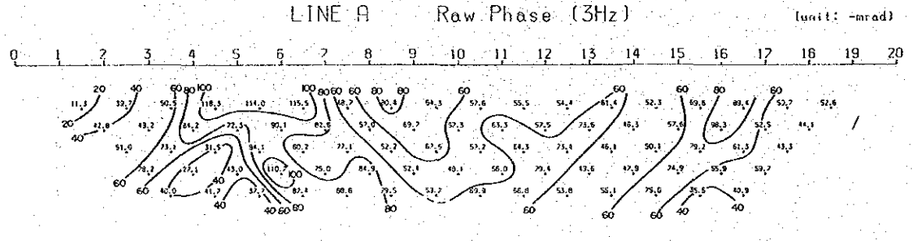

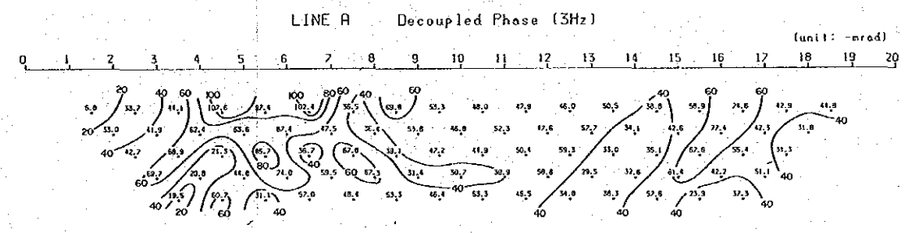

Fig.40 Phase Difference at Five Frequencies (Line A)

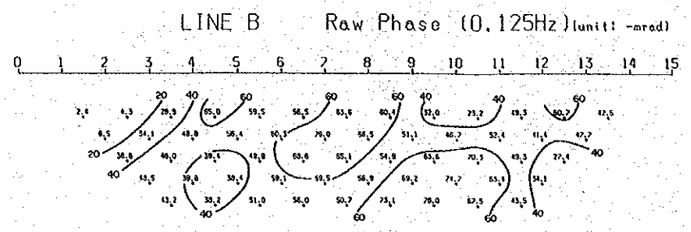

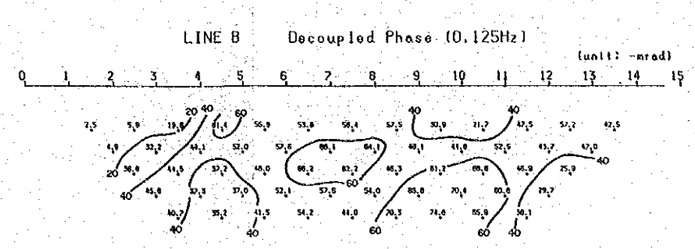

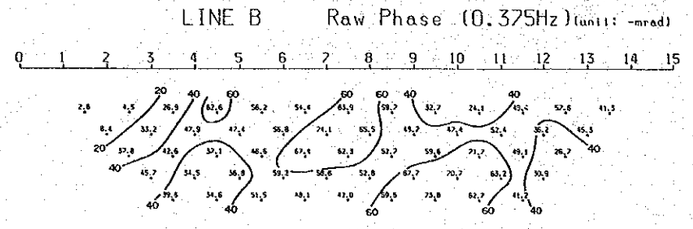

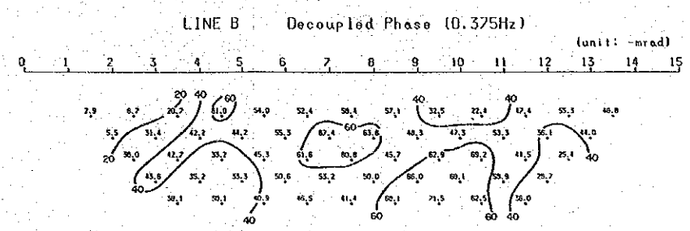

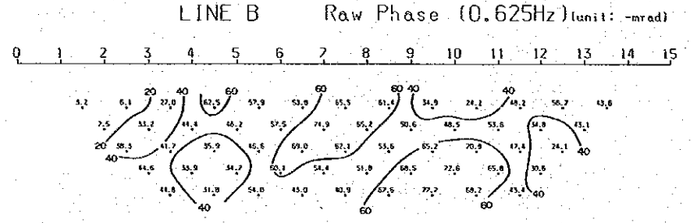

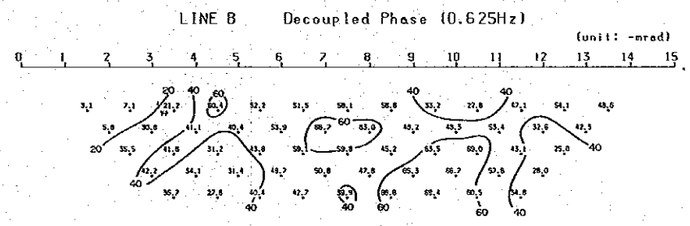

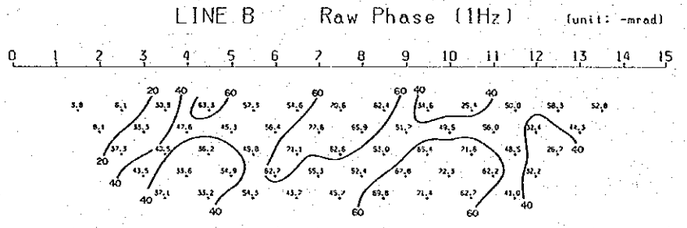

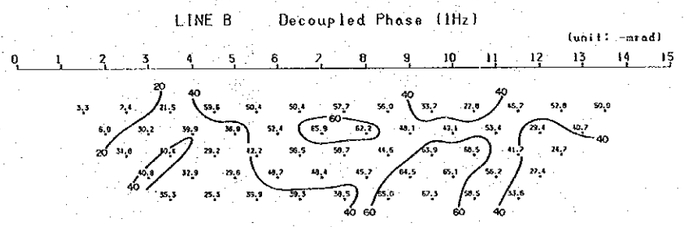

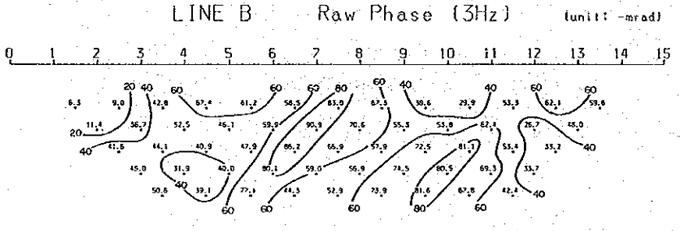

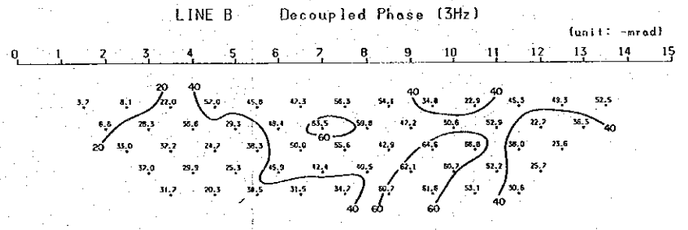

Fig.41 Phase Difference at Five Frequencies (Line B)

Two predominant high-PFE anomalous zone (larger than 8% of PFE) are obtained at southern side of station No.8 (MJT-1 site) and northern side of No.15 The former pattern is more distinct than the latter pattern. Those distribution corresponds with low resistivity zone being smaller than 50 ohm-m. Another small high PFE zone is recognized in deep part of Nos. 8 -10 and Nos.11-13. On the other hand, PFE values are decreased, corresponding with high resistivity part larger than 200 ohm-m.

The Line B (Fig.36 PFE)

High PFE zones over 8% are distributed at shallow to deeper parts of No.6 to No.9 and at deep to shallower parts of No.9 to No.12.

Distribution pattern of those PFE anomalies indicates that high anomalous zone is generally present at Maden and Mat Streams, continuing from shallow part to deeper part, while low PFE zones are recognized at south end of the Line A (south of No.3) and West of No.3 of the Line B. The former of low PFE area corresponds with distribution of unaltered porphyry granite (Pg2) having no mineralization, whereas the latter correspons with unmineralized area bordering by fault which runs parallel with Maden Stream.

Relationship between PFE values and Copper grades is described in paragraph 1-6-4

(3) Pseudo-Section of Phase.

Pseudo-sections of phase were drawn on each Hertzs of 0.125, 0.375, 0.625, 1, and 3, then ferequency dependance of phase was investigated. Decoupled results mentioned in the latter part are also shown together on the pseudo-sections.

The Line A (Fig. 40)

In comparison with those sections each other, each section shows same pattern. Accordingly, it is presumed that electromagnetic coupling is quite small. In shallow part between No.4 and No. 7, area of 80 mrad spreads in proportion to high frequency, and electromagnetic coupling phenomenon occurs slightly. Distribution of apparent resistivity (Fig. 35 AR) shows that there is a very samll amount of low apparent resistivity with values smaller than 10 ohm-m in the survey area. 86 % of rock samples collected in the area have resistivity larger than 500 ohm-m. The

fact indicates that the area is less susceptible to electromagnetic coupling because the resistivity of rock in the area is large.

The Line B (Fig. 41)

Five pseudo-sections of decoupled phase are all similar in contoured patterns, and they are also correspond to the phase pattern of undecoupled 0.125 Hz. Consequently it is considered that the electromagnetic coupling is removed from the response.

(4) Phase, Magnitude and Cole-Cole Spectra.

Phase,magnitude and Cole-Cole Spectra are shown in the pseudo-section. All spectra after decoupling are also illustrated in the section.

Line A (Fig. 42)

(A) Phase spectrum :

A negative phase spectrum was detected at the lower sections of No.4 to No.7, and No.16 to No.18. PFE and phase are of high value and resistivity is of low value in this part. Pre-decoupled spectra are A-type (ascending to the right), except for the negative phases, while decoupled spectra are horizontal or descending to the right and also convex spectra (X-type). Sharply curved X type spectra observed through measurement of rocks are present in the two abovementioned two negative phase areas.

(B) Magnitude spectrum

This is generally a spectrum ascending to the right, and steeply dipped spectra are detected at the lower parts of No.4 to No.7 and No.16 to No.18. Decoupled spectra are mostly gently dipped or horizontal, but the steep spectra of the two parts mentioned above remain steeply-diping, compared with the spectra in the other parts.

(C) Cole-Cole diagram

Most diagrams belong to C-type and descend to the right, but A-type diagrams are detected in

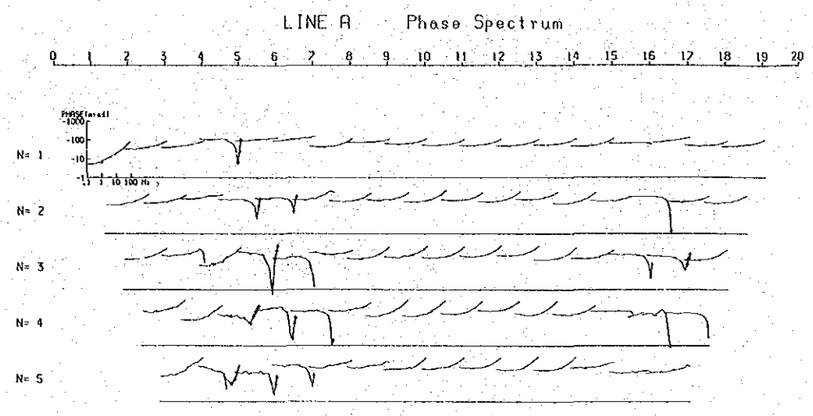

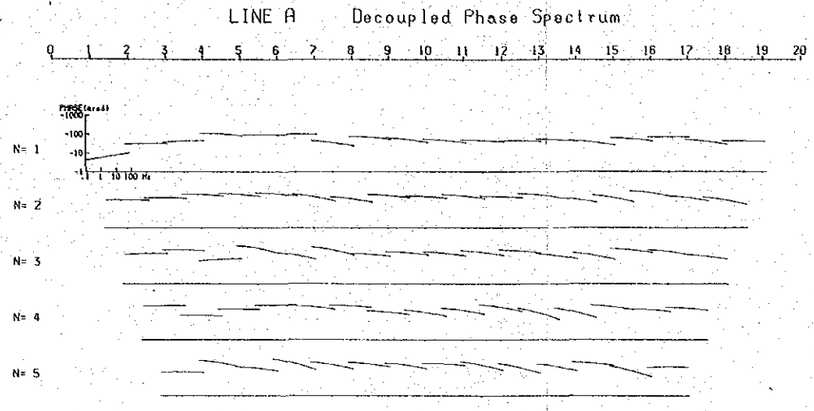

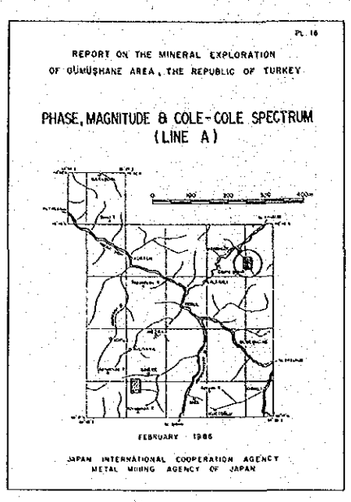

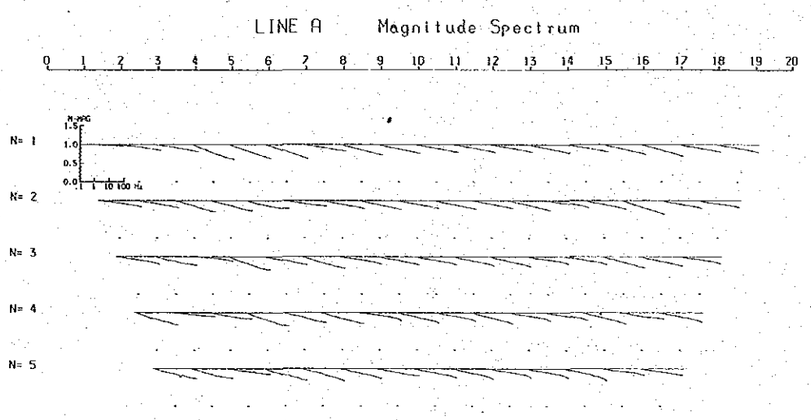

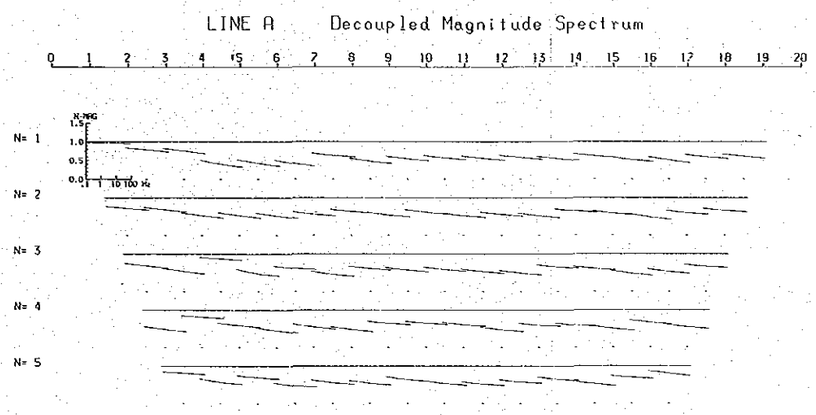

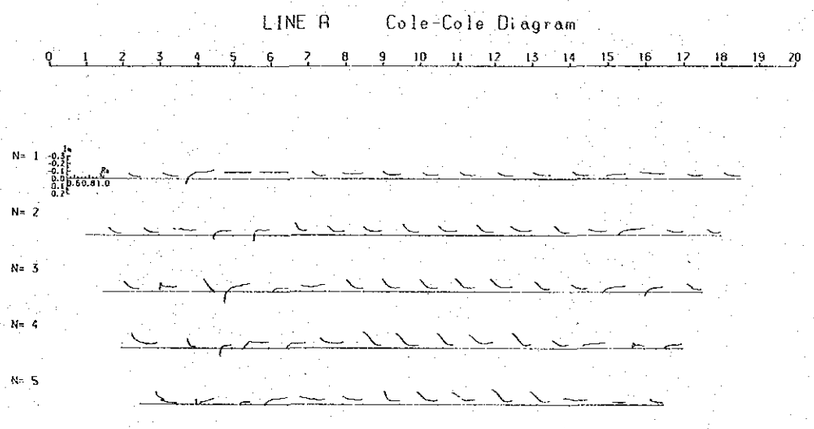

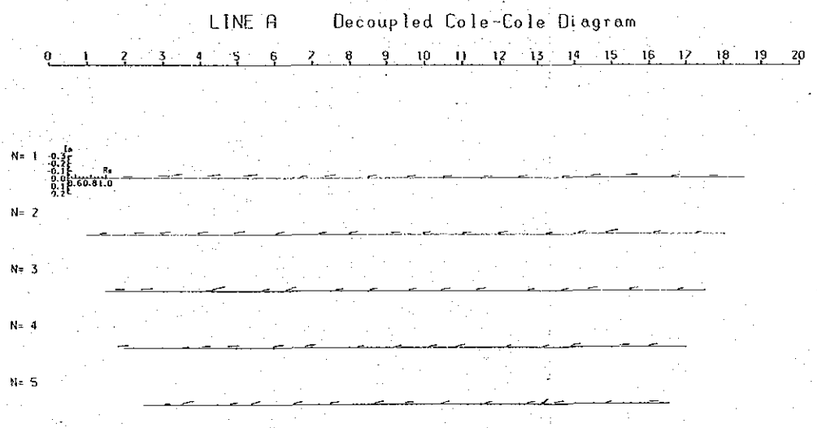

Fig.42 Phase, Magnitude and Cole-Cole Spectrum (Line A)

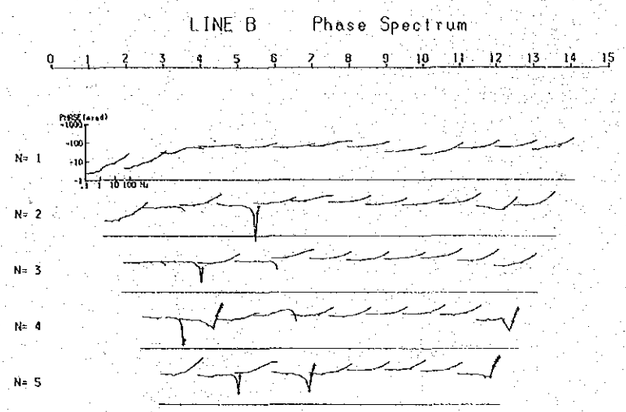

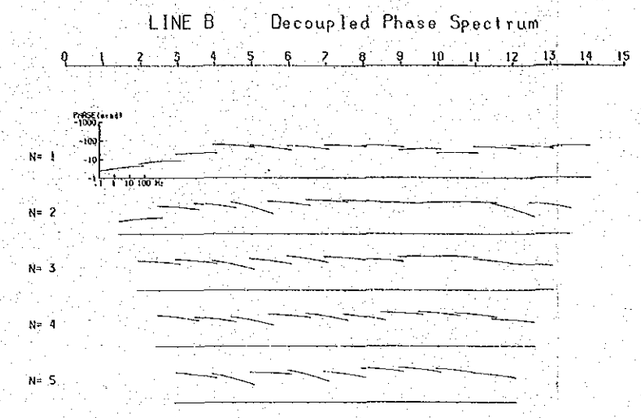

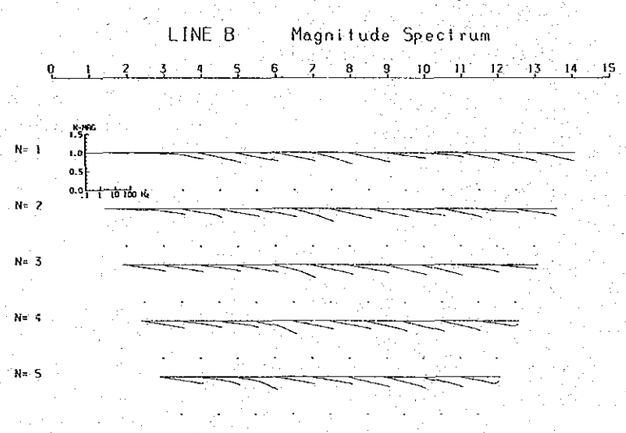

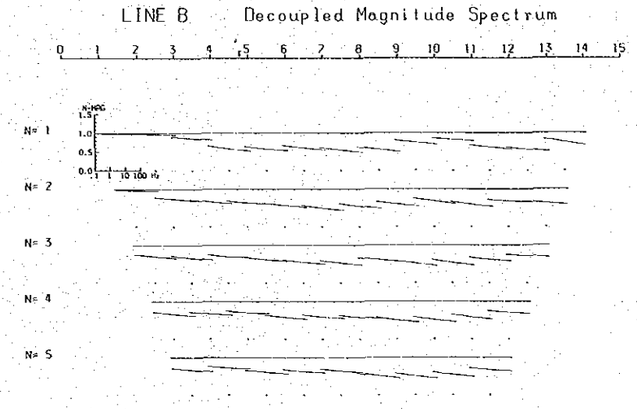

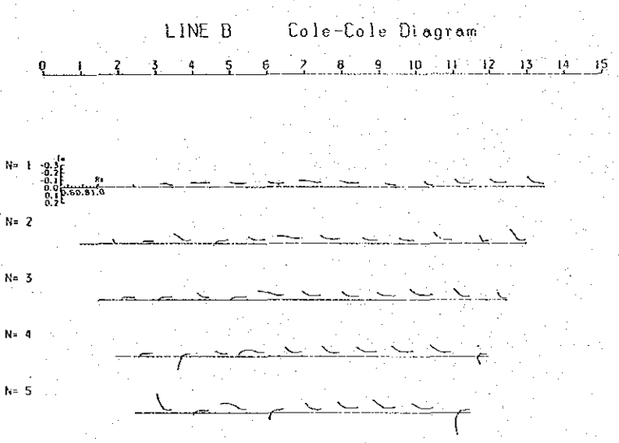

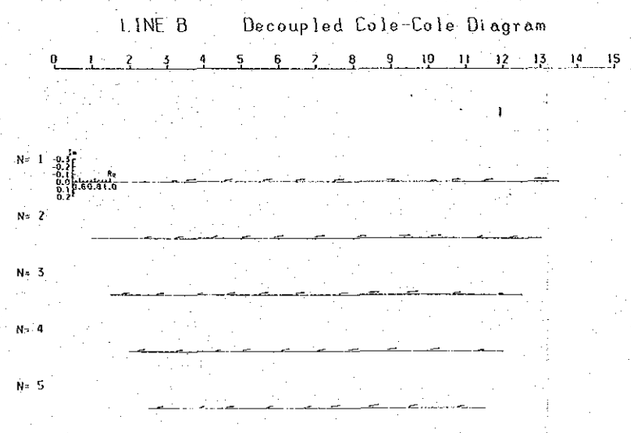

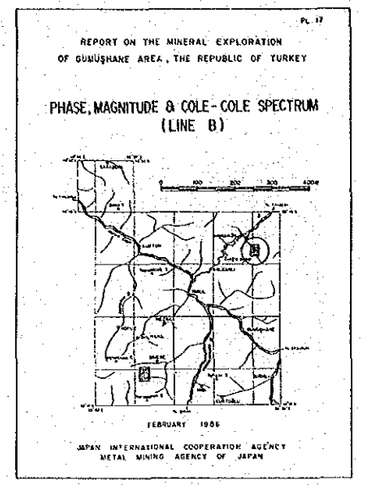

Fig.43 Phase, Magnitude and Cole-Cole Spectrum (Line B)

the same places as the anomalous magnitudes and phases mentioned above. Horizontal B-type diagrams are also recognized at shallow parts of No.4 to No.6, and at deep parts of No.14 to No. 16. The Cole-Cole diagram after decoupling is mainly A-type, and steeply dipping parts are also located at the same places as the phase- and magnitude-anomalies.

Line B (Fig. 43)

(A) Phase spectrum

Negative phases are observed at lower parts of No.3 to No.7, and No.11 to No.13 on the survey line. The spectra are commonly flat up to around 10 Hz, and become A-type, increasing simply at high frequency. After decoupling, the spectra type are flat or gently descending to the right. The spectra are flat or convex X-type at areas of high PFE and phase on their sections (No. 6 to No.12). The spectrum is descending steeply to the right at the negative phase part as in the case of Line A.

(B) Magnitude spectrum

Most spectra ascend to the right, but a steeply dipping spectra are obtained at No.5 to No.8. Gently sloping or flat spectra are shown for areas of high resistivity, at the western part of the survey line and at the shallow part of No.9 to No.11. Magnitude spectra after decoupling are gently ascending to the right.

(C) Cole-Cole diagram

The diagrams are generally shown flat or descend to the right, but the spectrum ascends to the right at the negative phase. In the Cole-Cole diagram after decoupling, the spectra are seen to ascend to the right or be flat, but the slope is steeper. Characteristics of the spectra resemble those of Line A.

(5) Decoupled Percent Frequency Effect

Decoupled phase, magnitude and Cole-Cole diagram are each explained in the above sections,

along with the undecoupled raw data. Thus only the case of PFE is described below.

Line A (Fig. 44 upper figure)

This section has almost the same contour pattern as PFE in Fig.35 , but values of PFE are somewhat greater than those of undecoupled PFE. This tendency is especially remarkable at No. 4 to No.7, and in the shallow part of No.16.

Line B (Fig. 44 lower figure)

It is pointed out that PFE values tend to increase at some portion in the section as in the case of Line A, but the contour pattern is similar to Fig.36.

(6) *Model Simulation for IP Anomaly*

Above mentioned anomalies are qualitatively interpreted and evaluated on the pseudo-sections. Model simulations were applied in order to interpret quantitatively the anomaly source, its location, and meaning of PFE and resistivity. The model simulations were carried out on Lines A and B.

Line A (Fig. 45)

A predominant PFE anomaly is detected at the southern part of the MJT-1 site, and at the northern part of the MJT-2 site on this line. Their results are shown in Fig.45 (A) and (B). In Fig.45 (A), andesite lava is code 2 and code 3, porphyrytic granite is code 6 and the strongly mineralized area is code 8 and code 9. Porphyritic granite (Pgl, code 6) is assumed to be of high resistivity and low PFE owing to fresh rock.

The simulation model is suitable because the apparent resistivity and PFE pattern obtained by simulation are mostly similar to the survey result.

On the other hand, in the anomalous part (Fig.45)(B) of the northern section of the line, andesite (code 3), porphyritic granite (code 4) and high PFE (code 4) are assumed.

The simulation result corresponds closely to the survey result, except that the form of low apparent resistivity is different around No. 15 and high PFE occurs at the northern end of the line. The reason may be that survey data is insufficiently at the end of the survey line and some data

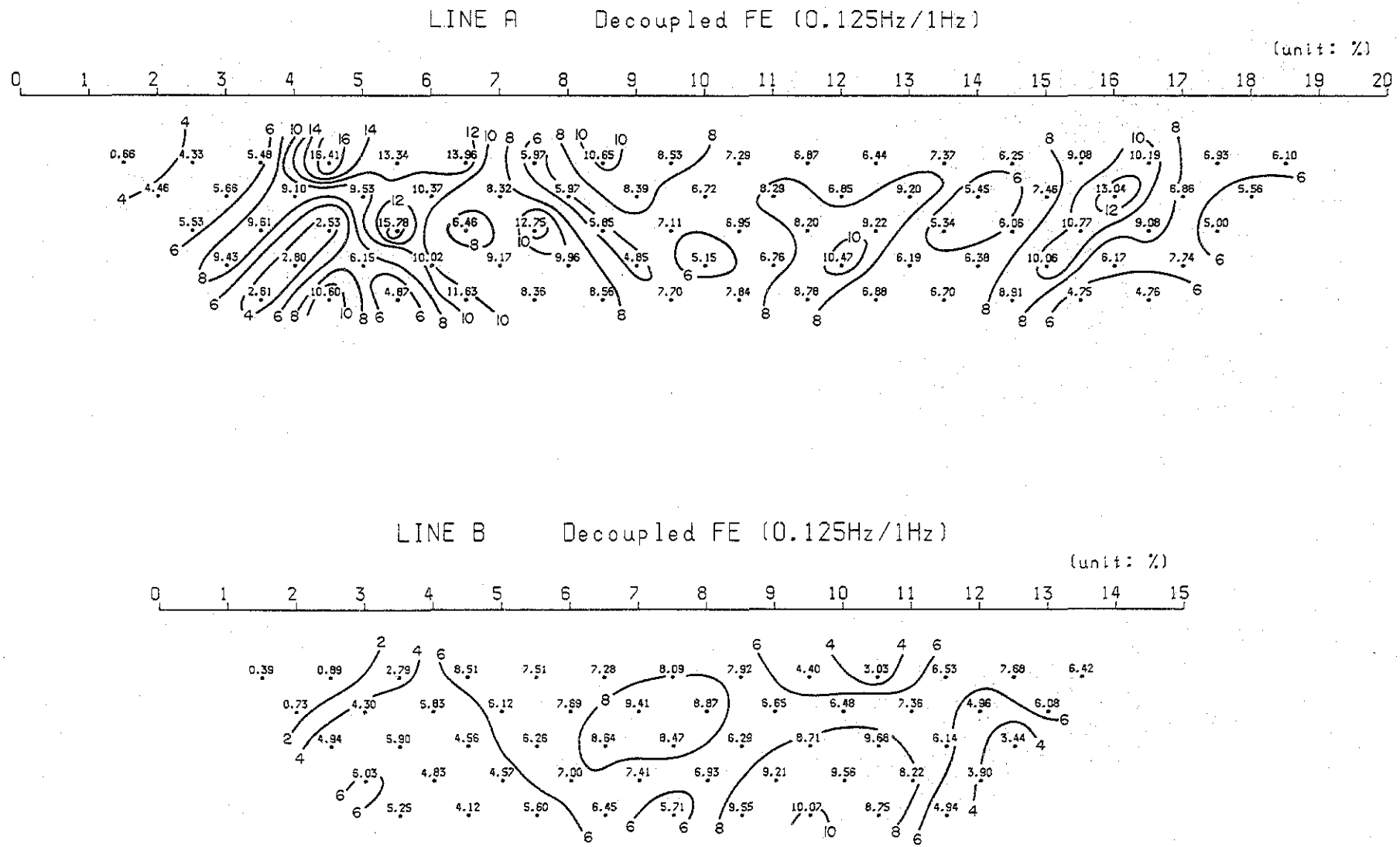

Fig.44 Decoupled PFE (Line A, Line B)

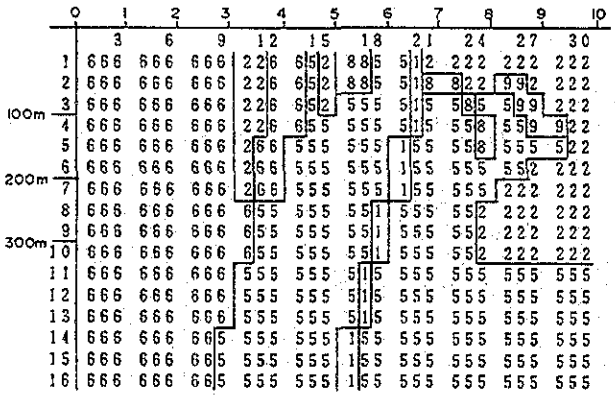

MODEL NO. A-1

CODE	RESISTIVITY OHM M	F.E. %
1	100.	6.0
2	200.	8.0
3	0.	.0
4	0.	.0
5	50.	8.0
6	500.	1.0
7	0.	.0
8	2.	20.0
9	2.	8.0

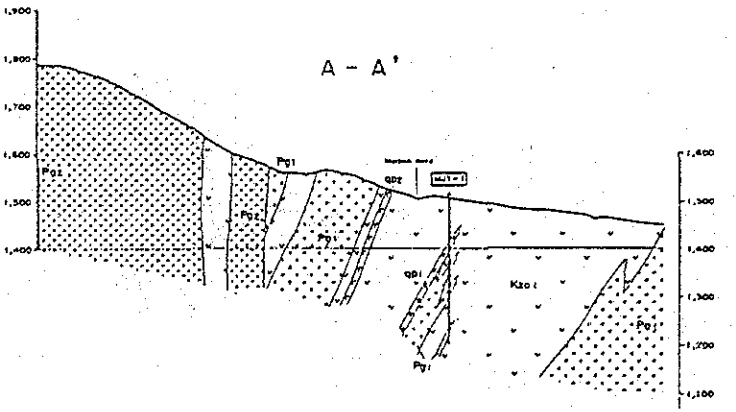

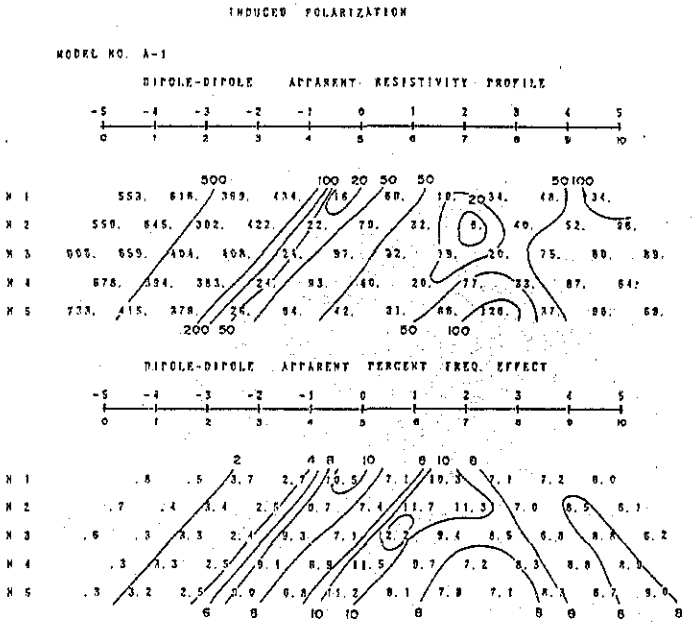

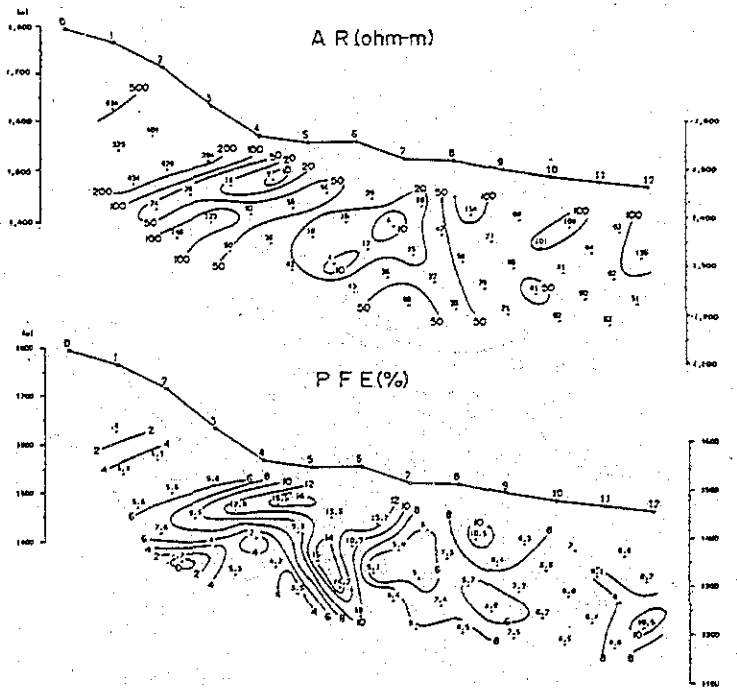

Fig.45 Result of Model Simulation (Line A) (A)

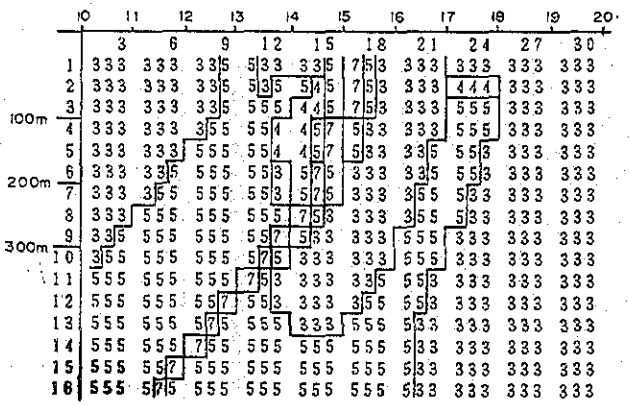

MODEL NO. A-2

CODE	RESISTIVITY OHM M	F.E. %
1	0.	.0
2	0.	.0
3	100.	6.0
4	20.	20.0
5	50.	8.0
6	0.	.0
7	50.	6.0
8	0.	.0
9	0.	.0

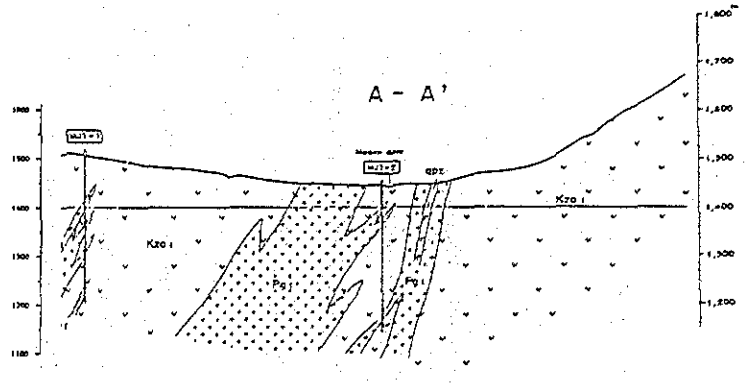

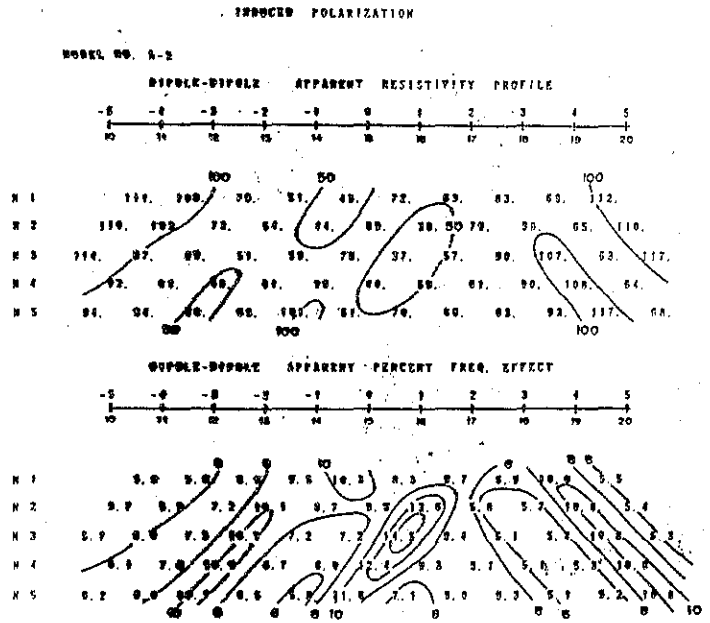

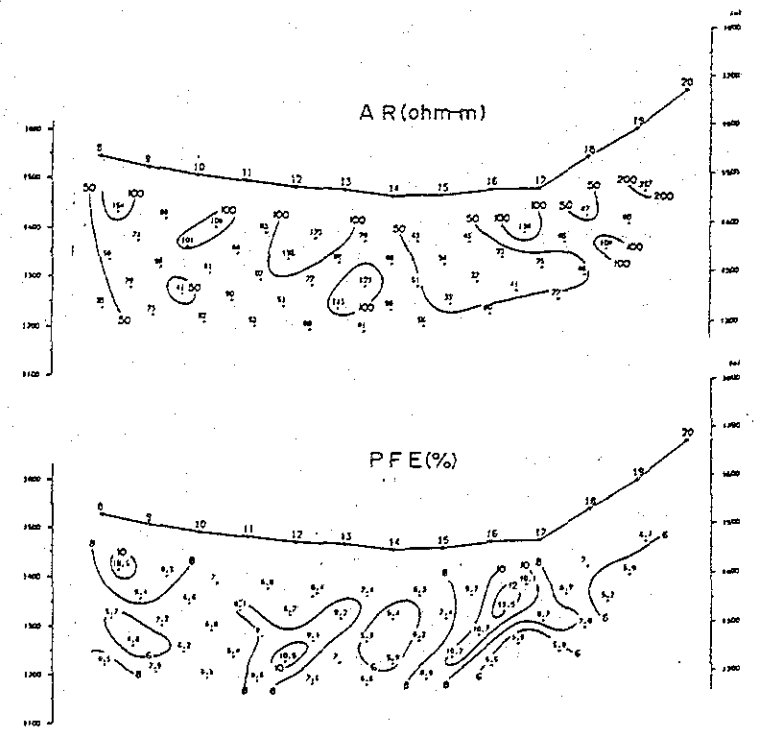

Fig.45 Result of Model Simulation (Line A) (B)

have been are extrapolated to outside of the area in the process of simulation.

Line B (Fig. 46)

Porphyritic granite (Pg1, code 4) is distributed on the eastern side from Maden Stream on this line, and a PFE anomaly larger than 8 % and a high resistivity zone (cord 5 and code 6) were detected in the shallow part from No.7 to No.13. Andesite (code 1 and code 2) around Maden stream, unmineralized andesite (code 3) and limestone (code 7) further on the western side, are also present. Code 8 is the inferred low resistivity zone located along the fault.

The simulation result reveals that position of high resistivity and distribution of PFE fit well with the observed value. Porphyritic granite (code 5) isthe weakly mineralized part. The fault inferred on the western side of Maden River by geological survey is also confirmed to dip about 45° and is accompaniedby the low resistivity zone of the simulation interpretation. The western side of the fault is indicated as an unmineralized zone by the interpretation as well as by geological survey.

(7) Discussion and Interpretation Map

Discussion

The SIP survey was insufficient to obtain distribution of resistivity and PFE on plan because the survey was carried out only on the two survey lines which connect the three drill holes of this year and which cross at a right angle. Thus the interpretation was done with an aim of unravelling geophysical response conditions and continuity to deeper zones within the neibouring parts of the survey lines. Geological and mineralization conditions between those drill holes were also interpreted in conjunction with measurement results of drill cores.

(a) Most apparent resistivity values are around 100 ohn-m. Low resistivity values of less than 50 ohm-m are mainly located around No.5 and No.15 of Line A. The former is lower in resistivity than the latter.

On the other hand, high resistivity zones (over 200 ohm-m) were detected at both end parts of Line A, around No.10, and in the western part of Line B. The high resistivity in the southern end of Line A corresponds to porphyritic granite(Pg2). At the western end of Line B, it is

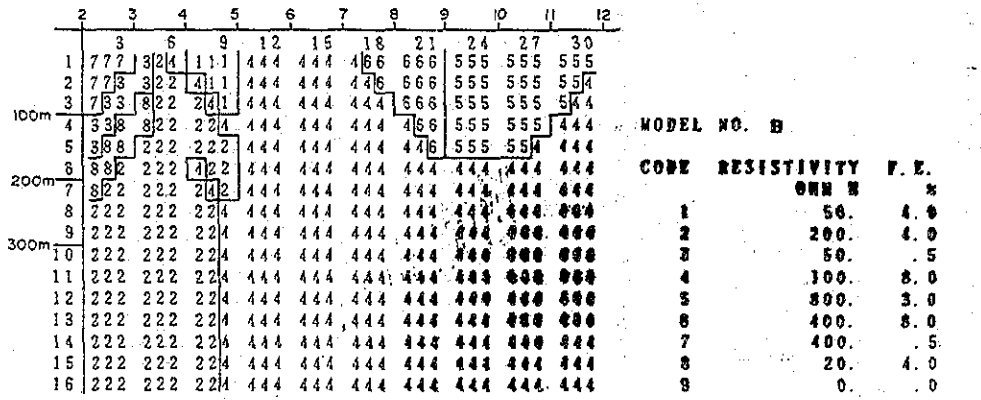

MODEL NO. B

CODE	RESISTIVITY OHM M	F. E. %
1	50.	4.0
2	200.	4.0
3	50.	.5
4	100.	8.0
5	800.	3.0
6	400.	8.0
7	400.	.5
8	20.	4.0
9	0.	.0

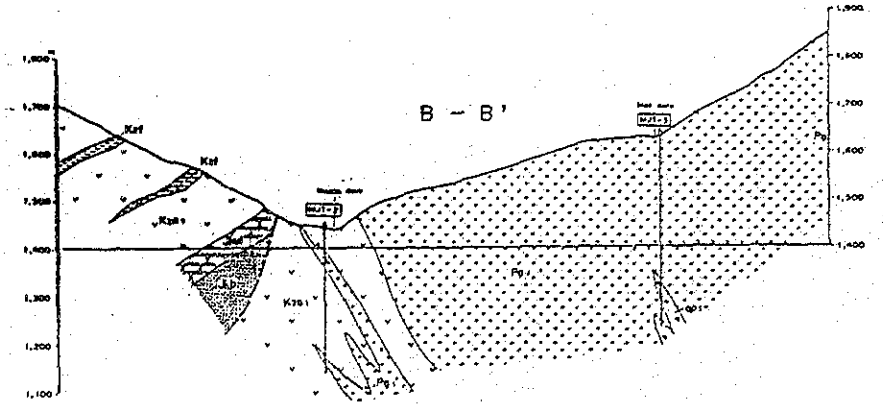

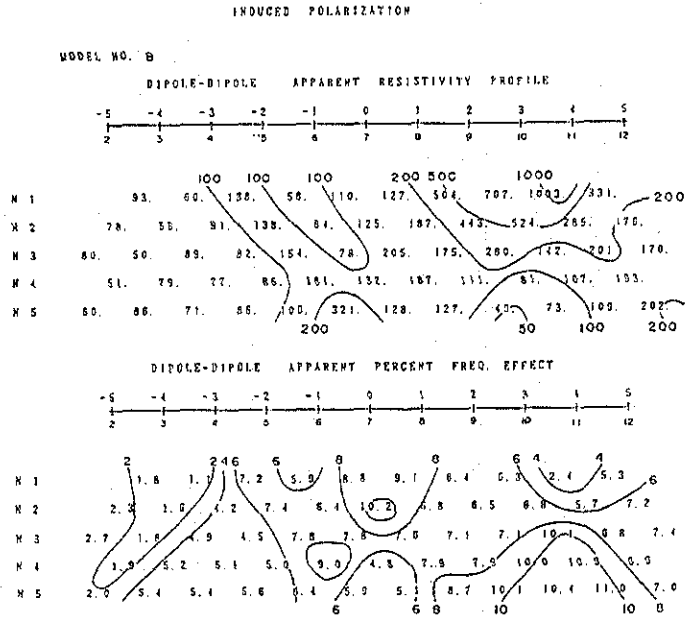

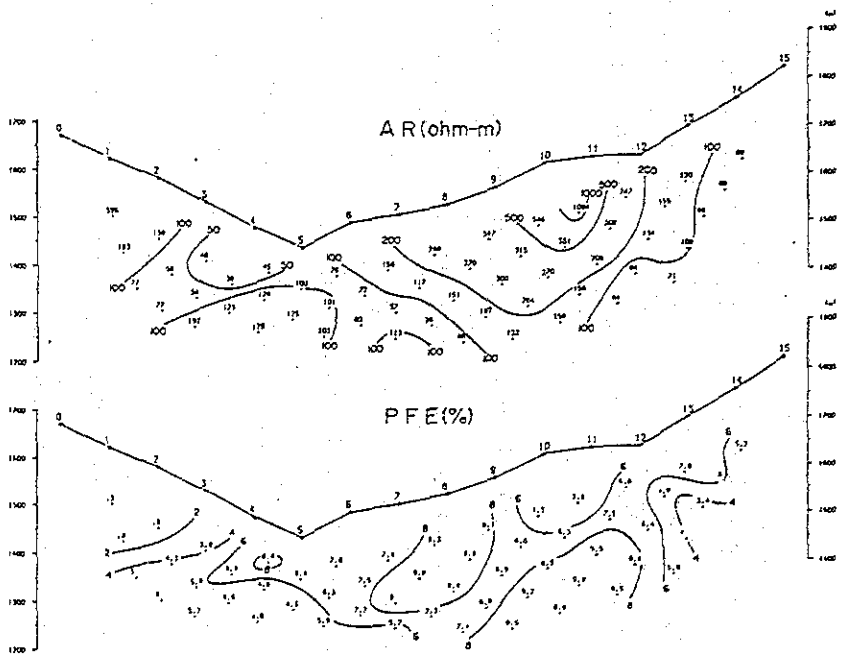

Fig.46 Result of Model Simulation (Line B)

unmineralized, bordering on the inferred fault, and corresponds to the geological survey result which indicates existing andesite lava and pyroclastic rock (Zigana Formation). The fault presumably dips about 45° through the pseudo-section of PFE and apparent resistivity.

(b) PFE values are grouped into three populations, and the values over 4% are constitute 95.6 % of them. Results of drilling core and rock measurements indicate that PFE values of fresh or weakly mineralized samples are less than 1.5 % in value. In the whole survey area, the zone of values larger than 4% in PFE is regarded as the anomalous mineralized zone. High PFE values were detected at No.5 and No.16 of Line A and at No.10 of Line B. Two values of the former correspond to the low resistivity zone, but the latter is located in the high resistivity zone.

(C) 19 samples were collected from drilling cores, and measured for their SIP properties. The result (Table 12) indicates that PFE values are proportional to phase, while both values (PFE and phase) are inversely proportional to resistivity values. On the other hand, grades of copper and molibdenum are not correlative with PFE, phase, resistivity, etc. X and Y type phase spectra amongall these phase spectra, show high values of phase and PFE, but do not correspond to high grade samples of copper and molibdenum. They tend, rather, to belong to A and D types of phase spectra. It is inferred that ore grades are not so apparent from SIP responses.

The interpretation result reveals that remarkably high PFE anomalies are responses to emplacement of pyrite, and that responses are most marked at No.5 of Line A, and weakest at the northern and north-eastern area, depending upon pyritization. This zone of strong pyritization is situated in the phyllic zone. Accordingly, the northern and eastern areas from the MJT-2 site are promising for copper bearing mineralization.

Interpretation Map (Fig. 47)

The survey result is summarized in the interpreted map. Anomalous areas and the promising area for copper mineralization are marked on the map with respect to the plan maps of apparent resistivity (n = 1) and of percent frequency effect (n = 1).

PL. 18

REPORT ON THE MINERAL EXPLORATION
OF GÜMÜŞHANE AREA, THE REPUBLIC OF TURKEY

GEOPHYSICAL INTERPRETATION MAP OF THE HASANDERE AREA

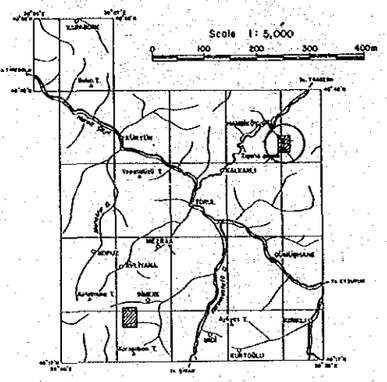

FEBRUARY · 1986

JAPAN INTERNATIONAL COOPERATION AGENCY
METAL MINING AGENCY OF JAPAN

LEGEND

- SIP SURVEY LINE
- MJT-1 DRILLING SITE
- HIGH PFE ZONE 8 %
- LOW PFE ZONE 2 %
- HIGH RESISTIVITY ZONE 200 ohm-m
- LOW RESISTIVITY ZONE 50 ohm-m
- EXPECTED HIGH Cu % ZONE

Fig.47 Geophysical Interpretation Map in the Hasandere Area

Table12 Relationship between SIP responce and Cu,Mo % of drilling core Sample

Sample No.	Depth (m)	R o c k	Phase (-mrad)	PFE (%)	Resist. (ohm-m)	Spectrum type	Cu (%)	Mo (%)	R e m a r k s
Drilling No. MJT - 1									
21	52.10	Alternated andesite	-2.2	0.50	162	D	0.06	0.001	Sericite-chlorite、diss.pyrite
22	99.80	Alternated andesite	-4.3	-0.19	126	D	0.09	0.009	Diss.pyrite
23	139.90	Porphyrtic granite(pgl)	21.8	4.56	219	D	0.08	0.004	Pyrite-quartz vein
24	150.80	Alternated andesite	561.6	134.17	449	Y	0.10	0.001	Epidote, pyrite along fissures
25	184.50	Porphyrtic granite(pgl)	208.2	38.71	1,795	X	0.09	0.019	Diss.pyrite
26	200.10	Basaltic andesite	3.5	0.45	4,757	A	0.06	0.001	Propyliza.
27	250.90	Andesite	8.8	1.43	1,299	A	0.03	0.00	Filmy pyrite
28	274.30	Basaltic andesite	117.8	18.20	547	X	0.04		Propyliza.,diss.pyrite
29	297.90	Basaltic andesite	376.2	88.31	1,361	X	0.01		Propyliza.,diss.pyrite
Drilling No. MJT - 2									
31	44.70	Porphyrtic granite(pgl)	7.8	1.60	294	D	0.15	0.003	Diss.pyrite、sericite-chlorite
32	51.70	Alternated andesite	6.7	1.49	824	D	0.40	0.010	Propyliza.、diss.pyrite
33	154.30	Alternated andesite	541.2	144.57	550	X	0.12	0.003	Diss.pyrite along fissures
34	200.00	Alternated andesite	221.2	37.22	2,035	Y	0.12	0.004	Diss.pyrite along fissures
35	250.10	Alternated andesite	21.2	3.30	10,068	A	0.19	0.008	Diss.pyrite along fissures
36	299.30	Basaltic andesite	32.1	4.91	4,303	B	0.13	0.004	Diss.pyrite along fissures
Drilling No. MJT - 3									
41	151.05	Porphyrtic granite(pgl)	36.7	5.53	849	A	0.21	0.006	Sil.、sericite、molybdenite-qz
42	199.20	Porphyrtic granite(pgl)	32.4	4.69	3,754	B	0.15	0.011	Sil.、sericite、diss.pyrite
43	250.00	Porphyrtic granite(pgl)	19.4	3.08	6,253	B	0.13	0.007	Sil.、molybdenite、diss.pyrite
44	301.20	Porphyrtic granite(pgl)	38.6	0.83	1,694	X	0.07	0.004	Sil.、sericite、diss.pyrite